The Effects of Extrinsic and Intrinsic Noise on a Tumour and a Proposed Metastasis Model

by

Herbert Tang

A thesis

presented to the University of Waterloo

in fulfillment of the

thesis requirement for the degree of

Doctor of Philosophy

in

Applied Mathematics

Waterloo, Ontario, Canada, 2015

© Herbert Tang 2015

I hereby declare that I am the sole author of this thesis. This is a true copy of the thesis, including any required final revisions, as accepted by my examiners.

I understand that my thesis may be made electronically available to the public.

Abstract

Cancer is a ubiquitous disease that afflicts millions of people worldwide and we will undoubtedly encounter it at some point in our lives, whether it be random strangers on the news, or someone much closer. As such, research into cancer (and cures for cancer) has been an intense area of focus. Malignant tumours show three main characteristics: 1) aggressive and uncontrolled growth, 2) invasion into surrounding tissue, and 3) the ability to leave the primary tumour site and invade another organ (metastasis). Mathematical models of these three aspects began in earnest about half a century ago, for example with Laird[70] in 1964 proposing that tumour growth was gompertzian. With the advent of the modern computer, complex partial differential equation (PDE) models of tumour growth which incorporate the other two features of malignant tumours have become accessible to the average researcher. Utilizing a mixture of both analytical and numerical methods, this thesis aims to add to the schema of cancer research by examining the effects of noise on a well established model of tumour growth, and a promising model for mitosis that we hope to eventually adapt to describe metastasis.

The tumour model that we will examine is a single species reaction-diffusion model that captures the first two aspects of tumour growth. The reaction part determines how fast the tumour grows and the diffusion part describes how quickly the cancer cells spread within the domain. Adding noise to the model is a method of describing the disorder that is in a typical tumour, and allows us to determine error bounds on the tumour size and survival time, which gives us a sense of how accurate the estimates of those two quantities are. This method of estimating the uncertainty in survival time also allows us to further determine how modifications to the model (such as changing the diffusivity or adding chemotherapy) affects the error in the system.

Our model of mitosis is an excitable system that admits a traveling wave as a possible solution. Mitosis is a process that occurs in a very spatially specific manner within the embryo and this model describes how a signal propagates from the centre of the embryo outwards. When we allow noise to perturb the system we will see that the model allows noise induced traveling

waves in what would normally be a stable system in a deterministic setting. This means that the parameter range under which signalling can occur is relaxed and traveling waves occur more readily than expected. In terms of metastasis, where the tumour microenvironment is especially noisy and chaotic, that might explain why metastasis is so prevalent in malignant tumours.

Adding noise to well established PDE models gives it an extra layer of fidelity that allows us to extract additional information from the model not available in the traditional deterministic setting. Using both a numerical and an analytical approach, this thesis develops and demonstrates general methods for estimating the uncertainty in the model outputs and also a method for calculating when a system might admit a noise induced instability in an otherwise stable system. More specifically, the error bounds in the estimates of tumour size and survival time in the tumour growth model may be of future use to doctors treating patients, and the noise induced effects of the mitosis model helps us to understand further how metastasis arises out of a developing tumour.

Acknowledgements

A profound thank you to all those who were very patient with me during the completion of this thesis.

Dedication

This thesis is dedicated to my parents, who helped me see this through to the end.

Contents

List of Figures

Chapter 1

Introduction and Background Material

1.1 What is Cancer?

Cancer is a group of diseases where mutated cells (cancer cells) form an abnormal mass of tissue (a tumour) that grows aggressively, eventually forms its own vascular networks (angiogenesis) and resists the normal cell kill (apoptosis) and repair mechanisms of the human body. In general, we say a tumour is malignant when it displays the potential to grow out of control, ability to invade into its surrounding tissue, and the capability to spread to a different organ in the body (metastasize)[1]. This last property, metastasis, is theorized to occur in several distinct stages that are a result of the first two features activating certain contextual signals within the tumour microenvironment, and has certain parallels to mitosis in a growing embryo[14]

Hanahan and Weinberg[2][3] have proposed several "hallmarks" that explain how cancer cells are able to sustain their aggressive growth and avoid the normal defence mechanisms of the human body. Of interest to us is the fact that such aggressive tendencies means that tumours growth in a haphazard and irregular manner. In particular, the vascular network inside a tumour is extremely chaotic and the blood vessels can vary greatly in size. This means that different parts of the tumour receive varying amounts of oxygen and nutrients leading to hypoxic regions where

the oxygen supply is low, or even necrotic regions where the tumour cells are already dead. This heterogeneity in the tumour microenvironment is the key new aspect that chapters 2 and 3 aims to model mathematically.

Metastasis, the ability for cancer cells to invade a different organ in the body, is a property that is theorized to arise as a result of certain signals expressed inside a growing tumour[14]. Once cancer cells receive this signal, it then undergoes what is sometimes referred to as the "invasion-metastasis" cascade where it gains the ability to leave the primary tumour site, invade into the blood stream, travel to a different organ, and then somehow entrench themselves in this new organ and develop a new separate tumour. The signal that activates this cascade is hypothesized by Weinberg[14] to be the same signal that is activated in certain parts of an embryo during embryogenesis because the same transcription factors that carry this signal have been found in both tumour cells and embryos. The mitosis model of chapter 4 describes how a signal propagates within an embryo, and lends itself perfectly for a possible adaptation into a model for this very first step in metastasis.

1.2 Outline

This thesis explores the three important aspects of a malignant tumour in 2 separate models. Chapters 2 and 3 explore a tumour growth model that describes local invasiveness and replicative potential. The mitosis model of chapter 4 is a starting point for what we hope is eventually model for metastasis.

This introductory chapter and the appendices will develop the theory needed to understand and develop the methods used in this thesis. In particular we will carefully define and explain what stochastic processes and stochastic differential equations are, what we mean by finding a solution, and how we would go about doing so. Then, we will explore how to incorporate diffusion (or more general spatial effects) into the model. One important distinction is the difference between extrinsic and intrinsic noise, and the different mathematical methods needed to describe

them.

In chapters 2 and 3 we will explore the effects of extrinsic and intrinsic noise on a tumour growth model. The original model is a reaction-diffusion type PDE model and variations on its basic premise have been explored extensively in the current literature (such as Murray[6] and Swanson: 2002[5], 2003[63][64], 2008[65]). The goal of this model is to estimate the visible tumour diameter, which is a way of determining when a tumour would be visible on a CT scan, and the survival time, which is defined as when the tumour becomes visible until patient death[5]. Adding noise to the model is one way to represent the inherent chaos and heterogeneity in the tumour microenvironment, and allows us to estimate the error bounds on these estimates of tumour size and survival time. These error bounds provide information on the uncertainty of the estimates and gives us a sense of how accurate they are. Moreover, the error bounds on tumour size could potentially be used to help surgeons determine how much extra area around a tumour should be removed during surgery for example, and the error bounds on survival time gives us another way to consider how different situations and therapies affect how long the patient would live.

The mitosis model describes an embryo sending out a mitosis signal from its centre outwards towards the edges, and it is a multi species reaction-diffusion type model that supports a traveling wave solution (the mitotic signal) under certain conditions[31]. In the context of mitosis, noise in this model could also represent heterogeneity within the embryo but it is more useful to think of noise in this context as the natural randomness of chemical reactions that need to happen in order for the traveling wave to occur. Chemical reaction noise is more substantial when the population number is small[18][40] (such as in the initial formation of a tumour) and we will see in that an appropriate amount of noise can induce a traveling wave in this model even when its deterministic counterpart would be stuck in its stable steady state (known as “Stochastic Coherence” or “Stochastic Resonance”[29]). Such noise induced instabilities means that the parameter range under which the system can support a signal is broadened, and thus possibly more likely to occur

than expected.

1.3 Stochastic Processes

A stochastic process is a system that evolves in time (or space) according to some underlying probability distribution. A stochastic differential equation is a differential equation with random coefficients and whose solutions must necessarily be a stochastic process. This section will explain and give the necessary and analogous definitions for limits, continuity, differentiability etc needed in order to understand what it means to solve a stochastic differential equation.

Einstein's study of Brownian motion, the random movement of pollen grains suspend in water, is probably the key historical example from a physics point of view. He took a probabilistic approach that is analogous to a random walk, and the resultant equation for the probability density laid the foundation for what we now call a master equation. (Smoluchowski also took this same approach independently of Einstein.) Langevin, on the other hand, took a more direct approach by adding a random forcing term to the deterministic ODEs (i.e. using Newton's 2nd Law of Motion), and differential equations of this type are now commonly referred to as the Langevin equation, or more generally a stochastic differential equation (SDE, SODE (ordinary), or SPDE (partial)). We will find that Brownian motion is in fact *not differentiable*, which means the Langevin equation is not actually a valid equation until we define what we mean by its solution.

1.3.1 What is noise?

Following earlier works by van Kampen[18], we will very broadly classify noise as either ***intrinsic*** or ***extrinsic***. The two types of noise ostensibly require slightly different mathematical treatment, the first requires a master equation while the second is usually modeled using a Langevin equation, but there is often overlap both theoretically and mathematically between the two types of noise. In general, for this thesis, when we say intrinsic or extrinsic we are referring to how the noise will be treated mathematically.

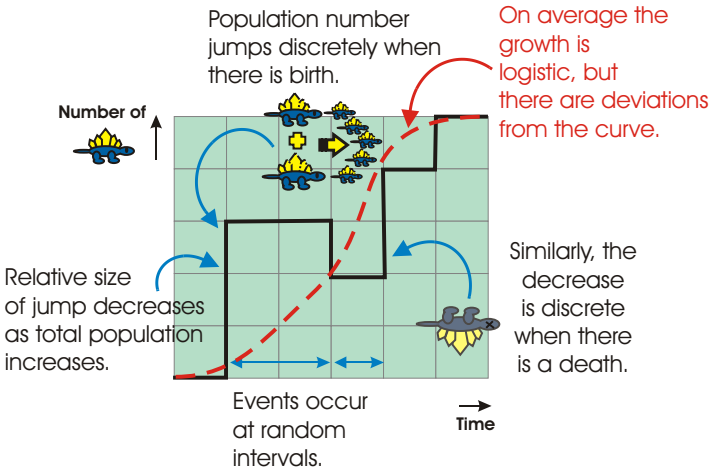

Figure 1.1: A schematic of intrinsic noise in logistic growth.

Consider population growth, when a birth occurs, the population must increase by an integer increment (1, 2 (twins), 3 (triplets), etc), and similarly with death. That means population growth is fundamentally a ***discrete*** process. Moreover, births and deaths do not occur at regular intervals, they occur at ***random*** times and we cannot predict when they will occur with absolute certainty. In contrast, the solution to the logistic growth equation is smooth; it assumes that population changes are infinitesimally small and occur infinitely often. Thus, the ODE formulation of logistic growth is at best an approximation (albeit a good one when the population is large). In fact, the ODE describes the ***average*** behaviour over a large number of realizations; by that we mean if we had many identical experiments that satisfied the conditions of logistic growth (e.g. bacteria in a petri dish) then, although each experiment will give results that have discrete jumps at different times, taking the average of all the experiments at each time would give us back

the logistic growth curve. These ideas are illustrated in figure 1.1. We will call these deviations away from the deterministic or macroscopic equation due to discrete number effects and inherent randomness ***intrinsic*** or ***internal noise***.

Extrinsic or ***external noise*** is noise that can (in principle) be switched off and can be meaningfully separated from the system dynamics. For example, in logistic growth of say rabbits, the food supply and environmental conditions could be affected by random factors such as inclement weather, then the carrying capacity of the system would no longer be constant, but a random function of time. Or, in the case of an electric circuit, one might have a fluctuating voltage source which affects the output of the system. For Brownian motion, one might consider the random collisions from the smaller water molecules to be external noise (because they are all contained in the random forcing term of the equation for Langevin's approach) but physically it doesn't make sense since you can't really turn off the water molecules. However, if the pollen particle is large enough then the collisions from the smaller water molecules would be negligible, and in that sense we can turn off the noise in our equations.

One must keep in mind that this stochastic approach is only an approximation. If we had a super computer that could compute a system of simultaneous equations for each and every molecule in the experiment (on the order of Avogadro's number) then we would be able to treat Brownian motion (or any similar system) as deterministic. Thus, what we call noise is actually just a reflection of our own ignorance of the system - it is a way for us to make the problem manageable and actually gleam useful results.

1.4 Definitions

What follows are some standard definitions for stochastic processes. These definitions will mostly follow a mix of Yaglom[73], Gardiner[54], and van Kampen[18][22], but similar definitions can be found in Gillespie's book[41], and Lemons[55]. The goal of this chapter is to define and understand what we mean by a stochastic differential equation. In this section the

stochastic process will be a function of one variable only (time), some standard knowledge of random variables and rules of probability will be assumed.

Let $\tilde{\omega}$ be a random variable with a given set of possible outcomes (the phase space). A **stochastic process**

$$\xi_t = \xi_t(\tilde{\omega}) \tag{1.1}$$

is a **random function** that depends on both $\tilde{\omega}$ and t. In particular, there are two ways to interpret such a function:

- If we fix $\tilde{\omega}$ then ξ_t is a function of time, and each ξ_t corresponding to a particular (given) $\tilde{\omega}$ is called a *realization* or *sample path* of the stochastic process. This is essentially what happens when we perform numerical simulations of a stochastic differential equation (more on this later).

- If we fix $t = t_0$ then ξ_{t_0} is a random variable with parameter t_0 and ξ_{t_0} can be interpreted as a family of random variables over all possible $\tilde{\omega}$. In our case t is time, so we usually have $t \in [0, T]$ where T is some fixed number, or $t \in \Re$.

Since ξ_t is a random function, it must follow some probability distribution. We denote the probability distribution function as

$$F(x;t) = P\left\{\xi_t \leq x\right\}, \tag{1.2}$$

and the corresponding probability density by

$$f(x;t) = \frac{\partial F(x;t)}{\partial x}. \tag{1.3}$$

The usual definitions for joint probabilities follows, for example

$$F(x_1, x_2; t_1, t_2) = P\left\{\xi_{t_1} \leq x_1, \xi_{t_2} \leq x_2\right\} \tag{1.4}$$

is the probability distribution function for $\boldsymbol{\xi}_{t_1,t_2} = (\xi_{t_1}, \xi_{t_2})$. In order to completely specify a stochastic process this distribution function must satisfy the usual rules of ordinary statistics ($f(x;t) \geq 0$ and $\int f(x;t)dx = 1$) and also a *symmetry condition* and a *compatibility condition* (see Yaglom[73] equations 1.4 and 1.5).

There are two special kinds of stochastic processes that we are interested in:

- An n-dimensional stochastic process $\boldsymbol{\xi}_t$ is called **stationary** if it remains the same when each t_i in is shifted along the time axis by the same amount:

$$F(x_1, x_2, ..., x_n; t_1 + \tau, t_2 + \tau, ..., t_n + \tau) = F(x_1, x_2, ..., x_n; t_1, t_2, ..., t_n). \tag{1.5}$$

- Assuming $t_1 < t_2 < ... < t_n$, a **Markov Process** is one where the conditional probability only depends on the most recent condition:

$$f(x_n; t_n | x_1, ..., x_{n-1}; t_1, ..., t_{n-1}) = f(x_n; t_n | x_{n-1}; t_{n-1}). \tag{1.6}$$

  Such processes are called "without memory" and it is easy to build up joint probabilities using conditional probabilities and the product rule (or Bayes' Theorem).

For this thesis, we will always assume the Markov property, but in general, solutions to a stochastic differential equation are not necessarily stationary.

The **mean** (or 1st moment, or expected value) of a stochastic process is

$$\mu(t) = \langle \xi_t \rangle = \int_{-\infty}^{\infty} x f(x;t) dx. \tag{1.7}$$

If ξ_t is stationary then $\mu(t) = m$ a constant (i.e. does not depend on t). Next, the **correlation**

function (or 2nd moment) is given by

$$B(t_1, t_2) = \langle \xi_{t_1} \xi_{t_2} \rangle = \int_{-\infty}^{\infty} \int_{-\infty}^{\infty} x_1 x_2 f(x_1, x_2; t_1, t_2) dx_1 dx_2. \tag{1.8}$$

In this case, if ξ_t is stationary then $B(t_1, t_2) = B(t_2 - t_1)$, a function of the time difference only. Moreover, if there is a τ_c such that $B(\tau) \approx 0$ for $\tau > \tau_c$, then we call τ_c the **correlation time** of the stochastic process. If $\mu(t) = m$ and $B(t_1, t_2) = B(t_2 - t_1)$ we say the stochastic process is **wide-sense stationary**. In general this is a relaxed definition of stationarity, but Yaglom[73] claims that in practice one rarely encounters a situation where a stochastic process is wide-sense stationary but not stationary. Related to the correlation is the variance (or 2nd cumulant)

$$\langle\langle \xi_{t_1} \xi_{t_2} \rangle\rangle = \langle \{\xi_{t_1} - \mu(t_1)\}\{\xi_{t_2} - \mu(t_2)\} \rangle = B(t_1, t_2) - \mu(t_1)\mu(t_2). \tag{1.9}$$

Higher order moments and cumulants can be defined analogously. We are usually only interested in the mean and variance of the solution to a stochastic differential equation since those are quantities we can physically measure in an experiment.

We say a stochastic process is **mean-square continuous** if the limit

$$\lim_{h \to 0} \left\langle (\xi_{t+h} - \xi_t)^2 \right\rangle = 0 \tag{1.10}$$

exists for all t. Alternatively, this is equivalent to saying that the correlation function $B(t_1, t_2)$ is continuous at the point $t_1 = t_2 = t$ for all t. One can show that, for a wide-sense stationary process, this is the same as requiring that $B(\tau)$ is continuous at $\tau = 0$ (i.e. if it is continuous at $\tau = 0$ then it is continuous everywhere)[73].

Similarly, we say a stochastic process is **mean-square differentiable** if there exists a random

variable ξ_t' such that the limit

$$\lim_{h\to 0}\left\langle\left(\frac{\xi_{t+h}-\xi_t}{h}-\xi_t'\right)^2\right\rangle = 0 \tag{1.11}$$

exists for all t. Again, in terms of the correlation function, this is equivalent to saying $B(t_1, t_2)$ is differentiable (in the ordinary vector calculus sense) at the point $t_1 = t_2 = t$ for all t.

In general a stochastic differential equation (SDE) is given by

$$\frac{du}{dt} = A(u, t; \tilde{\omega}) \tag{1.12}$$

where u and A may possibly be vectors with multiple components. In a deterministic setting, a unique solution is determined by specifying an initial condition $u(t_0) = u_0$ at some initial time t_0, and varying u_0 over the phase space will give you *all* possible solutions regardless of the choice of t_0, in other words, a different initial condition at a different time t_1 must give a solution that falls under the previous possibilities, but for a SDE the situation is different as you get a different solution space for *each* t_0[22]. This is because the initial condition $u(t_0, \tilde{\omega}) = u_0$ must be a sure variable (i.e. the probability of observing $u = u_0$ is exactly equal to 1 at $t = t_0$), and hence the variance at $t = t_0$ must be exactly zero, thus the variance changes as a function of t_0.

A **Langevin equation** is a special case of a SDE and has the form

$$\frac{du}{dt} = A(u) + C(u)\eta(t), \tag{1.13}$$

where $\eta(t)$ is a random function, but A and C are ordinary deterministic functions. This equation is named after Paul Langevin who first studied Brownian motion using an equation of this form in 1908[45]. In practice, one normally arrives at a Langevin equation by simply taking the original deterministic dynamics and adding a random function as a forcing term with $C(u)$ set equal to a constant (hence the name additive noise). Since the noise is simply attached to the end of the

deterministic dynamics, this is also what we referred to earlier as **extrinsic noise**.

1.4.1 Example: White Noise and Weiner Processes

White noise, denoted $\eta(t)$, is defined by giving its mean and correlation:

$$\langle \eta(t) \rangle = 0, \quad \langle \eta(t_1)\eta(t_2) \rangle = \delta(t_1 - t_2). \tag{1.14}$$

It is a wide-sense stationary process with zero correlation time. It is called white noise because its Fourier spectrum is a flat line[54]. The Weiner process is integrated white noise, and is defined by the stochastic differential equation

$$\frac{dW}{dt} = \eta(t), \tag{1.15}$$

with initial condition $W(t_0) = w_0$. The Weiner process is also called Brownian motion because it is possible to show that Einstein's considerations lead to the same equation[54]. We can show, using ordinary calculus, that the mean of a Weiner process is constant by multiplying each side by the probability density $f(x;t)$ and integrating so that we have

$$\frac{d\langle W \rangle}{dt} = \frac{d}{dt}\left(\int_{-\infty}^{\infty} W(t) f(x;t) dx \right) = \int_{-\infty}^{\infty} \eta(t) f(x;t) dx = \langle \eta(t) \rangle = 0. \tag{1.16}$$

Applying the initial condition, this means that $\langle W \rangle = w_0$ for all time. With a bit of work, one can also show in a similar manner[54] that the correlation function is given by

$$\langle W(t_1)W(t_2) \rangle = min(t_1 - t_0, t_2 - t_0) + w_0^2. \tag{1.17}$$

Thus the Weiner process is not differentiable (see Doob[46] for further discussion). However, we can solve this conundrum in two ways. The first way is to require that the correlation time be small but non-zero (i.e. not a delta function), then it can be shown that the process is differ-

entiable and ordinary calculus applies (Stratonovich[51] and van Kampen[52] has more detailed explanations). Since any real noise source would not actually be white, this is an acceptable resolution, and one must keep in mind that white noise should only be treated as an idealization of the physical situation. If we insist on using white noise, then we need to look at the integral form of the equation.

A stochastic process is **mean-square integrable** on $[0,t]$ if and only if there exists a random variable, denoted by $\xi^{(-1)}(t)$ or $\int_0^t \xi(u)du$ such that the limit

$$\lim_{\epsilon\to 0}\left\langle \left(\epsilon\sum_{i=1}^{t/\epsilon}\xi(i\epsilon)-\int_0^t \xi(u)du\right)^2\right\rangle = 0, \tag{1.18}$$

exists, where ϵ is a sequence of values chosen so that t/ϵ are integers.

Suppose $\eta(t)$ is white noise, if we integrate the Langevin equation

$$\int \frac{du}{dt}dt = \int A(u)dt + \int C(u)\eta(t)dt, \tag{1.19}$$

the first two integrals are well defined under ordinary calculus but the last one is not. One often uses the differential form of the Wiener process to write $dW(t)=\eta(t)dt$ so that the last integral can be written as $\int C(u(t))dW(t)$. The question here is: since $u(t)$ is a random function, which value of $u(t)$ should we use in the Riemann sum? Suppose we partition the interval $[0,t]$ into n subintervals $0<t_1<...<t_n$. The **Itô stochastic integral** (developed by Kiyoshi Itô in the 1940s[49][50]) is given by the limit of the Riemann sum

$$\int_0^t C(u(t'))dW(t') = \lim_{n\to\infty}\left\{\sum_i C(u(t_{i-1}))[W(t_i)-W(t_{i-1})]\right\}, \tag{1.20}$$

where the limit is taken in the mean-square sense as defined earlier, with u taken at the left end point of the intervals. As an alternative to the Itô integral, the **Stratonovich integral** (named

after Ruslan Stratonovich, who published his version in 1966[51]), takes the midpoint

$$\int_0^t C(u(t'))dW(t') = \lim_{n\to\infty}\left\{\sum_i C\left(\frac{u(t_i)-u(t_{i-1})}{2}\right)[W(t_i)-W(t_{i-1})]\right\}, \tag{1.21}$$

where again the limit is taken in the mean-square sense. Without going any further into the details, the Itô integral is well defined when the noise is strictly white, whereas the Stratonovich integral works when the correlation time is non-zero. More details can be found in Gardiner[54] and van Kampen[18]. Thus the integrated form of the Langevin equation

$$u(t) - u(0) = \int_0^t A(u)dt + \int_0^t C(u)\eta(t)dt, \tag{1.22}$$

is well defined even when the noise is white, and a solution to the SDE exists in this integrated sense, provided an interpretation rule is supplied for how the stochastic integral is treated[52].

For a stochastic PDE one can imagine analogous vector calculus definitions to the definitions for stochastic differentiation and integration mentioned in this chapter. However, most researchers usually appeal to much more complicated set and measure theory methods[75][76][77] that are difficult to understand. Fortunately, chapter 2 of this thesis deals with a variation of the stochastic heat equation and the existence and uniqueness of solutions to that problem have been studied extensively[35][58]. We will be interested in finding the mean and the variance of the solution to the stochastic PDE of interest.

Appendix A explains how to numerically integrate a stochastic PDE using a standard Euler method[35]. Most simulation methods for stochastic PDEs adopt Itô's interpretation, and we do the same when considering extrinsic noise. Moreover, recall each realization we generate is equivalent to fixing $\tilde{\omega}$ at each time t. Thus, by generating many sample paths, we are in fact generating a sample distribution for $\tilde{\omega}$ at each t, and taking the mean and variance at each time point will give us an estimate of the mean and variance of the stochastic process as a function of time.

1.5 Master Equation

Instead of a SDE, an alternate way of studying stochastic processes is to use what is called the master equation. This involves assuming that the stochastic process is Markov, then manipulating the rules of probability to arrive at a differential equation that governs the time evolution of the probability density[18]. The master equation itself is usually not solvable directly, so numerical and approximation methods are often needed. Appendix B explains how to numerically simulate exact realizations of processes governed by a particular master equation (known as Gillespie's Algorithm[40]), and the next section explains an approximation method developed by van Kampen[19].

From the product rule of probability we have that

$$f(x_1, x_2; t_1, t_2) = f(x_2; t_2|x_1; t_1)f(x_1; t_1), \tag{1.23}$$

and integration over x_1 of this equation gives

$$f(x_2; t_2) = \int_{-\infty}^{\infty} f(x_2; t_2|x_1; t_1)f(x_1; t_1)dx_1. \tag{1.24}$$

If we further assume the process is Markov, for $t_1 < t_2 < t_3$, we can show that

$$f(x_1, x_2, x_3; t_1, t_2, t_3) = f(x_3; t_3|x_2; t_2) \cdot f(x_2; t_2|x_1; t_1) \cdot f(x_1; t_1). \tag{1.25}$$

If we integrate the above over x_2 then

$$f(x_1, x_3; t_1, t_3) = f(x_1; t_1) \int_{-\infty}^{\infty} f(x_3; t_3|x_2; t_2)f(x_2; t_2|x_1; t_1)dx_2, \tag{1.26}$$

and using the product rule again $f(x_1, x_3; t_1, t_3) = f(x_3; t_3|x_1; t_1)f(x_1; t_1)$, we have

$$f(x_3; t_3|x_1; t_1) = \int_{-\infty}^{\infty} f(x_3; t_3|x_2; t_2)f(x_2; t_2|x_1; t_1)dx_2. \tag{1.27}$$

This is the **Chapman-Kolmogorov equation** and it relates all the **transition probabilities** $f(x_i; t_i|x_j; t_j)$ as one integral equation. For a stationary Markov process, we can write

$$f(x_2; t_2|x_1; t_1) = p(x_2|x_1; \tau), \tag{1.28}$$

where $\tau = t_2 - t_1$. Then the Chapman-Kolmogorov equation can be written as

$$p(x_3|x_1; \tau' + \tau) = \int_{-\infty}^{\infty} p(x_3|x_2; \tau')p(x_2|x_1; \tau)dx_2, \tag{1.29}$$

where $\tau' = t_3 - t_2$.

For a large class of systems known as jump processes (examples of which are Brownian motion and chemical reactions), one can show that, over a very short time, the transition probability is given by[53]

$$p(x|z, \tau') = (1 - a_0\tau')\delta(x - z) + \tau' w(x|z) + o(\tau') \tag{1.30}$$

where $w(x|z)$ is the transition probability per unit time, and a_0 is the zeroth jump moment

$$a_0(z) = \int_{-\infty}^{\infty} w(x|z)dx. \tag{1.31}$$

In words, the above equation for $p(x|z)$ means that the transition probability from state z to state x is given by the probability that no jump occurs (i.e. you are already in state x) + the probability that a jump occurs over a time interval τ'. Substituting this result into the Chapman-Kolmogorov equation yields (after some work)

$$\frac{\partial}{\partial\tau}p(x_3|x_1; \tau) = \int_{-\infty}^{\infty} \left[w(x_3|x_2)p(x_2|x_1; \tau) - w(x_2|x_3)p(x_3|x_1; \tau)\right] dx_2. \tag{1.32}$$

This is called the **Master Equation** and it has the form of a gain-loss type differential equation with the probability of entering into state x_3 (given you were at x_1) minus the probability of leaving state x_3 (given you were in state x_3 already). If the system is discrete, this equation takes on the form

$$\frac{dP_n(t)}{dt} = \sum_m \left[W_{nm}P_m(t) - W_{mn}P_n(t)\right]. \tag{1.33}$$

1.5.1 Example: Logistic Growth

Consider logistic growth, a one species model of tumour cells given by

$$\frac{dc}{dt} = f(c) = rc\left(1 - \frac{c}{K}\right), \tag{1.34}$$

where c is the tumour cell *density*, r is the growth rate, and K is the carrying capacity. Rewritten in terms of the *number* of tumour cells C, we must introduce a new parameter Ω, that has dimensions of volume, so that we have:

$$\frac{dC}{dt} = rC\left(1 - \frac{C}{\Omega K}\right). \tag{1.35}$$

In order to consider the effects of intrinsic noise, we will explicitly include the discreteness of births and deaths by recasting logistic growth in terms of the following reaction scheme

$$C \xrightarrow{\nu_1} C + 1, \quad \nu_1 = r \cdot \frac{C}{\Omega}, \tag{1.36}$$

$$C \xrightarrow{\nu_2} C - 1, \quad \nu_2 = \frac{r}{K}\frac{(C)(C-1)}{\Omega^2}, \tag{1.37}$$

where ν_i can be identified with the reaction rates in equation 1.34 but are now to be interpreted as the transition rates W in the master equation (known as the principle of mass action, see Appendix E), and we have assumed that only unit births and deaths can occur at any time.

A convenient way to rewrite this reaction scheme is in terms of the stoichiometry matrix $\mathbf{S}$,

which tells us how each reaction changes the population, and the propensity vector $\boldsymbol{\nu}$ which is a list of the transition rates. For our example, we have

$$\mathbf{S} = \begin{pmatrix} 1 & -1 \end{pmatrix}, \quad \text{and} \quad \boldsymbol{\nu} = \left(r \cdot \frac{C}{\Omega}, \frac{r}{K} \left(\frac{C}{\Omega} \right) \left(\frac{(C)(C-1)}{\Omega^2} \right) \right)^T, \tag{1.38}$$

specifically written in this way so that in the thermodynamic limit where $C \to \infty$ and $\Omega \to \infty$ in such a way that $C/\Omega \to c$ a constant, we can approximate $\nu_2 = \frac{r}{K}\frac{(C)(C-1)}{\Omega^2}$ by $\nu_2 = \frac{r}{K}\frac{C^2}{\Omega^2}$ and recover the deterministic equations

$$\frac{dc}{dt} = \mathbf{S} \cdot \boldsymbol{\nu} = f(c). \tag{1.39}$$

The convenience of this notion will become apparent when we consider the Linear Noise Approximation in the next section.

Using the discrete form of the master equation (equation 1.33), and the transition rates as identified above, we can now write down the master equation for logistic growth as a stochastic process:

$$\begin{aligned} \frac{dP}{dt} &= r(C-1)P(C-1) + \frac{1}{\Omega}\frac{r(C+1)^2}{K}P(C+1) - rCP(C) - \frac{rC^2}{\Omega K}P(C), \\ &= r\left(\mathbf{E}^{-1} - 1\right)CP + \frac{1}{\Omega}\frac{r}{K}\left(\mathbf{E} - 1\right)C^2P. \end{aligned} \tag{1.40}$$

where E_i^k is the step operator given by

$$\mathbf{E}_i^k f(..., n_i, ...) = f(..., n_i + k, ...), \tag{1.41}$$

and is another convenient piece of notation that will reappear shortly. Notice that this is a discrete-differential equation with non-linear transition rates and there is no known solution method. So we will need to appeal to numerical simulations using the Gillespie algorithm (shown in figure 1.2) and approximation methods.

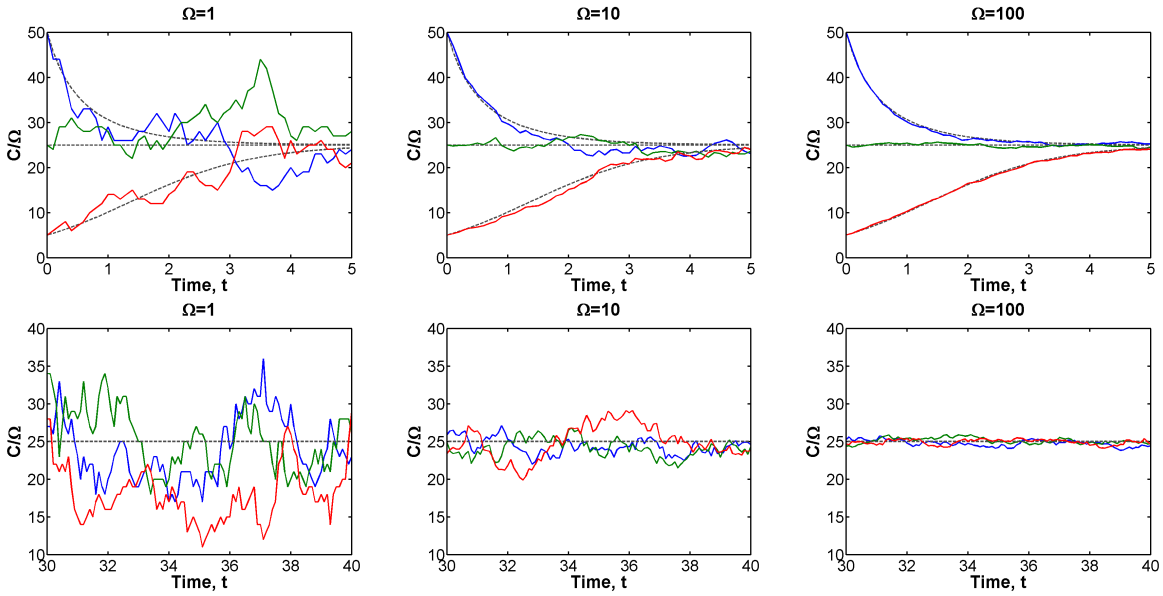

Figure 1.2: Some simulations of logistic growth as a stochastic process using Gillespie's algorithm (coloured solid lines; explained in Appendix B), with $r = 1$, $K = 25$, $\Omega = 1, 10, 100$, and started at three different initial conditions. Dashed grey lines are numerical simulations of deterministic logistic growth with the same initial conditions. Top row shows t=[0,5] as the system relaxes to equilibrium and bottom row shows t=[30,40] as the system fluctuates about the equilibrium. As discussed in the text, the ODE model represents the average of the stochastic model over a large number of realizations. Plots shown have concentration $c = C/\Omega$ as the y axis and time as the x axis. Thus, in terms of cell number, we have approximately, from left to right, 25, 250, and 2500 total cells in the system. Note how as we increase the number of cells, the relative magnitude of the fluctuations decreases as $1/\sqrt{N}$ and we approach the deterministic model. This scaling will reappear in the next section.

One might also try solving for the moments instead by multiplying the master equation by the appropriate power of C and taking the sum over all values, but the equations for the first two moments yield

$$\frac{d\langle C\rangle}{dt} = r\langle C\rangle - \frac{1}{\Omega}\frac{r}{K}\langle C^2\rangle, \tag{1.42}$$

$$\frac{d\langle C^2\rangle}{dt} = r\langle C\rangle + 2r\langle C^2\rangle + \frac{1}{\Omega}\frac{r}{K}\langle C^2\rangle - \frac{1}{\Omega}\frac{r}{K}\langle C^3\rangle, \tag{1.43}$$

which are not closed (i.e., involve higher-moments) and cannot be solved explicitly. Thus, even for the moment equations we will require an approximation method to close the system.

1.5.2 System Size Expansion of the Master Equation

The master equation in general is a discrete-differential equation that we cannot solve exactly. Hence we will need to develop methods to find approximate solutions to the master equation. The method we will discuss was developed by van Kampen and is known as the Linear Noise Approximation, or perhaps more suggestively, the system size expansion[19]. For clarity, we will apply the approximation to the reaction part first, then discuss the effect of transport on the fluctuations in the next section.

For this general overview of the expansion method, we will specialize our discussion to chemical reaction networks. Chemical reactions are an example of intrinsic noise - reactions occur because of random collisions between the reactant molecules and deviations away from the deterministic model arise because the events are discrete and occur randomly[62].

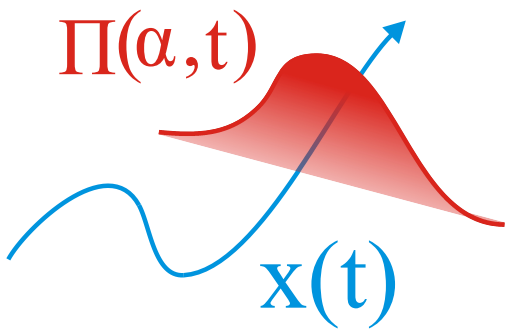

Figure 1.3: Idea: There is an envelope of fluctuations about the deterministic trajectory of the concentration and the variance of these fluctuations scales as $\frac{1}{\Omega}$.

Suppose that there are N species of reactant molecules, and let $\mathbf{n}$ denote the *number* of molecules of each species. Let Ω be a measure of the system size or volume. We will assume that we can separate the fluctuations $\boldsymbol{\alpha}$ from a deterministic evolution of the reactant concentrations $\mathbf{x}$ in the following manner:

$$n_i = \Omega x_i + \sqrt{\Omega}\alpha_i. \tag{1.44}$$

This square-root scaling of the fluctuations is motivated by Poisson processes, where the relative size of the fluctuations is inversely proportional to the square-root of the number of molecules (which we saw heuristically in figure 1.2), and leads to a consistent perturbation expansion when

there is only one globally stable steady state in the corresponding deterministic equations. Written more suggestively in terms of concentrations,

$$\frac{n_i}{\Omega} = x_i + \frac{1}{\sqrt{\Omega}}\alpha_i.$$

We will assume that the second term on the right hand side, which governs the fluctuations, will be small as $\Omega \to \infty$ compared to the first term, in such a way so that the term on the left hand side stays constant even though it appears to depend on a higher power of Ω. This is known as the ***thermodynamic limit***.

For discrete chemical reaction networks, we can write the master equation in this form[34]

$$\frac{dP(\mathbf{n},t)}{dt} = \Omega \sum_{j=i}^{R} \left[\left(\prod_{i=1}^{N} \mathbf{E}_i^{-S_{ij}} \right) - 1 \right] \nu_j \left(\frac{\mathbf{n}}{\Omega} \right) P(\mathbf{n},t). \tag{1.45}$$

where $\mathbf{S}$, $\boldsymbol{\nu}$ and $\mathbf{E}_i^k$ are the stoichiometry, propensity, and step operator as defined in chapter 1.

The next step is to then expand the step operator and transition probabilities as a series in powers of $\frac{1}{\sqrt{\Omega}}$. Substituting these series into the master equation and equating terms of the same order, we get that, at the zeroth order, the concentration must obey the deterministic dynamics

$$\frac{dx_i}{dt} = \left[\mathbf{S} \cdot \boldsymbol{\nu}(\mathbf{x})\right]_i = f_i(\mathbf{x}). \tag{1.46}$$

At the next order, we get a linear Fokker-Planck equation for the probability distribution of $\boldsymbol{\alpha}$:

$$\frac{\partial \Pi}{\partial t} = -\sum_{i,j} J_{ij} \frac{\partial \left(\alpha_j \Pi\right)}{\partial \alpha_i} + \frac{1}{2} \sum_{i,j} D_{ij} \frac{\partial^2 \Pi}{\partial \alpha_i \partial \alpha_j}, \tag{1.47}$$

where $\mathbf{J}$ is the Jacobian matrix of the linearized dynamics

$$J_{ij}(t) = \left. \frac{\partial f}{\partial x_j} \right|_{\mathbf{x}(t)}, \tag{1.48}$$

and D is the diffusion matrix given by

$$\mathbf{D} = \mathbf{S} \cdot \text{diag}[\nu] \cdot \mathbf{S}^T. \tag{1.49}$$

This Fokker-Planck equation can then be used to calculate the moments of α, and hence N. One can show that the solution to the linear Fokker-Planck equation, equation (1.47), is a (time-dependent) multi-variate Gaussian, so to this level of approximation, all we need to know are the first and second moments to completely specify the distribution, which can be found by multiplying equation (1.47) with α_i or $\alpha_i\alpha_j$ and integrating by parts to give:

$$\frac{d}{dt}\langle\alpha_i\rangle = \sum_j J_{ij}\langle\alpha_j\rangle, \tag{1.50}$$

$$\frac{d}{dt}\langle\alpha_i\alpha_j\rangle = \sum_k J_{ik}\langle\alpha_k\alpha_j\rangle + \sum_k J_{kj}\langle\alpha_i\alpha_k\rangle + D_{ij}. \tag{1.51}$$

In particular, using our ansatz $\mathbf{n} = \Omega\mathbf{x} + \sqrt{\Omega}\boldsymbol{\alpha}$ and the initial condition $P(\mathbf{n}, 0) = \delta_{\mathbf{n},\mathbf{n_0}}$, which implies $\langle\boldsymbol{\alpha}(0)\rangle = \mathbf{0}$, we have that

$$\frac{d}{dt}\langle\mathbf{n}(t)\rangle = \mathbf{f}(\langle\mathbf{n}(t)\rangle). \tag{1.52}$$

As a consequence, to the lowest order approximation, the average of the stochastic model obeys the deterministic rate equations, and this equation can be interpreted as the macroscopic equation that governs the system in the limit of no fluctuations.

1.5.3 Back to Logistic growth

Recall, when we considered the stochastic version of logistic growth we were unable to solve for the first and second moments because the system of equations were not closed (see equations 1.42 and 1.43). We now apply the linear noise approximation to close the system of equations and get approximate solutions for the mean and variance.

Recall for logistic growth we have that

$$\frac{dx}{dt} = f(x) = rx\left(1 - \frac{x}{K}\right), \tag{1.53}$$

where we have replaced the density of tumour cells $c = C/\Omega$ with the concentration x as required by equation 1.46 above. Hence the Jacobian is given by

$$J = \frac{df(x)}{dx} = r - \frac{2rx}{K}. \tag{1.54}$$

The stoichiometry and propensity are given by

$$\mathbf{S} = \begin{pmatrix} 1 & -1 \end{pmatrix}, \quad \text{and} \quad \boldsymbol{\nu} = \left(rx, \frac{rx^2}{K}\right)^T, \tag{1.55}$$

where again we have replaced c with x. Note that, as before, the second term in the propensity should be $\nu_2 = \frac{r}{K}\frac{(C)(C-1)}{\Omega^2}$, but in the thermodynamic limit as $\Omega \to \infty$ and $C \to \infty$, we can make the approximation $\nu_2 = \frac{r}{K}\frac{(C)(C-1)}{\Omega^2} \approx \frac{r}{K}\frac{C^2}{\Omega^2} = \frac{rx^2}{K}$. Using equation 1.49, this means that the diffusion matrix D is

$$D = \begin{pmatrix} 1 & -1 \end{pmatrix} \begin{pmatrix} rx & 0 \\ 0 & \frac{rx^2}{K} \end{pmatrix} \begin{pmatrix} 1 \\ -1 \end{pmatrix} = rx + \frac{rx^2}{K}. \tag{1.56}$$

Then, using equations 1.50 and 1.51, and a bit of algebra, we get for the first moment

$$\frac{d\langle C\rangle}{dt} = r\langle C\rangle\left(1 - \frac{\langle C\rangle}{\Omega K}\right). \tag{1.57}$$

For the variance, which is defined as $\langle\langle C^2\rangle\rangle = \langle C^2\rangle - \langle C\rangle^2$, note that in the simple one species

case, we have

$$\begin{aligned}\langle\langle C^2\rangle\rangle &= \langle C^2\rangle - \langle C\rangle^2, \\ &= \langle \Omega^2 x^2 + 2\Omega^{\frac{3}{2}} x\alpha + \Omega\alpha^2\rangle - \Omega^2 x^2, \\ &= \Omega^2 x^2 + 2\Omega^{\frac{3}{2}} x\cancelto{0}{\langle\alpha\rangle} + \Omega\langle\alpha^2\rangle - \Omega^2 x^2, \\ &= \Omega\langle\alpha^2\rangle. \end{aligned} \tag{1.58}$$

This yields

$$\frac{d\langle\langle C^2\rangle\rangle}{dt} = \Omega\frac{d\langle\alpha^2\rangle}{dt} = 2\left(r - \frac{2r\langle C\rangle}{\Omega K}\right)\langle\langle C^2\rangle\rangle + r\langle C\rangle + \frac{r\langle C\rangle^2}{\Omega K}. \tag{1.59}$$

These estimates of the mean and variance, can now be solved explicitly by first solving for the mean and then substituting the result into the variance. They are plotted, along with some stochastic simulations using the Gillespie algorithm, in figure 1.4.

1.5.4 Limitations of the Linear Noise Approximation

Although van Kampen's Linear Noise Approximation works well for chemical reactions and provides a general recipe for approximating the probability distribution of the fluctuations in a stochastic system with internal noise, it is important to understand the assumptions that limit the usefulness of this expansion method.

1. The Linear Noise Approximation gives us a leading-order correction to the macroscopic behaviour, but the ansatz, equation 1.44 and the perturbation expansion requires that the magnitude of the fluctuations is small compared to the deterministic solution.

2. The Gaussian nature of the noise is a consequence of truncating the expansion after the first two terms and is no longer true once higher order terms are included[61].

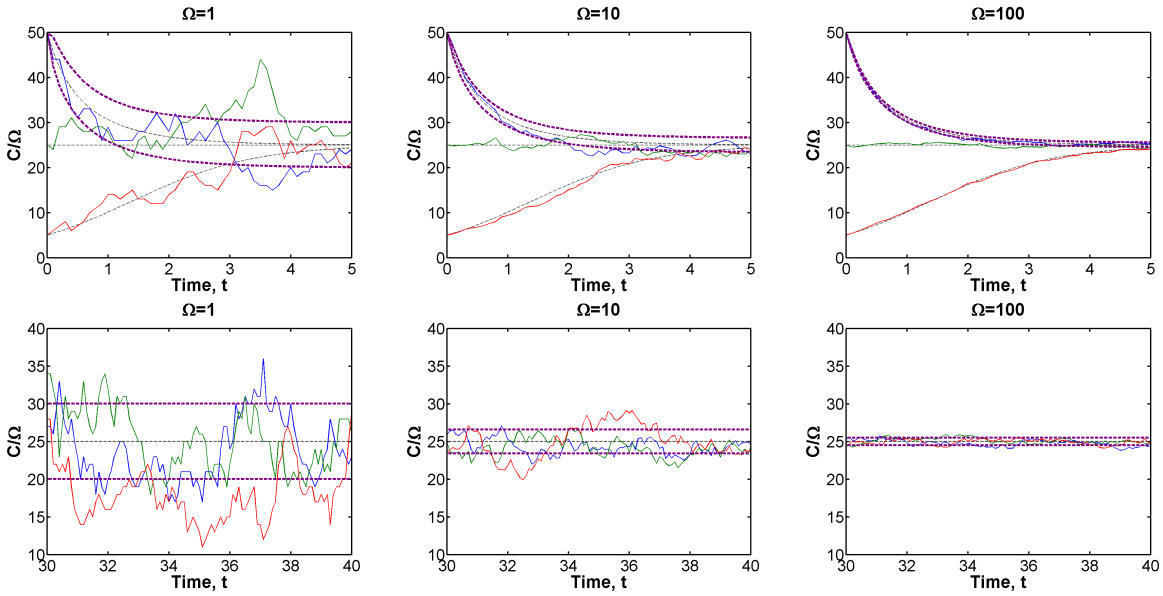

Figure 1.4: Same plots as figure 1.2 but now with the estimate of the variance added using the linear noise approximation. Specifically, the mean was plotted by using equation 1.57, and the fluctuation envelope was calculated by evolving equation 1.59 and then plotting $\langle c \rangle \pm \sqrt{\langle\langle c^2 \rangle\rangle}$. Note how the variance envelope initially grows with time then settles into equilibrium along with the deterministic system.

3. The Linear Noise Approximation is a local expansion about a deterministically stable trajectory. The criterion that the trajectory is stable ensures ensures that the fluctuations remain sub-dominant to the deterministic behaviour. To see this, consider for simplicity the one species versions of equations 1.57 and 1.59:

$$\frac{d\langle \alpha \rangle}{dt} = J\langle \alpha \rangle, \tag{1.60}$$

$$\frac{d\langle \alpha^2 \rangle}{dt} = 2J\langle \alpha^2 \rangle + D. \tag{1.61}$$

The first equation tells us that α obeys the ***linearization*** of the deterministic dynamics and hence its applicability is strictly local. The second equation gives us the magnitude of the fluctuations, and demonstrates that there is an interplay between the Jacobian and the diffusion. If the system is stable, then the Jacobian is negative (more generally it has eigenvalues with negative real parts) and that ensures that the fluctuations do not grow

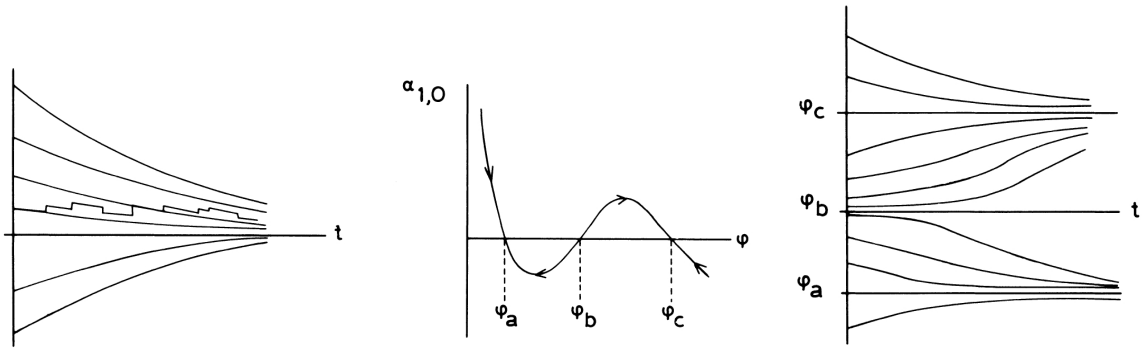

(a) If there is only one globally stable steady state, then all solutions tend towards this steady state, and the effect of fluctuations is to make the stochastic trajectory jump from one solution to another, which nonetheless have to converge.

(b) Suppose we have a bistable system with two stable steady states and one unstable one.

(c) Then, solutions must converge towards ϕ_A or ϕ_C and there is a non-zero probability of switching between the two.

Figure 1.5: The linear noise approximation is a local approximation method. Figures from van Kampen[18]

unbounded, specifically, it ensures that they do not grow to the same order of magnitude as the macroscopic part in finite time[18].

If there are multiple stable steady states, then the approximation is valid only for trajectories close to a particular steady state as there will be a non-zero probability that one may jump from the basin of attraction of one steady state to another. This jump probability cannot be calculated by the Linear Noise Approximation and other methods are needed[18]. This last point emphasizes the fact that the Linear Noise Approximation is a local expansion about the stable steady state and does not tell us any global properties of the system. A heuristic picture of this need for a single stable fixed point is given in figure 1.5.

1.6 Spatially Extended Stochastic Systems

Here we will be interested in converting a reaction-diffusion equation into a stochastic process through the master equation. The previous section demonstrated how to deal with the reaction

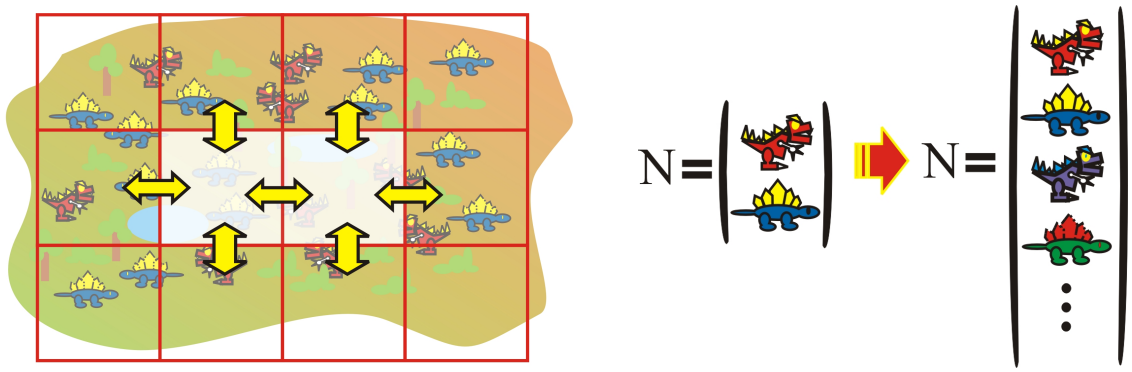

(a) Idea: We discretize space and consider diffusion as a reaction that moves the reactant molecule from one bin into another.

(b) This means that we can consider each species in each bin to be different species, and extend all our previous work appropriately.

Figure 1.6: Extending reaction stoichiometry to include transport.

part. In order to turn diffusion into a stochastic process we will adapt Smoluchowski's analysis of Brownian motion, where he considered Brownian motion as a random walk[47] (since Smoluchowski's original 1906 paper[48] is in German, reference is an English explanation by Kac in 1947).

If we discretize our coordinate space into bins, diffusion (or any kind of transport in general) is simply a process that moves one member of the population from one bin to another. In other words, we can consider it as a reaction that decreases by one the number of a particular reactant species in one bin and increases by one the number of the same reactant species in another.

With this simple bit of insight, it is straightforward to modify the Gillespie algorithm to include diffusion. We simply consider each species in each bin to be different species, and then extend the stoichiometry and propensity appropriately to include diffusion as a reaction (a picture of this situation is provided in figure 1.6). Details on how to extend Gillespie's Algorithm is explained in Appendix B.

From an analytic standpoint, let us label each bin with the Greek index λ. We will denote each reactant species in each cell by $\mathbf{N}^{\lambda}$. A pictorial representation is presented in figure 1.7. To consider the contribution due to diffusion, we will first let our grid spacing $\rightarrow 0$ so that we can

(a) We will discretize coordinate space into bins of equal volume and denote them by the set λ. Since reaction is just another kind of reaction, the spatial orientation doesn't matter as long as we take it into account appropriately in our stoichiometry.

(b) The reactant species in each bin are labeled $\mathbf{N}^{\lambda}$,

Figure 1.7

switch to a continuous description in the following way:

$$\lim_{\Omega \to 0} \frac{\mathbf{N}^{\lambda}(t)}{\Omega} = \mathbf{n}(\mathbf{r},t). \tag{1.62}$$

where r is the position of the center of the bin λ, and n is the number density.

Next, van Kampen[18] has shown that the contribution of diffusion to the first moment is simply

$$\frac{\partial \langle \mathbf{n}(\mathbf{r},t) \rangle}{\partial t} = \mathbf{D}\nabla^2 \langle \mathbf{n}(\mathbf{r},t) \rangle . \tag{1.63}$$

So the combined effect of both reaction and diffusion is

$$\frac{\partial \langle \mathbf{n}(\mathbf{r},t) \rangle}{\partial t} = \mathbf{f}(\langle \mathbf{n}(\mathbf{r},t) \rangle) + \mathbf{D}\nabla^2 \langle \mathbf{n}(\mathbf{r},t) \rangle , \tag{1.64}$$

which we once again identify as the deterministic or macroscopic equation.

For the second moment, we have this complicated equation which involves the Dirac delta

function[20]

$$\frac{\partial}{\partial t}\left\langle\langle n_i(\mathbf{r_1},t)n_j(\mathbf{r_2},t)\rangle\right\rangle = D\left(\nabla_1^2+\nabla_2^2\right)\left\langle\langle n_i(\mathbf{r_1},t)n_j(\mathbf{r_2},t)\rangle\right\rangle + 2D\nabla_1\cdot\nabla_2\left\{\delta(\mathbf{r_1}-\mathbf{r_2})\left\langle n_i(\mathbf{r},t)\right\rangle\right\}, \tag{1.65}$$

which is not amenable to analysis or numerical simulation. However, if we define the factorial cumulant as

$$[n_i(\mathbf{r_1},t)n_j(\mathbf{r_2},t)] = \left\langle\langle n_i(\mathbf{r_1},t)n_j(\mathbf{r_2},t)\rangle\right\rangle - \delta(\mathbf{r_1}-\mathbf{r_2})\left\langle n_i(\mathbf{r_1},t)\right\rangle, \tag{1.66}$$

then the evolution for this quantity is given by

$$\frac{\partial}{\partial t}[n_i(\mathbf{r_1},t)n_j(\mathbf{r_2},t)] = D\left(\nabla_1^2+\nabla_2^2\right)[n_i(\mathbf{r_1},t)n_j(\mathbf{r_2},t)], \tag{1.67}$$

which is much simpler. To recover the variance, we simply add back the correct term when necessary using the solution for the first moment.

1.6.1 Example: Fisher's equation

We will discuss Fisher's equation in more detail in the next section on excitable media. For the purposes of this section it is simply logistic growth with diffusion added:

$$\frac{\partial c}{\partial t} = \underbrace{rc\left(1-\frac{c}{K}\right)}_{\text{Logistic Growth}} + \underbrace{D\nabla^2 c}_{\text{Diffusion}}. \tag{1.68}$$

With the preceding results, one can show that the stochastic version of Fisher's equation with intrinsic noise has mean which obeys

$$\frac{\partial\langle c(\mathbf{r},t)\rangle}{\partial t} = r\langle c(\mathbf{r},t)\rangle\left(1-\frac{\langle c(\mathbf{r},t)\rangle}{K}\right) + D\nabla^2\left\langle c(\mathbf{r},t)\right\rangle, \tag{1.69}$$

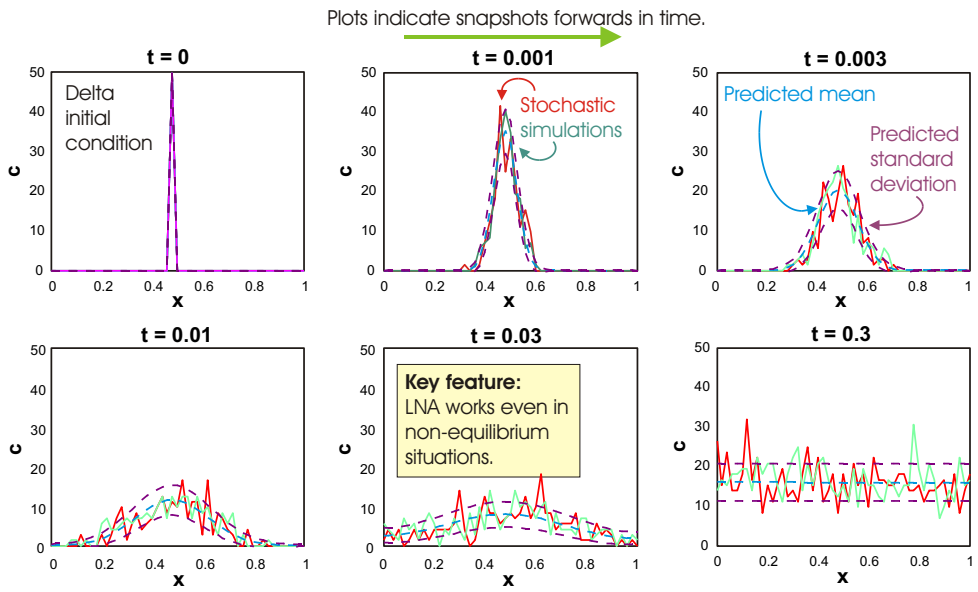

Figure 1.8: A plot of some numerical simulations of Fisher's equation as a stochastic process with the same parameters and boundary conditions as figure 1.12 in chapter 2. The solid lines are two independent numerical simulations using Gillespie's algorithm. The dashed lines are the approximate mean and variance as given by equations 1.69 and 3.1 respectively.

and factorial cumulant,

$$\begin{aligned}\frac{\partial\left[c(\mathbf{r_1},t)c(\mathbf{r_2},t)\right]}{\partial t} &= \left\{\left(r-\frac{2r\langle c(\mathbf{r_1},t)\rangle}{K}\right)+\left(r-\frac{2r\langle c(\mathbf{r_2},t)\rangle}{K}\right)\right\}\left[c(\mathbf{r_1},t)c(\mathbf{r_2},t)\right]\\ &+\delta(\mathbf{r_1}-\mathbf{r_2})\left\{r\langle c(\mathbf{r_1},t)\rangle+\frac{r\langle c(\mathbf{r_1},t)\rangle^2}{K}-r\langle c(\mathbf{r_1},t)\rangle\left(1-\frac{\langle c(\mathbf{r_1},t)\rangle}{K}\right)\right\}\\ &+2\delta(\mathbf{r_1}-\mathbf{r_2})\left(r-\frac{2r\langle c(\mathbf{r_1},t)\rangle}{K}\right)\langle c(\mathbf{r_1},t)\rangle\\ &+D\left\{\nabla_1^2+\nabla_2^2\right\}\left[c(\mathbf{r_1},t)c(\mathbf{r_2},t)\right]. \qquad (1.70)\end{aligned}$$

Numerical simulations of these results and some corresponding stochastic simulations are shown in figure 1.8. The plots show how Fisher's equation evolves with time, and demonstrate how the Linear Noise Approximation accurately captures the variance of the system when internal noise is added to the system. In particular, the variance envelope predicted by the Linear Noise Approximation varies in both space and time and only settles into a steady state as the system itself settles into a steady state.

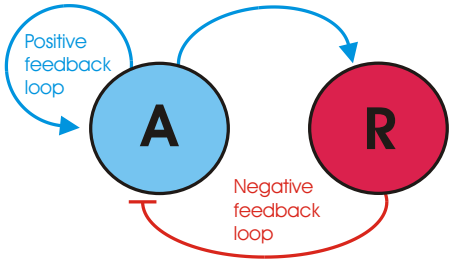

Figure 1.9: The activator A activates itself and activates its repressor R at the same time. This leads to both a positive and a negative feedback loop on A. Most excitable systems have feedback behaviour hierarchy similar to this, and in figure 1.10 the positive feedback acts on a faster timescale than the negative feedback.

1.7 Excitable Media

In very general terms, excitable systems usually involve feedback loops that act on different time scales, such as in the schematic in figure 1.9, that lead to limit cycle behaviour as depicted in figure 1.10 which involves a very quick rise to the excited state, and then a slow relaxation back to the lower equilibrium state. The most famous example of a spatially homogeneous excitable system is perhaps the Hodgkin-Huxley model (1952)[8] and the simplified version developed by Fitzhugh (1961)[9] and Nagumo (1962)[10] to describe the action potential in neurons.

The "all or nothing" principle of excitable media makes it a very useful model for cell signalling (such as for cell cycles[30]) as there is clear differentiation between an "on" or "off" state. Moreover, when diffusion is added to the system, excitable systems differ from simple oscillatory ones by exhibiting spatial inhomogeneities such as patterning or traveling waves[7]. We will examine Fisher's equation[26] and the Vilar model[13] as relevant examples that will display this kind of behaviour. Then, we will see how adding noise to the model can cause an otherwise stable system to exhibit (continued) oscillatory behaviour. In chapter 4 we will look at how noise affects an excitable mitosis model that we hope can be adapted to model metastasis in the future.

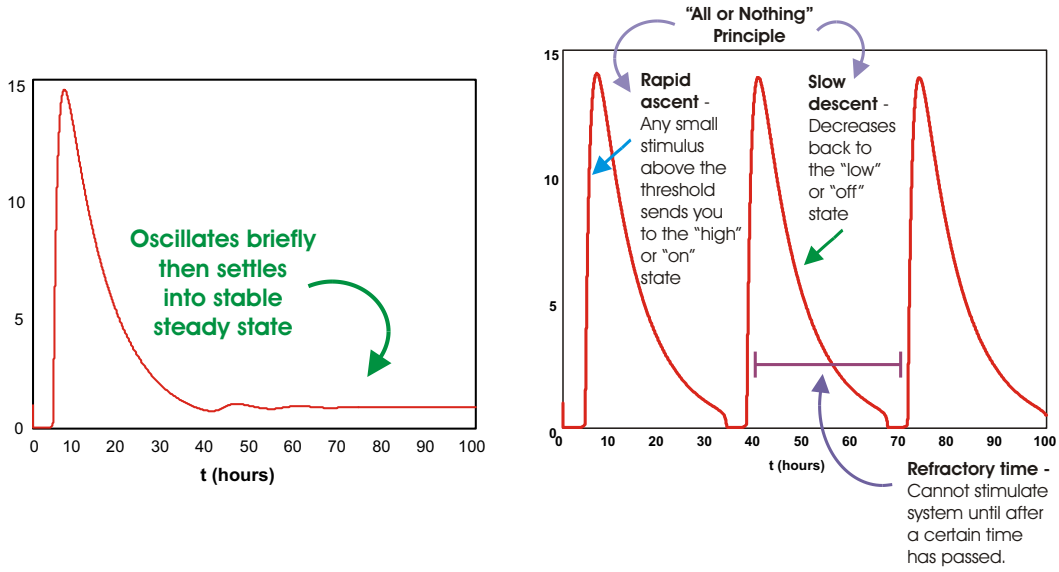

(a) Stable

(b) Limit Cycle

Figure 1.10: In general, excitable systems exhibit either asymptotic stability or limit cycle behaviour in the absence of noise. Notice in b) that excitable systems have a very particular kind of limit cycle behaviour, and that is usually created by different time scales in the positive and negative feedback.

1.8 Example: Fisher's equation

If we add diffusion to logistic growth, we get what is known as Fisher's equation (or the Fisher-Kolmogorov equation):

$$\frac{\partial c}{\partial t} = \underbrace{rc\left(1 - \frac{c}{K}\right)}_{\text{Logistic Growth}} + \underbrace{D\nabla^2 c}_{\text{Diffusion}}. \tag{1.71}$$

Fisher[26] proposed this equation in his 1937 paper to describe the spread of a local mutation, that is somehow beneficial or advantageous to the population, from its initial mutation cite to its neighbours in the form of a wave. Quoting Fisher in his original paper[26]:

> "If at any point of the habitat a mutation occurs, which happens to be in some degree, however slight, advantageous to survival, in the totality of its effects, we may expect the mutant gene to increase at the expense of the allelomorph or allelomorphs previously occupying the same locus. This process will be first completed in the neighbourhood of occurrence of the mutation, and later, as the advantageous gene is diffused in the surrounding population, in the adjacent portions of its range."

Variations of this equation have been used to model tumour growth, which is just a different kind of mutation, and will be explored in detail in chapters 2 and 3 (see figure (1.11)).

Depending on the system size, parameters and boundary conditions, we will see qualitatively different behaviour. Following Powathil[23] and Murray[6], we will assume no flux boundary conditions throughout the rest of this report to model the effects of a solid boundary, such as the skull in brain tumours. In general, with no flux boundary conditions, we will simply see the system reach a spatially homogeneous steady state at the stable equilibrium of the logistic growth term (see figure 1.12). However, under certain situations, it is possible to observe a traveling wave, which is a wave that propagates without change of shape, until the wavefront hits the boundary (see figure 1.13). Traveling wave instabilities are an important aspect of this model

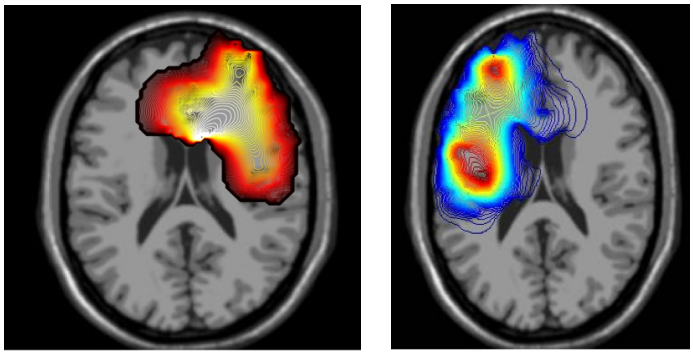

Figure 1.11: Application of Fisher's equation to brain tumours in two dimensions using a sample CT scan to simulate the situation in a real brain. Colours represent tumour cell density. Figures from Powathil[23]

as the higher concentration of the wave front can be used to represent a signal passing through the cell[30][32].

1.8.1 Role of Noise in Excitable Media

Fisher's equation is an example of a wider class of systems known as excitable systems. Greenberg and Hastings (1978)[7] provide the following description for excitable media:

> "In a spatially homogeneous environment an excitable media is characterized by a globally stable equilibrium state, and also by a threshold mechanism which produces a large amplitude response to a sufficiently large stimulus. This response is temporary, however, and the system soon returns to its equilibrium configuration."

Excitable systems exhibit either limit cycle behaviour or asymptotic stability depending on the parameter values. Near the bifurcation value, noise can induce limit cycle-like behaviour in an otherwise stable system by causing the system to undergo large trajectories in the phase space near where the limit cycle would be if we were past the bifurcation value. A heuristic argument is shown in figure 1.14. We will explore an example of a biological system that can be modeled by such a system in detail.

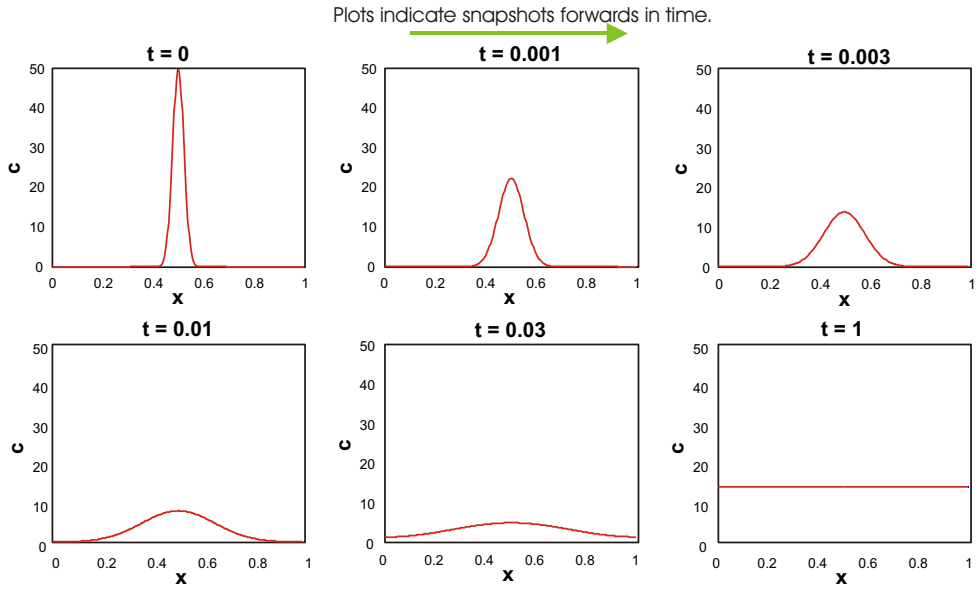

Figure 1.12: Simulation of Fisher's equation in one dimension with $r = 4$, $K = 15$, $D = 1$, and no flux boundaries at $x = 0$ and $x = 1$. The system simply diffuses then grows towards the stable steady state at $c = 15$. Notice that the equilibrium solution is uniform in space.

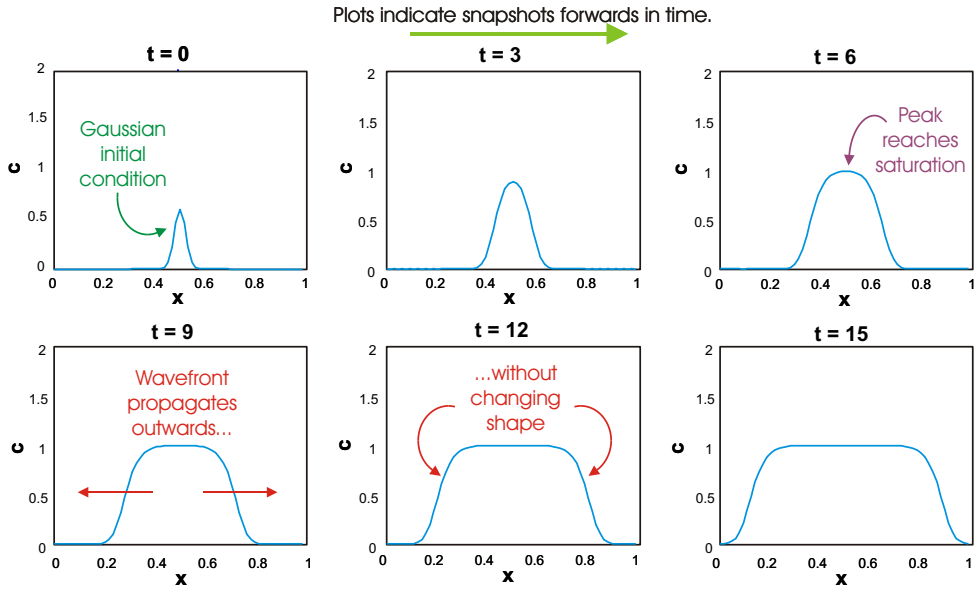

Figure 1.13: With $r = 1$, $K = 1$, $D = 1/5000$ it is now possible to observe a traveling wave. Notice how once the peak reaches the stable steady at $c = 1$, the shape of the slope no longer changes and simply travels outwards.

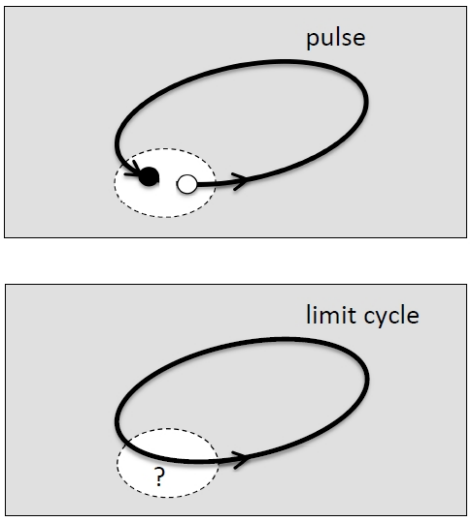

(a) Top panel: In the stable regime of the state space, all solutions eventually settle at the stable fixed point (the black dot). Noise in the system will perturb the system out of the steady state. These systems are called excitable because if the perturbation is large enough (outside the white circle) then the system is forced to undergo a large loop in the phase space. Bottom panel: the corresponding trajectory in the limit cycle regime, the idea being that the large excursion is similar to the limit cycle. Figure from Rué[33]

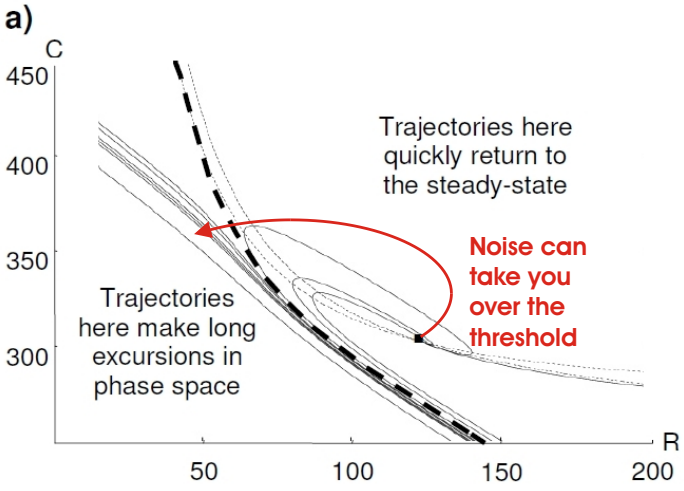

(b) Same idea, but specifically from the circadian clock example below. The dotted line represents the threshold which determines whether large excursions occur or not. This can be found numerically[12].

Figure 1.14: Heuristic idea behind excitability.

Example: Circadian Clock

The following is a model for circadian clocks or circadian rhythms first proposed by Vilar et al[13] based on "common positive and negative control elements found experimentally". Scott et al[12] studied the reduced model below, which is more amenable to analysis:

$$\frac{\partial A}{\partial t} = \gamma_A g\left(\frac{A}{K_A}, f_A\right) - \delta_A A - \kappa_C AR, \tag{1.72}$$

$$\frac{\partial R}{\partial t} = \gamma_R g\left(\frac{A}{K_R}, f_R\right) - \delta_R R - \kappa_C AR + \delta_A C, \tag{1.73}$$

$$\frac{\partial C}{\partial t} = \kappa_C AR - \delta_A C, \tag{1.74}$$

where

$$g\left(\frac{A}{K_A}, f\right) = \frac{\frac{1}{f} + \left(\frac{A}{K_A}\right)^n}{1 + \left(\frac{A}{K_A}\right)^n}. \tag{1.75}$$

Put in very simple terms, this model has an activator-repressor (A and R respectively in the mode equations) hierarchy that is similar to the schematic shown in figure 1.9. The only difference is that there is an intermediate complex C that mediates the negative feedback. For a nominal parameter set, the key control parameter is the ratio of the decay rates $\epsilon = \delta_R/\delta_A$, and in fact, the plots in figure 1.10 are plots of the repressor R when ϵ is low enough for the stable steady state to appear, and when ϵ is suitably high to exhibit a limit cycle.

When we consider the effect of intrinsic noise on this model, we once again need to introduce the parameter Ω that is a measure of the system size or volume. For small values of Ω, the relative effects of noise (i.e. fluctuations on the order of 1 or 2 molecules) are large because the number of reactants in the system is small, so the system is more easily perturbed into an excited state and can undergo a large oscillation. For large Ω, the relative effects of noise are small, so the system behaves tends to stay in its stable steady state, and the wait time between oscillations increases. Finally, for a medium amount of noise, we see regular, well behaved oscillations that are close in ampltiude and period to the system in its limit cycle regime. This

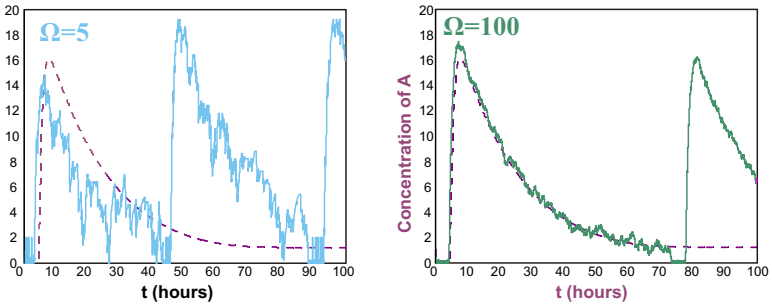

(a) High Noise

(b) Medium Noise

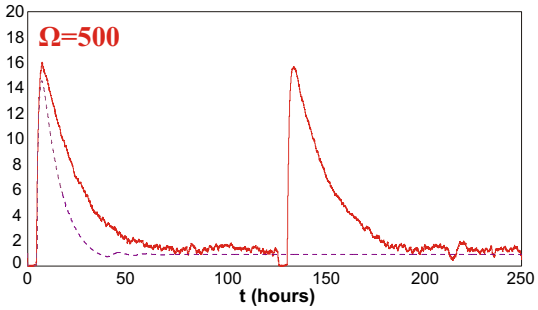

(c) Low Noise

Figure 1.15: All three figures are plots of the repressor R. The solid line represents a stochastic simulation, and the dashed line represents the corresponding deterministic behaviour for a parameter set that exhibits stability. In (a) one can see that, when there are a low number of molecules, noise leads to frequent oscillations and large variations in the amplitude of the oscillation. As we increase the number of molecules, we see in (b) that the amplitude and frequency of oscillation is more regular. As $\Omega \to \infty$ the system reaches the deterministic limit (i.e. a stable steady state), and the time between oscillations increases, as shown in (c). It has been shown that a medium amount of noise leads to, in some sense, the most regular amplitude and period and reproduces the limit cycle behaviour most closely - sometimes known as stochastic coherence[27][28].

particular tuning of noise to create sustained oscillations is sometimes called stochastic coherence or stochastic resonance[27][28], and there is speculation that some biological systems (such as neural signalling in human brains) have evolved to make use of such phenomena[29]. These effects are illustrated in figure 1.15.

If we now add back diffusion, and for the sake of simplicity assume that R and C diffuse at

the same rate, then we have

$$\frac{\partial A}{\partial t} = \gamma_A g\left(\frac{A}{K_A}, f_A\right) - \delta_A A - \kappa_C AR + D_1 \frac{\partial^2 A}{\partial x^2}, \tag{1.76}$$

$$\frac{\partial R}{\partial t} = \gamma_R g\left(\frac{A}{K_R}, f_R\right) - \delta_R R - \kappa_C AR + \delta_A C + D_2 \frac{\partial^2 R}{\partial x^2}, \tag{1.77}$$

$$\frac{\partial C}{\partial t} = \kappa_C AR - \delta_A C + D_2 \frac{\partial^2 C}{\partial x^2}. \tag{1.78}$$

A straightforward but lengthy linear stability analysis, assuming all parameters are fixed as before, except for $\epsilon = \delta_R/\delta_A$ which was the bifurcation parameter in the previous case, and $d = D_1/D_2$, which is the ratio of diffusion coefficients allows us to determine when we might expect each of the different types of behaviour to occur (see figure 1.16). In particular, we can now observe traveling waves (see figure 1.17), which we will use to represent cell signalling in chapter 4.

In analogy to the situation without noise, one would expect that noise added to this system in the stable parameter regime would be able to cause noise induced oscillations. An analysis of that situation will not be performed here. We will however, conduct a lengthy analysis of noise induced oscillations in an excitable mitosis model in chapter 4.

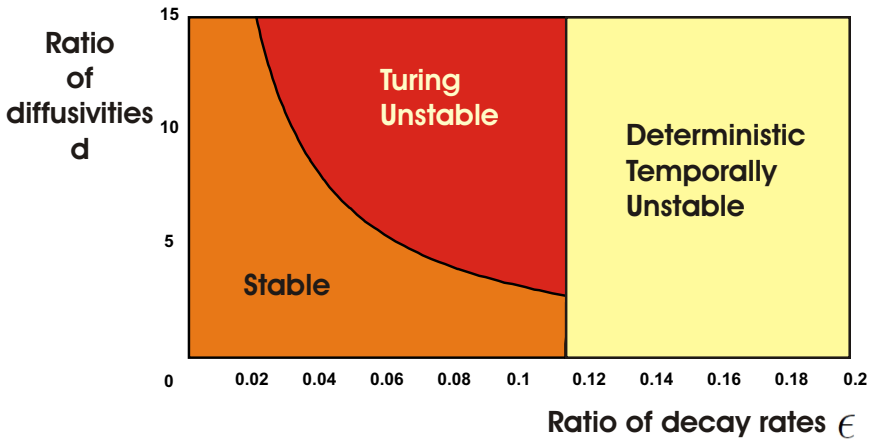

Figure 1.16: Bifurcation diagram obtained using linear stability analysis where $d = D_1/D_2$ and $\epsilon = \delta_R/\delta_A$. Turing instabilities are when the system is stable in the absence of diffusion, but unstable once diffusion is added. This leads to spatial patterns occurring (panel (c) in figure 1.17).

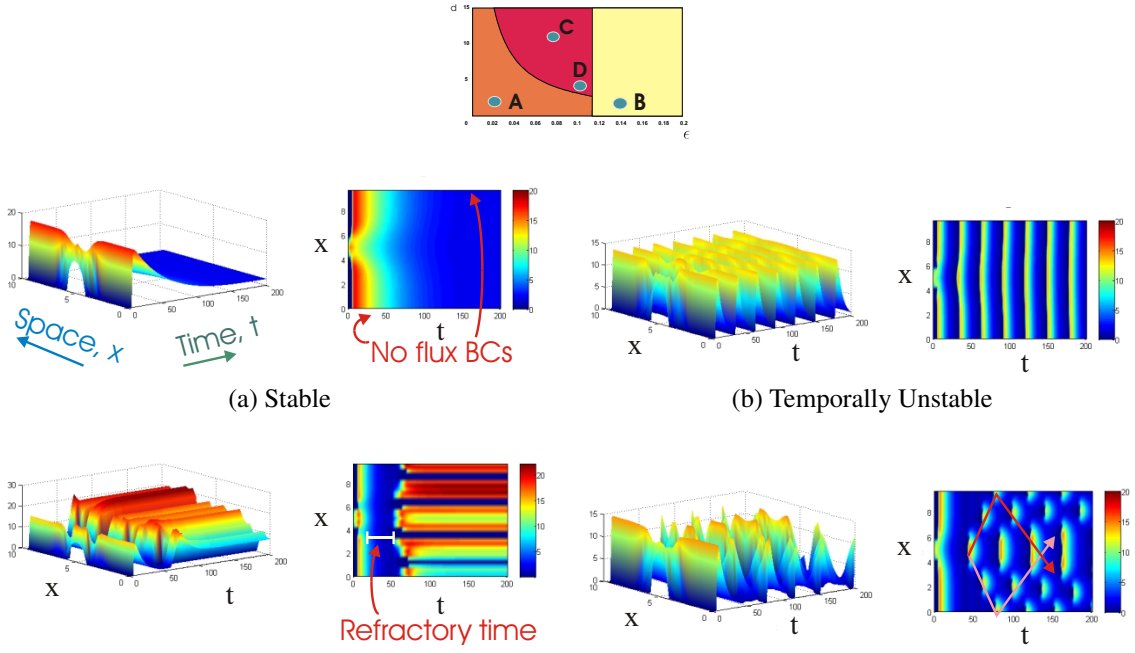

(a) Stable

(b) Temporally Unstable

(c) Spatially Unstable

(d) Traveling Wave

Figure 1.17: Different possibilities in the Vilar model when diffusion is is added.

Chapter 2

External Noise in a Tumour Model

Tracqui (1995)[4], Swanson (2002[5], 2003[63][64], 2008[65]) , Murray (2007)[6], Powathil (2007[68], 2009[23]), and Kohandel (2007)[69] (among others) have proposed deterministic reaction-diffusion type models to simulate the growth of brain tumours in humans. Although tumour cells do not actually diffuse, it has been suggested that diffusion reasonably approximates cell motility, and results using this model qualitatively agree with CT scans of brain tumours[4][6][23]. Once a model for tumour growth is chosen, it can then be used to estimate the survival time of a patient, which we will define as the growth of the tumour from a diameter of 3cm (when it is visible on a CT Scan) to 6cm (patient death).

This chapter will consider the effects of external noise on this system by adding a Langevin forcing term to the deterministic PDEs. The Langevin forcing term is one way to represent the chaotic structure and heterogeneity within the tumour microenvironment without having to know all the exact details of the structure for each and every patient by making the growth rate random in space and time. Analytic solutions to the stochastic PDE will not be attempted, instead, we will use extensive numerical simulations to generate sample paths of the system, and the resulting ensemble will be averaged at each time point to estimate the error bounds for the system. We will find that the error bounds are relatively small for the tumour model in this chapter, but it

does establish the method for possible future modifications.

2.1 Mathematical Details

In words, a single species tumour growth model would satisfy

rate of change of tumour cell population = motility of tumour cells+net proliferation of tumour cells,

with cell motility being represented by diffusion. For brain tumours, there are solid boundaries (e.g. the skull) which limits growth, so one might choose logistic growth for the proliferation term, which gives us Fisher's equation[26] as a starting point:

$$\frac{\partial n}{\partial t} = D\nabla^2 n + \rho n\left(1 - \frac{n}{K}\right).$$

Here, K is the carrying capacity or saturation limit for tumour cells within the brain. In practice, K is very large (Powathil estimates K to be about 10^5 cells/cm^2), so we are unlikely to reach the carrying capacity before patient death and the growth is essentially exponential. Thus our prototype for tumour growth is given by

$$\frac{\partial n}{\partial t} = D\nabla^2 n + \rho n, \tag{2.1}$$

where n is the concentration of tumour (cancer) cells, D is the diffusion coefficient, and ρ is the growth rate. This simple model in fact two thirds of what we think of as a malignant tumour, as it contains the potential to grow in an uncontrolled manner (the exponential growth term), and the ability to invade into its surrounding tissue (diffusion term). Metastasis will need to be modeled separately, and a proposed solution is in chapter 4. Although most tumours are a large collection of a number of different cells[2] (including possibly recruited normal cells[3]) one might think of the single species model as a simplification (cancer or normal) or as the growth of cancer stemcells[24][25] which would reproduce all the necessary differentiated cells.

There are many other possible choices for the growth term, and they have been used in the literature to model different situations. For example, it has been speculated as early as 1964 by Laird[70] that tumour growth is actually Gompertzian, Kohandel[69] uses a quadratic growth term to model vasculature, Anderson and Chaplain[71] add a chemotaxis term to mimic angiogenesis, Norris[72] use Michaelis-Menten Kinetics to model drug kintetics, and Powathil[68][23] adds a term to reprsent radiotherapy. Later on in this chapter we will modify the growth term slightly to reproduce the effects of chemotherapy.

It would be more realistic for the diffusion term to be space dependent, with $\nabla \cdot (D(x)\nabla n)$ instead of simply $D\nabla^2 n$, and indeed papers by Powathil[68] and Swanson's research group (e.g. Swanson (2003)[5], Rockne (2010)[66], Neal (2013)[67]) have different (constant) values for grey and white matter within the brain. A model of how the grey and white matter is distributed within the brain would be needed to take the different diffusibility into account, and most recently Neal et al (2013)[67] have taken comprehensive scans of each patient and tailored their mathematical models specifically for that patient. For this thesis we will simply we will keep the entire domain homogeneous and vary the diffusion constant D to determine its effects.

The aim of this chapter is to allow the growth rate to be random throughout the domain in the following way:

$$\frac{\partial n}{\partial t} = D\nabla^2 n + \rho\left[1 + \sigma(\mathbf{x}, t)\right] n, \tag{2.2}$$

where $\sigma(\mathbf{x}, t)$ is a random function of time and space, with no flux boundary conditions, and a gaussian or delta initial condition in the middle of the domain. This random growth rate represents the inherent heterogeneity within the chaotic tumour microenvironment without having to determine the exact details.

For simplicity, we will set $\sigma(\mathbf{x}, t) = \sigma\eta(\mathbf{x}, t)$, where σ is a constant in space and time. $\eta(\mathbf{x}, t)$ is commonly referred to as "space-time white noise"; it is Gaussian distributed, and can be

specified by giving the first two moments:

$$\langle \eta(\mathbf{x}, t) \rangle = 0, \tag{2.3}$$

$$\langle \eta(\mathbf{x}, t) \eta(\mathbf{x}', t') \rangle = \delta(\mathbf{x} - \mathbf{x}') \delta(t - t'). \tag{2.4}$$

The noise amplitude σ must be provided external to our current mathematical considerations (e.g. data fitting, physical considerations). This stochastic PDE was integrated numerically using a straightforward Euler scheme on a square 10cm by 10cm domain to very roughly represent the size of a human skull (see Appendices A and C for more details).

2.1.1 Visible Tumour Diameter and Survival Time

When a tumour is found in a patient, doctors rely on medical imaging devices to determine where the tumour is and what kind of treatment to apply. Any type of medical imaging technique will have a detection threshold under which tumour cells cannot be detected. According to Swanson[5] the CT Scan detection threshold is 8000 cells per mm^3. Illustrations of how this works can be found in figure 2.1.

To estimate the visible diameter of the tumour, we will count the number of grid boxes with density above the threshold value in our numerical simulations, multiply by the area of each grid box to get the total area, and use $A = \pi r^2$ to calculate the radius r, and hence visible tumour diameter (call it $V(t)$). This will only be an estimate since the stochastic simulation will not be a perfect circle (see figures 2.2 and 2.4). Following Swanson[5] we define survival time as the time it takes the tumour to grow from a (visible) diameter of 3 cm (the minimum size a tumour can be diagnosed) to a diameter of 6 cm.

For external noise, the most straight forward way of estimating the mean and variance of either measure of tumour diameter is to run a large number of numerical simulations and calculate the mean and variance of the ensemble. We will do this for different values of both σ (varying the

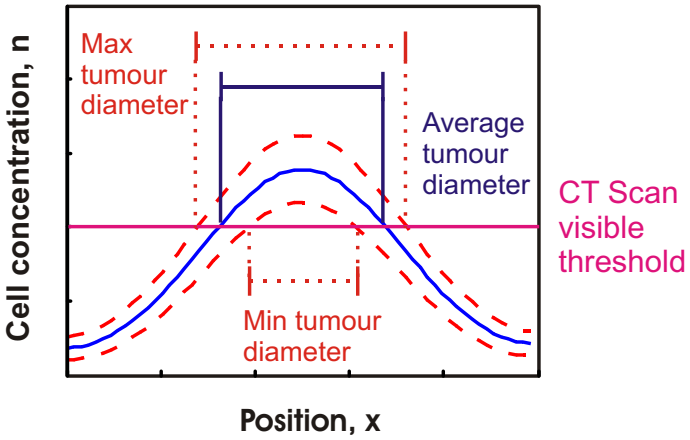

Figure 2.1: A one dimensional cross-section of the previous 2D model showing how the visible tumour diameter is calculated. Our goal is to calculate the dotted lines, which indicate mean +/- one standard deviation of the stochastic model. This will then give us the error bound on possible outcomes, and could be used to help estimate how large of an area treatment should be applied (e.g. radiation or surgery).

noise intensity) and D (varying the diffusivity of the tumour). Figures (2.1) and (2.3) illustrate how these calculated bounds can be put to use to estimate tumour diameter and survival time. Figures (2.5), (2.6), and (2.7) show actual numerical simulations of the model for $\sigma = 5$, and the error bounds estimated through repeated simulations.

2.2 Comparison between different values of σ

First, we will vary the noise strength σ. Although it makes sense for parts of the tumour microenvironment to have a negative growth rate, it shouldn't be excessively negative, so we will limit or choice of σ from 0.1 to 5. Figure (2.8) shows how changing σ affects the mean and standard deviation of the survival time. As one would expect, there is a more marked deviation from the deterministic model and a larger error when you increase the strength of the noise.

To quantify the effects of σ on the error, figure () is a plot of the standard deviation versus σ. This plot clearly demonstrates how the standard deviation increases as a function of σ, and that is verified by Pearson correlation coefficient[42][43] of 0.9995, indicating extermely strong posi-

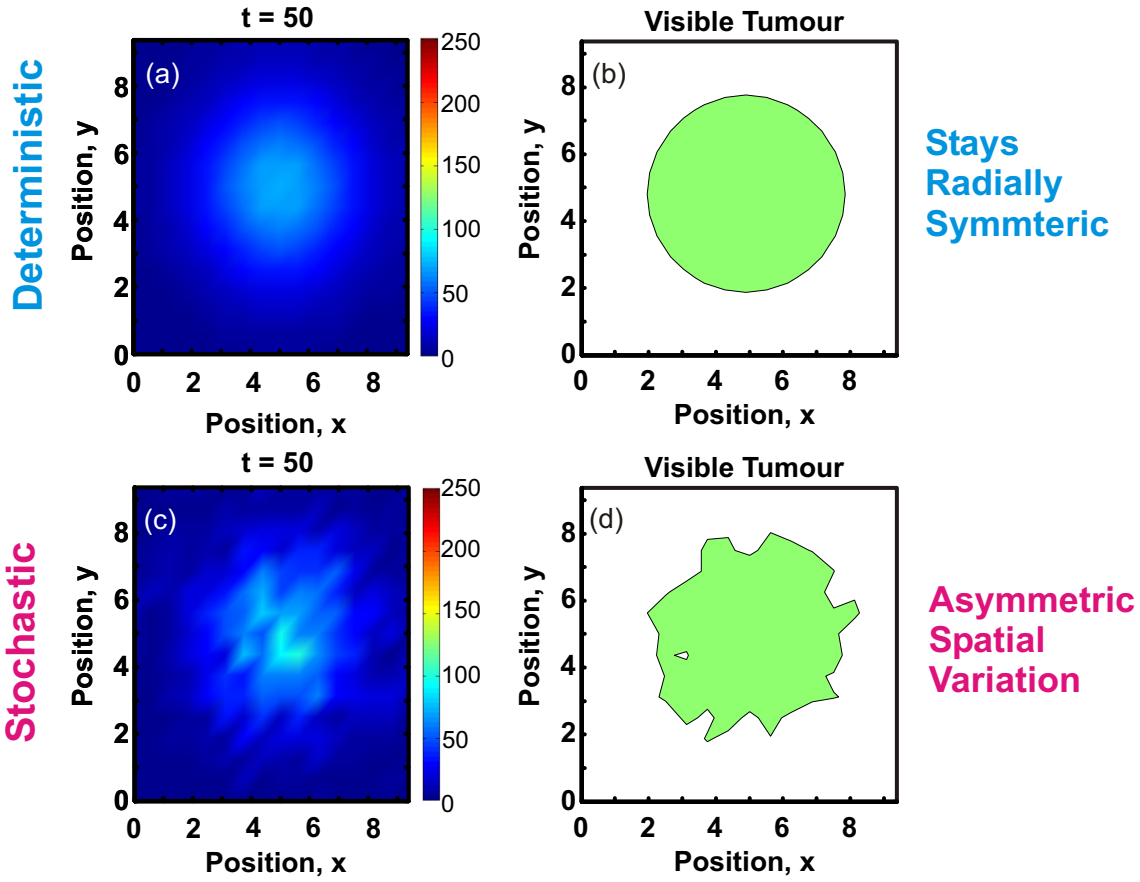

Figure 2.2: An illustration of the key difference between the deterministic and stochastic model. Given the same initial conditions, the deterministic model will always produce the same symmetrical pattern, but the stochastic model gives us a different asymmetrical solution each time.

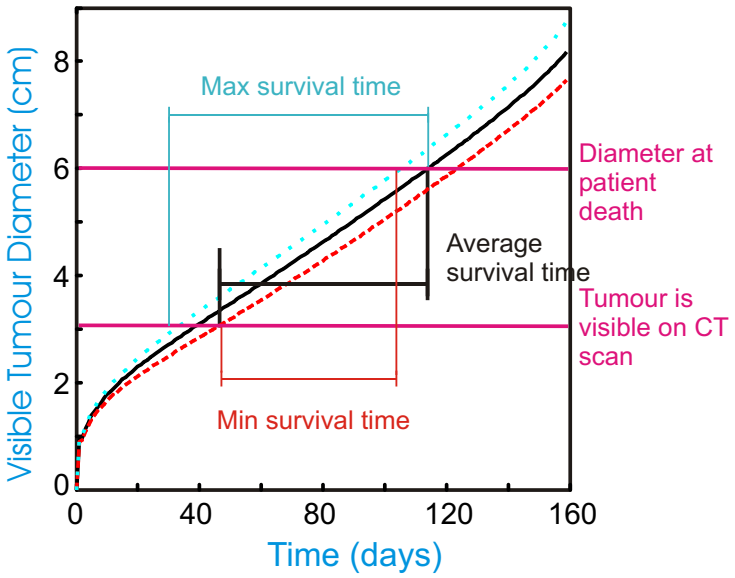

Figure 2.3: A schematic illustration of how we will estimate survival time. The goal is again to calculate the error bounds and give and estimate on the likely range of possible survival times.

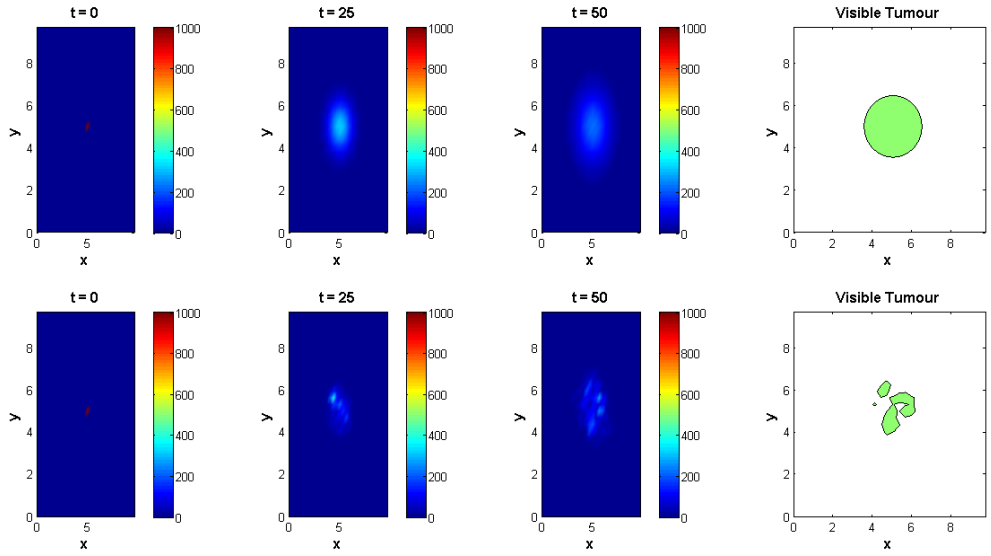

Figure 2.4: Comparison of the model with and without noise. Both sets of plots had $D = 5 \times 0.0013$ cm^2/day, $\rho = 0.012$/day (Swanson's parameter values for brain tumours) and $\sigma = 5$ in the bottom plots. The right most plot in each set shows a level set of the simulation and represents what a CT scan might see. Note the more realistic asymmetrical growth of the stochastic model compared to the always perfectly circular deterministic simulation.

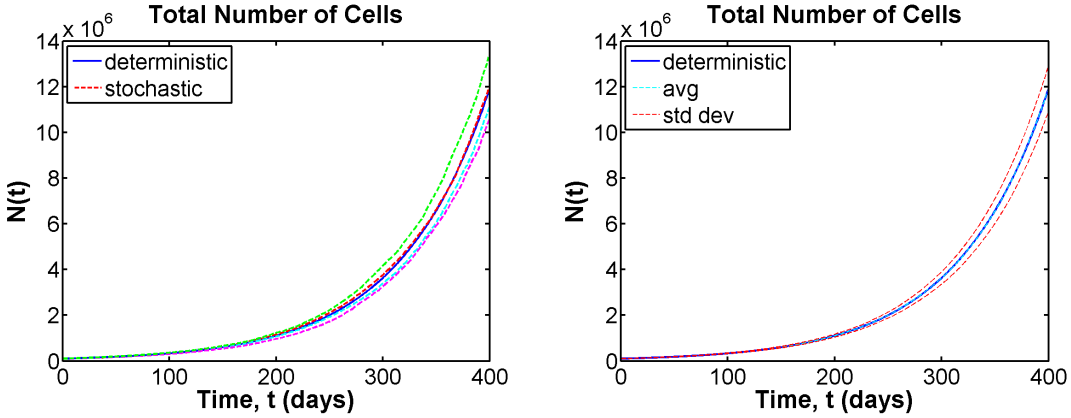

Figure 2.5: Plots that show the total number of cells in the system as a function of time (calculated by integrating the system over the whole domain). The two plots compare the model with and without noise for $\sigma = 5$. Left plot: Solid blue line is the deterministic trajectory, while the other coloured lines are sample realizations of the stochastic model. Right plot: mean and standard deviation over 50 realizations. Notice the average of the stochastic simulations is roughly the same as the deterministic trajectory, this is true because our simple model is linear.

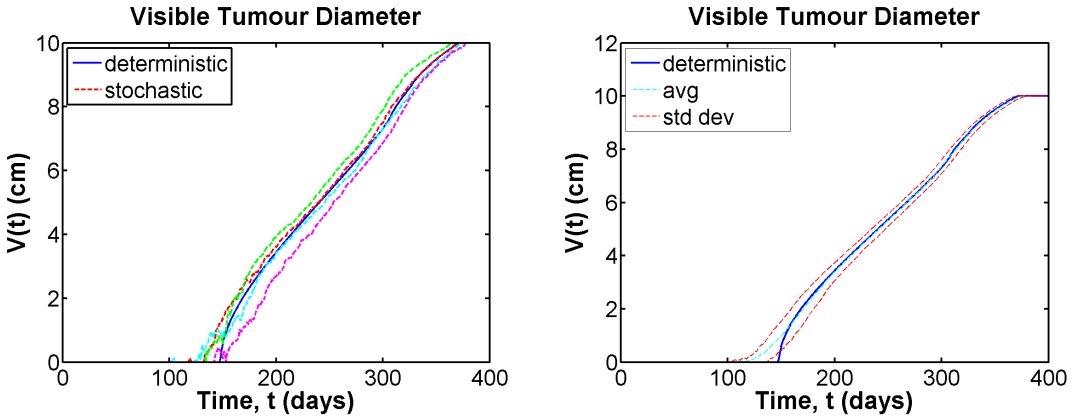

Figure 2.6: Visible tumour radius plots for $\sigma = 5$. Left plot: Solid blue line is the deterministic trajectory, while the other coloured lines are sample realizations of the stochastic model. Right plot: mean and standard deviation over 100 realizations. The effects of external forcing is relatively small.

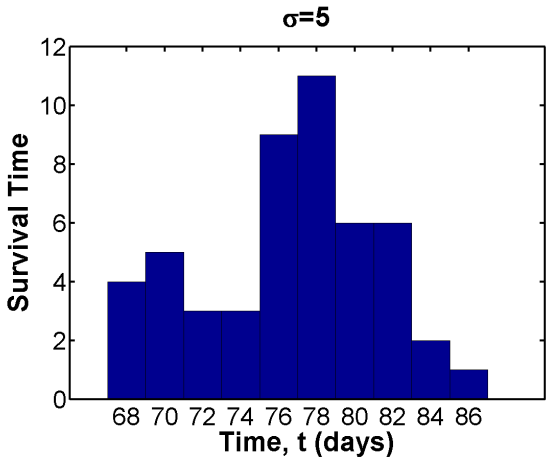

Figure 2.7: Histogram of survival times for $\sigma = 5$ over 50 simulations. The mean was 77.1 days, with a standard deviation of 4.7 days. The deterministic model gives a survival time of 78 days.

tive correlation. A standard least squares line[42][44] computed using Matlab's built-in function "lsline" was also added to the plot to visualize the strong positive relationship. However, even when σ is at our imposed maximum strength of 5 the standard deviation in survival time is only 4.7 days compared to an average of 77.1 days, so the effect of noise on the system is less than 10%.

2.3 Comparison between different values of D

From Swanson[5] the diffusion constant D can vary from about 2 to 100 times the nominal value of 0.0013cm^2/day between white and grey matter in the brain, with a factor of 5 being a good approximation for the average across the whole brain. Figures (2.10), (3.5), and (2.12) show some results of our model when the multiplication factor for D is varied from 1 to 25 (with $\sigma = 5$). As we can see from figure (3.5) the survival time decreases as we increase the diffusivity, and figure (2.12) shows how the standard deviation decreases as well. The Pearson correlation coefficient for standard deviation versus diffusivity was -0.9653 indicating a strong negative correlation and this shrinking standard deviation tells us that we are more confident in our estimate of survival time for more invasive tumours.

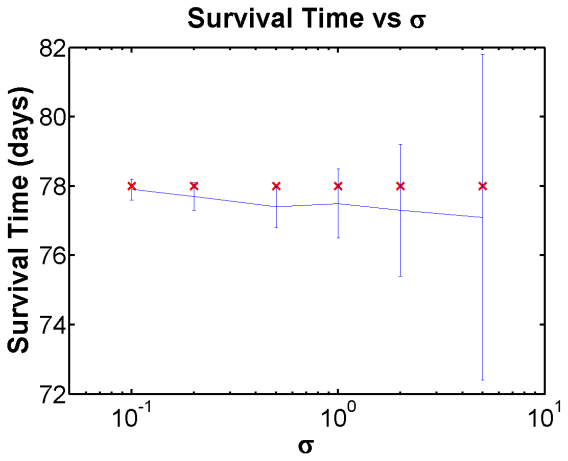

Figure 2.8: Plot of mean survival time and one standard deviation for different values of σ over 50 realizations each. The survival time for the deterministic model is 78 days (indicated by the red crosses on the plot).

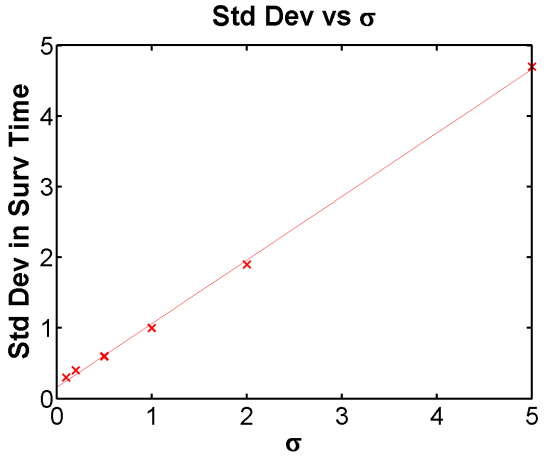

Figure 2.9: Plot of standard deviation versus noise strength σ. Least squares straight line plotted using Matlab. The Pearson correlation coefficient was 0.9995 indicating strong positive correlation.

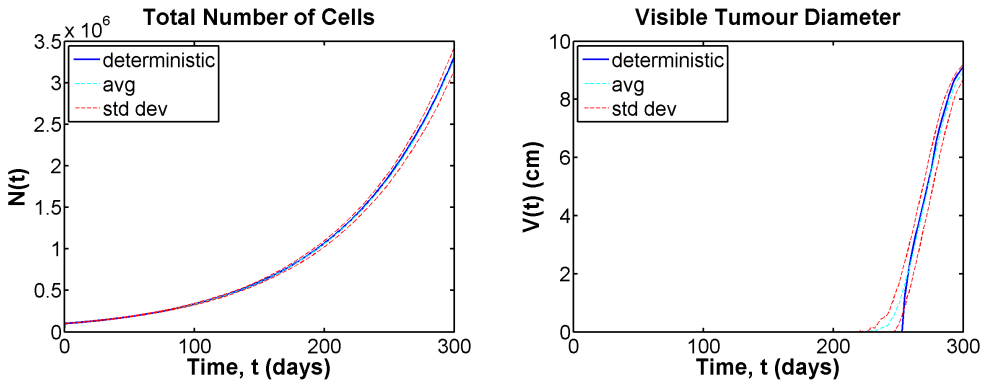

Figure 2.10: These are plots for the total number of cells and visible tumour diameter for $D = 15 \times 0.0013\text{cm}^2/\text{day}$ with $\sigma = 5$. The survival time was 15.3 days with a standard deviation of 2.4 days, which is a much shorter survival time as expected.

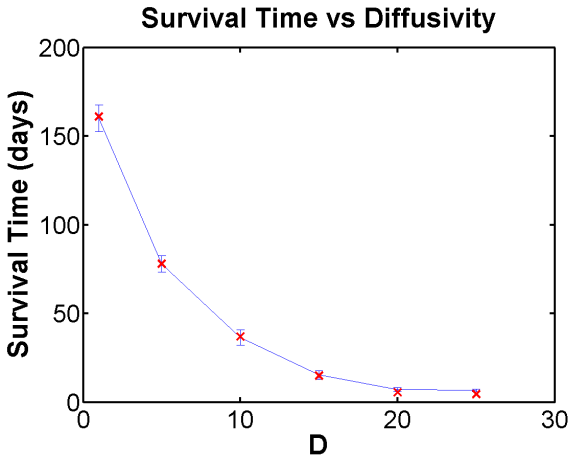

Figure 2.11: Plot of mean survival time and one standard deviation for different values of D (bottom axis is the multiplication factor for D) over 50 realizations each. Red crosses indicate the corresponding result for the deterministic model. the mean and standard deviation decrease for more invasive tumours.

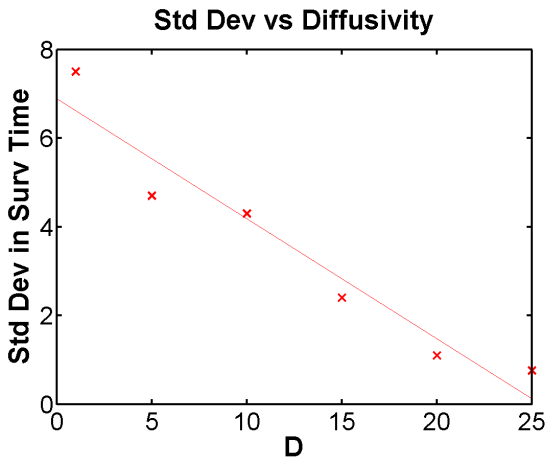

Figure 2.12: Plot of standard deviation versus diffusivity, with a leat squares straight line fitted using Matlab. The Pearson correlation coefficient was -0.9653, indicating a strong negative correlation.

2.4 Discussion

The estimate of the variance in tumour radius is a potentially useful tool for surgery or radiotherapy because it tells us how much around the visible tumour we should target in order to eliminate most of the tumour. Surgeons and radio oncologists always target a larger area than what can be seen on medical imaging techniques, but there is always the trade off of being too aggressive with treatment and causing major side effects, or being too conservative and leaving too much of the tumour behind, allowing it to regrow. Although the effects of noise is small in this chapter, perhaps with an accurate estimate of σ and a better model we can find a middle ground where we remove most of the tumour while minimizing side effects to the patient.

We saw that increasing σ increased the error bounds on survival time, indicating that more chaotic and heterogeneous tumour microenvironments are hard to predict and require a larger area to be treated. On the other hand, increasing the diffusivity means we have increased the invasiveness of the tumour cells, and in this we saw that the survival time decreases, and that we are more confident in that estimate. In other words, more invasive tumours lead to a swifter and surer death which agrees with our intuition.

2.5 Adding Chemotherapy

2.5.1 Deterministic Equations

Tracqui[4] and Powathil[23] have both explored adding the effects of chemotherapy to the deterministic PDE model in the following manner

$$\frac{\partial n}{\partial t} = D\nabla^2 n + \rho n - k(t)n, \tag{2.5}$$

where

$$k(t) = \begin{cases} k, & \text{if} \quad t \in [t_i, t_{i+1}], \\ 0, & \text{otherwise}, \end{cases} \tag{2.6}$$

with the constant k chosen so that the total dose (area under the integral) is the same regardless of the number of treatments. The question we would like to answer here is whether changing the number of doses makes any difference to the survival time of the patient. As before, external forcing will appear as multiplicative noise in the exponential growth term.

$$\frac{\partial n}{\partial t} = D\nabla^2 n + \rho \left[1 + A\eta(\mathbf{x}, t)\right] n - k(t)n, \tag{2.7}$$

Figure (2.13) shows graphically how the total number of cells changes when we change the number of doses of chemotherapy. The mean and standard deviation was estimated with $\sigma = 5$ and the results are relatively small once again. Figure (2.14) shows how the survival time curve changes with the number of doses. The one thing of note here is that the growth spike at the end occurs later in terms of absolute simulation time for fewer doses, possibly indicating a longer survival time.

Figure (2.15) refutes that idea however, as it clearly shows that more doses means a longer survival time (as we have currently defined it). Moreover, figure (2.16) shows that there is strong

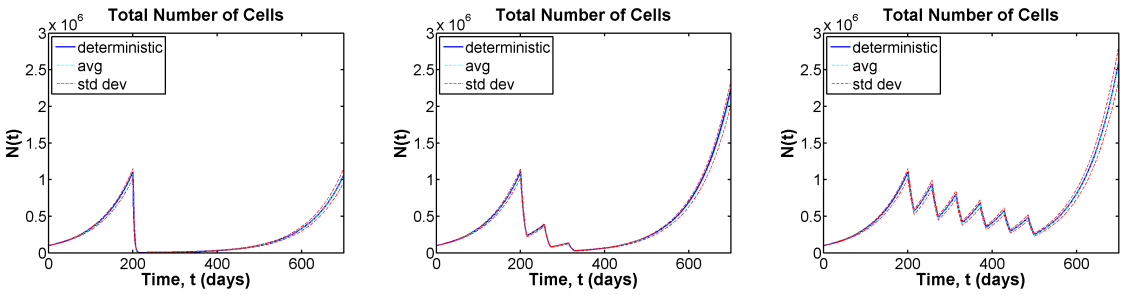

Figure 2.13: Plots of total number of cells for 1, 3, and 6 doses of chemotherapy, with mean and error bounds calculated over 50 realizations each and with $\sigma = 5$. As we saw before, noise is fairly small.

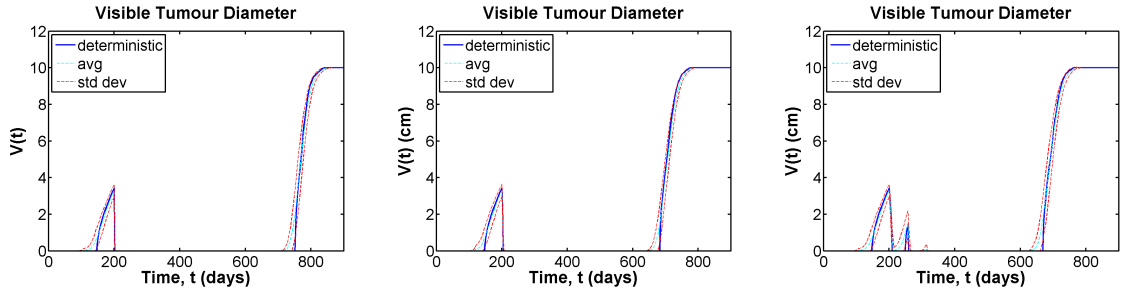

Figure 2.14: Plots of survival time for 1, 3, and 6 doses of chemotherapy, with mean and error bounds calculated over 50 realizations each and with $\sigma = 5$. Notice how the sudden growth at the end occurs earlier as we increase the number of doses, indicating an earlier death in terms of absolute simulation time.

positive correlation between the standard deviation and number of doses, so that too suggests more doses is better. So the question is whether one large dose is better or many smaller doses is better. One larger dose means a quicker, surer death once the tumour recurs, while many smaller doses means a longer potential survival time after relapse. As currently constructed, this model does not have a clear definition of remittance time (and we do not know whether it even accurately models such a situation) so we would have to chose more doses as the better option predicted by our model.

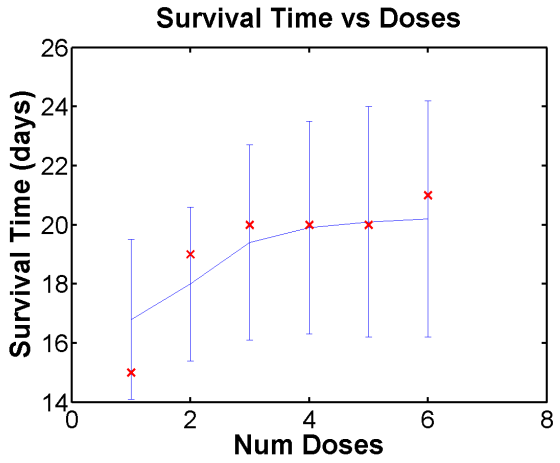

Figure 2.15: Plot of survival time versus number of doses. Red crosses indicate the corresponding result for the deterministic model. Notice how the mean survival time increases with the number of doses of chemotherapy.

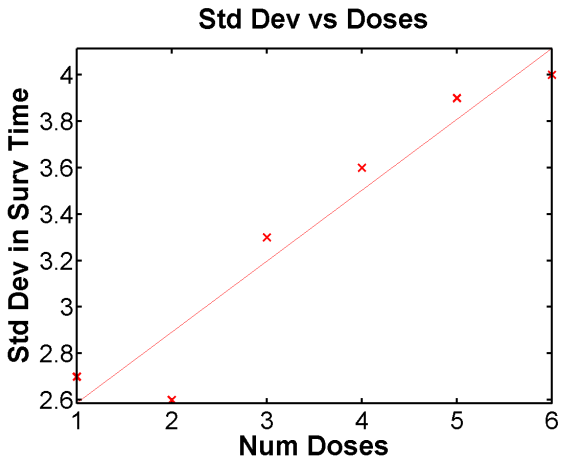

Figure 2.16: Plot of standard deviation versus number of doses, with least squares best fit line plotted using Matlab. The Pearson correlation coefficient was 0.9595, indicating a strong positive correlation. In other words, more doses meant a possibly longer survival time since both the mean and the standard deviation is larger.

2.6 What is the effect of External Noise?

In analogy to Brownian motion, external noise in our tumour model is one way to model the inherent heterogeneity within the chaotic tumour microenvironment with having to determine the exact details for each and every patient. This means we end up with a stochastic PDE that is difficult to solve analytically and we have to resort to numerical methods to estimate the mean and variance of the resultant stochastic process. We used external noise in this chapter to give error bounds on the visible tumour diameter and survival time, but found generally that the results were relatively small.

The correlation between noise and the three parameters we varied, σ, D, and number of doses, showed some relationships that agree with our intuition. The more noise in the system, the larger the error. The more invasive the tumour, the more confident we are in the estimated survival time. Finally, the more doses, the larger the error, indicating a longer possible survival time. These correlations give us a sense of how accurate our model is in predicting the survival time of a patient.

Chapter 3

Internal Noise in a Tumour Model

In this chapter we will examine how intrinsic noise affects the same tumour model as in the previous chapter. Internal noise differs from external noise in that it measures the fluctuations of the system due to inherent discrete number effects and randomness in chemical reactions. Furthermore, the system size parameter Ω introduced here is a physically well defined quantity that measures the total number of reactants in the system, unlike the noise amplitude σ for extrinsic noise which is ill defined and could potentially take on any number of meanings.

To analyze the situation with intrinsic noise, it is certainly possible to run a large ensemble of simulations using Gillespie's algorithm (Appendix B) as we did before, but we will not. Instead, we will use the extended version of the linear noise approximation as explained in chapter 1 to develop analytic expressions for the mean and variance of the system. We will see in this chapter that intrinsic noise has approximately the same effect on visible tumour diameter and survival time as a noise strength of $\sigma = 5$ for external noise, but the variance instead decreases with increased diffusivity and increased number of doses. We will find in this chapter that the large number of cells needed for a tumour to become visible means that the internal noise is fairly small.

3.1 Mathematical Details

Again we will consider diffusion with exponential growth in two dimensions,

$$\frac{\partial n}{\partial t} = D\nabla^2 n + \rho n,$$

but this time with internal noise added to the model. In other words, we will treat the exponential growth term as a chemical reaction using the principle of mass action[74] and diffusion as another type of reaction as explained previously. Our goal is to calculate the visible tumour diameter and survival time curves as in for internal noise analogous to the previous chapter. For internal noise, as discussed in the background material, we can use Van Kampen's Linear Noise Approximation to estimate the mean and variance for the system, which can then be used to calculate the mean and variance for the tumour diameter and survival time curves analytically. These analytic expressions allow us to not have to run a large number of stochastic simulations to estimate the mean and the variance, but we will still use a modified version of Gillespie's algorithm (explained in Appendix B) to generate some sample paths for the system (which can also be used to double check whether our analytic expressions are correct).

Van Kampen's Linear Noise Approximation tells us that (to first order) the mean of the system simply follows the original deterministic equation

$$\frac{\partial n}{\partial t} = D\nabla^2 n + \rho n,$$

so usual numerical methods for two dimensional reaction-diffusion equations can be used. There is only one species of reactant and only one chemical reaction in Fisher's equation, so the stoichiometry and propensity are given by $\mathbf{S} = 1$ and $\boldsymbol{\nu} = \rho n$ respectively. Using the general expression for the time evolution of the cumulant as found in equation 2.19 of Scott[11], one can

then show that the factorial cumulant for our tumour model must satisfy

$$\frac{\partial\left[n(\mathbf{r_1},t)n(\mathbf{r_2},t)\right]}{\partial t} = 2\rho\left[n(\mathbf{r_1},t)n(\mathbf{r_2},t)\right] + 2\rho\delta(\mathbf{r_1}-\mathbf{r_2})\langle n(\mathbf{r_1},t)\rangle + D\left\{\nabla_1^2+\nabla_2^2\right\}\left[n(\mathbf{r_1},t)n(\mathbf{r_2},t)\right], \tag{3.1}$$

where r_i is the position of the centre of grid box i in the discretization of our domain, along with Dirichlet conditions at the boundaries. For the initial condition, recall that the variance and factorial cumulant are related via the following equation:

$$\langle\langle n(\mathbf{r_1},t)n(\mathbf{r_2},t)\rangle\rangle = \left[n(\mathbf{r_1},t)n(\mathbf{r_2},t)\right] + \delta(\mathbf{r_1}-\mathbf{r_2})\langle n(\mathbf{r_1},t)\rangle. \tag{3.2}$$

We assume the variance is zero at $t = 0$, so the initial conditional for the factorial cumulant is simply $[n(\mathbf{r_1},0)n(\mathbf{r_2},0)] = -\delta(\mathbf{r_1}-\mathbf{r_2})\langle n(\mathbf{r_1},0)\rangle$.

For our 2D simulations, the evolution equation for the factorial cumulant is in fact a four dimensional equation. Also, we replace the Dirac delta function with a Kronecker delta function (divided by Ω) for the numerical simulation. Paraphrasing van Kampen[20], if we consider the dirac delta function to be a function of $\mathbf{r_2}$, we can make this identification between the two delta functions because $\delta(\mathbf{r_1}-\mathbf{r_2})$ vanishes except in the grid box that contains $\mathbf{r_1}$ in our discretized domain. So the integral over all space of the dirac delta is the volume of the box that contains $\mathbf{r_1}$, which is Ω. Hence we can say that in a discrete setting the dirac delta $\delta(\mathbf{r_1}-\mathbf{r_2})$ is equivalent to the Kroenecker delta $\delta_{1,2}/\Omega$.

For stochastic simulations, we will utilize a modified version of Gillespie's algorithm which makes use of the idea that we encountered in the background material where we treat diffusion as just a different kind of chemical reaction. Details on how this modification can be made is explained in Appendix B. Figure (3.1) illustrates the differences between the stochastic and deterministic models in two dimensions using a sample path generated by the Gillespie Algorithm.

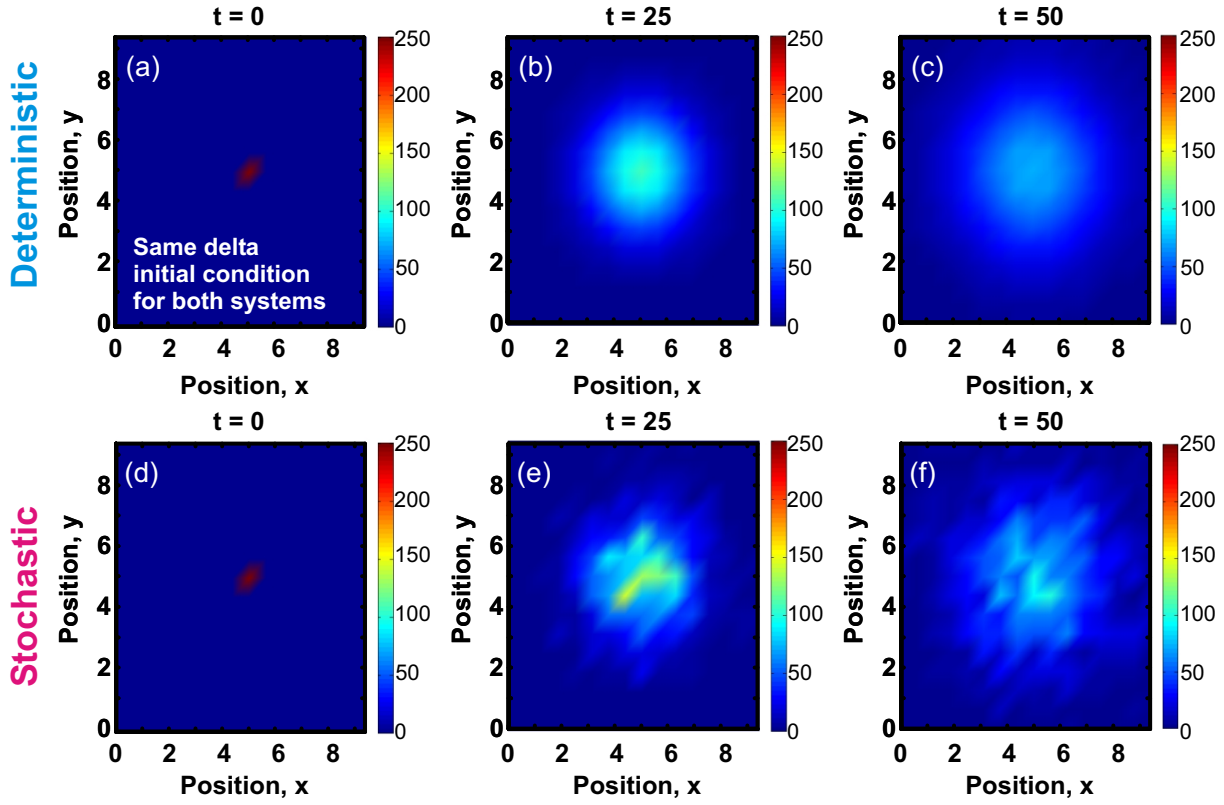

Figure 3.1: Plots showing the qualitative difference between the deterministic and stochastic models with parameters $N_0 = 1000$, $D = 5 \times 0.0013\text{cm}^2/\text{day}$, and $\rho = 0.012/\text{day}$ in both sets of simulations.

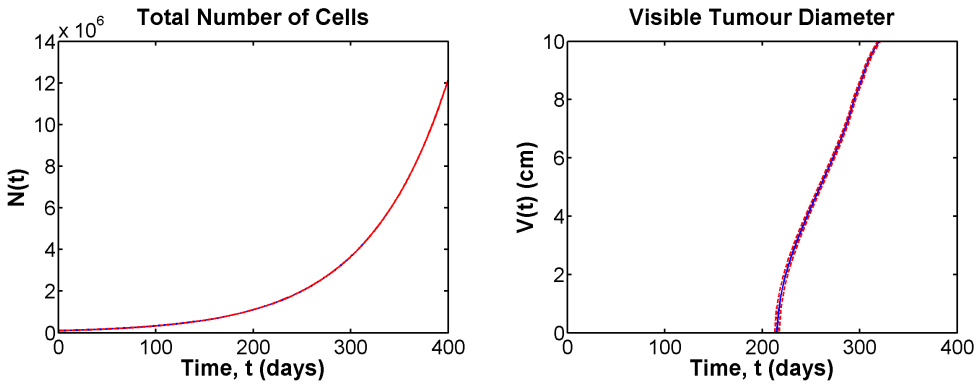

Figure 3.2: These plots show the estimated error bounds for the total number of cells and visible tumour diameter in the presence of internal noise. The mean for the survival time was 78 days (same as the deterministic case) with a standard deviation of 4.2 days. This very roughly corresponds to a noise strength of $\sigma = 5$ for external noise.

Figure (3.2) demonstrates the estimated error bounds on for internal noise with Ω set equal to the grid size of the simulations Δx^2. This choice of Ω ensures that there is exactly the same number of cancer cells in these simulations as the previous chapter. From the results in (3.2) one can see that the effect of internal noise is very small, and roughly corresponds to a noise strength of $\sigma = 5$ for external noise.

3.2 Comparison between different values of D

As with the previous chapter, we will once again vary the diffusivity D. Figure (3.3) shows a sample plot with $D = 15 \times 0.0013\text{cm}^2/\text{day}$, as compared to figure (3.2) which had $D = 5 \times 0.0013\text{cm}^2/\text{day}$. Figures (3.4) and (3.5) show how the survival time changes as we increase the diffusivity from 1 to 25 times the nominal value of $0.0013cm^2/\text{day}$. As one would expect, the survival time is shorter and the error bound is smaller as the tumour becomes more diffusive.

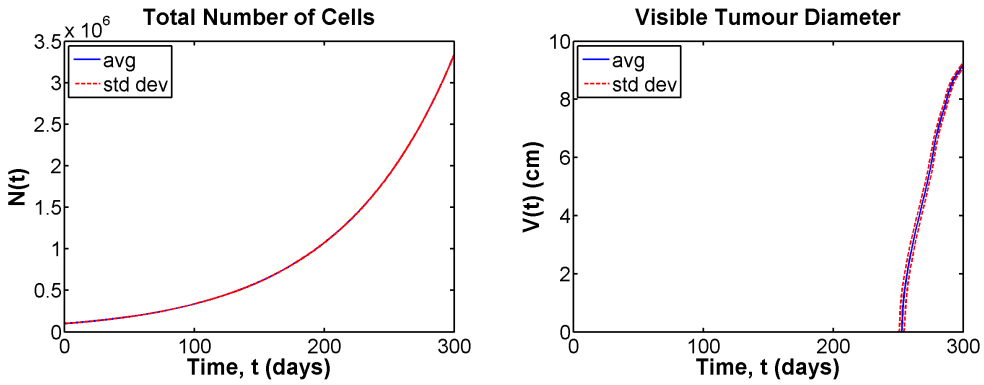

Figure 3.3: These are plots for the total number of cells and visible tumour diameter for $D = 15 \times 0.0013\text{cm}^2/\text{day}$. The survival time was 15 days with a standard deviation of 3.5 days, which is a much shorter survival time as expected.

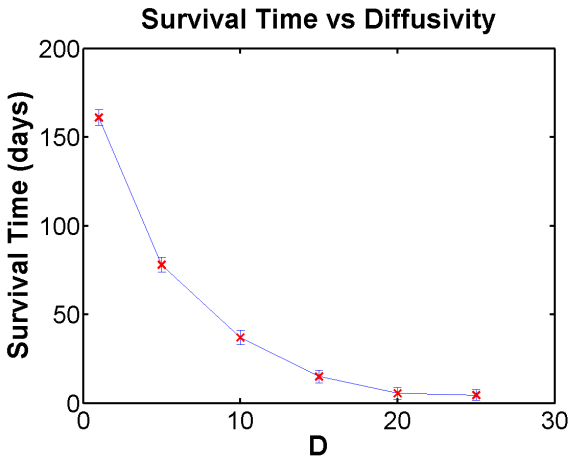

Figure 3.4: Plot of survival time vs D, where the bottom axis is the multiplication factor times $0.0013cm^2/\text{day}$. Both the mean and error bounds decrease as the diffusivity increases meaning the death of the patient is faster and surer.

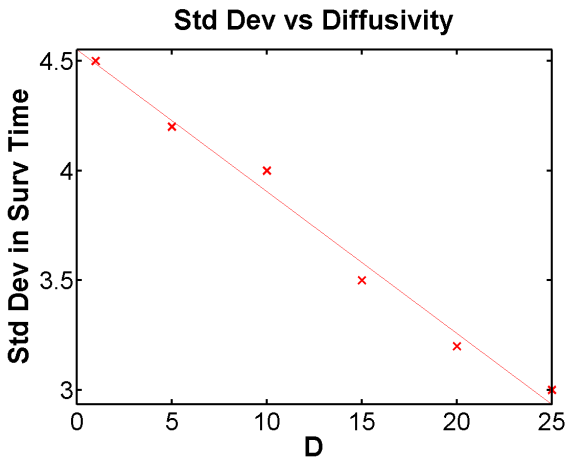

Figure 3.5: Plot of the standard deviation versus diffusivity with a least squares straight line fitted using Matlab. The Pearson correlation coefficient was -0.9930 which indicated a strong negative correlation between diffusivity and internal noise.

3.3 Adding Chemotherapy

As before, we again add chemotherapy by adding a time dependent decay term as follows:

$$\frac{\partial n}{\partial t} = D\nabla^2 n + \rho n - k(t)n, \tag{3.3}$$

where

$$k(t) = \begin{cases} k, & \text{if} \quad t \in [t_i, t_{i+1}], \\ 0, & \text{otherwise}, \end{cases} \tag{3.4}$$

with the constant k chosen so that the total dose (area under the curve) is the same regardless of the number of treatments. Figures (3.6) to (3.8) show what happens when we vary the number of doses, and we see in those pots the estimated error bounds for internal noise is quite small.

Figures (3.8) and (3.9) show how the mean and standard deviation change as we change the number of doses of chemotherapy. As we saw for external noise, the mean survival time increases with the number of doses, but for internal noise the error bounds actually decrease slightly as we increase the number of doses. Although the bounds do decrease, the actual change is very small

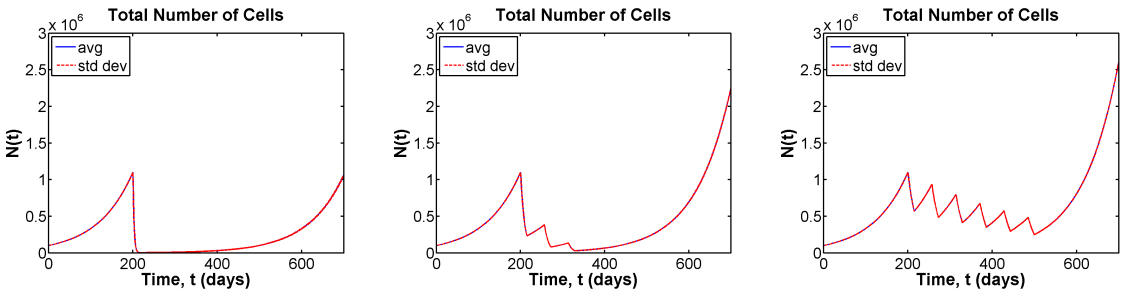

Figure 3.6: Plots for total number of cells and 1, 3, and 6 doses of chemotherapy with error bounds given by the Linear Noise Expansion. Noise is fairly small for such a large number of cells.

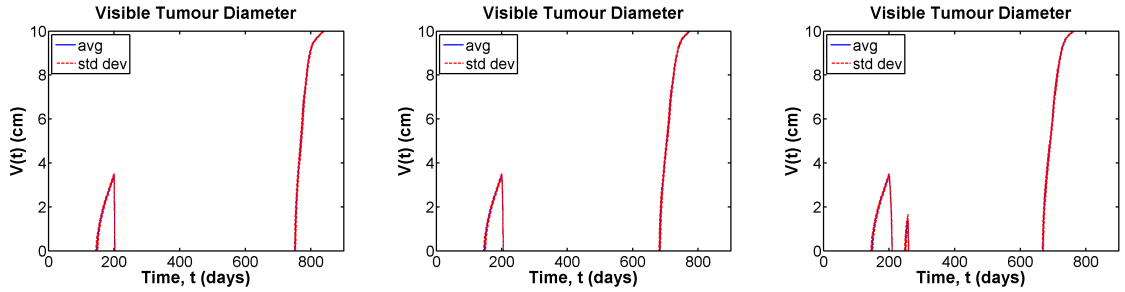

Figure 3.7: Visible tumour diameter for 1, 3, and 6 doses of chemotherapy with error bounds given by the Linear Noise Expansion. Noise is fairly small for such a large number of cells

(only 0.2 days between 1 and 6 doses) so we might say the error is essentially constant.

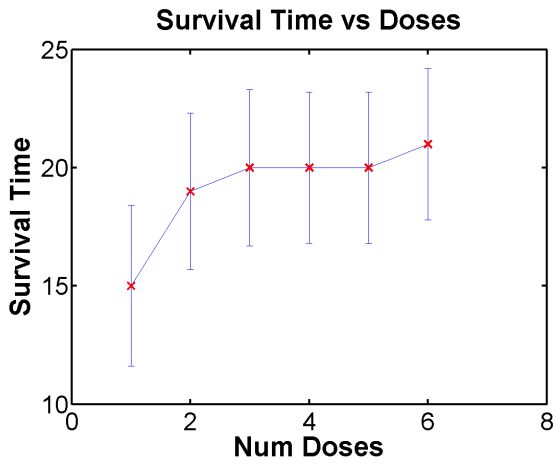

Figure 3.8: Plot of survival time versus number of doses. Survival time increases as we increase the number of doses but the error bound is very nearly the same across the number of doses.

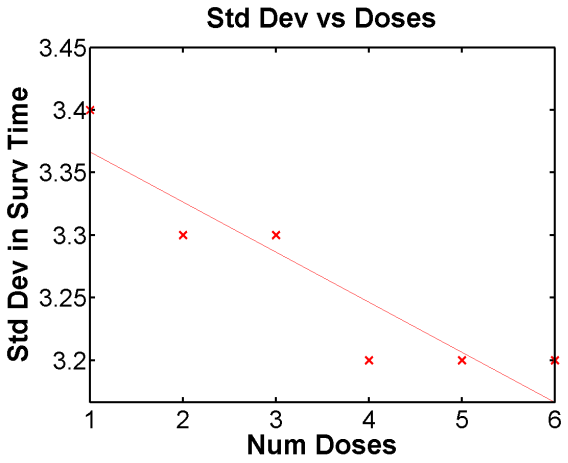

Figure 3.9: Plot of standard deviation versus number of doses with least squares line fitted using Matlab. Here the Pearson correlation coefficient was -0.9165 indicating strong negative correlation but the actual change in the error bound is very insignificant (only 0.2 days from 1 to 6 doses) so we could say that the error bound is essentially constant for internal noise.

3.4 Comparison between Internal and External Noise

Internal and external noise are two different ways of adding noise to the tumour model. Internal noise in this chapter replicates the randomness of cell division and cell movements, while external noise models the heterogeneity within the tumour microenvironment. In terms of direct comparison, an external noise strength of $\sigma = 5$ gave very nearly the same error bounds as $\Omega = \Delta x^2$ for internal noise.

As we can saw in the two chapters, both kinds of noise gave similar and intuitive results when we changed the diffusivity and number of doses for chemotherapy. Figures (3.10) shows how the standard deviation of the system changed as a result of both kinds of noise and they both agree that more diffusive tumours meant a quicker (lower surival time) and surer (smaller error bound) death. However, for the number of doses of chemotherapy, figure (3.11) shows that external and internal noise disagreed slightly on the error bounds as a function of the number of doses. Although the slope of the standard deviation versus number of doses plots is reversed for the two kinds of noise, the end result is that the error bound is roughly 3-4 days regardless of the number of doses, so the difference isn't significant.

The two kinds of noise introduced in the present and preceding chapter serve to demonstrate methods for calculating error bounds on visible tumour diameter and survival time. The former could eventually be of use to surgeons or radiologists in determining how much of an area they should operate on or irradiate during therapy, and the latter helps define how accurate our estimate of survival time is. A more accurate brain domain with a distribution of grey and white matter would be the next step in improving this model.

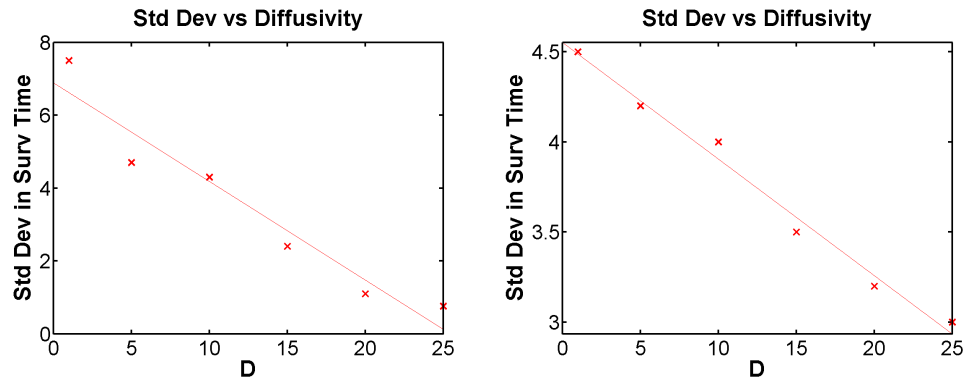

Figure 3.10: Plots of standard deviation versus diffusivity, external noise is on the left, internal is on the right. Both kinds of noise agree that more diffusive tumours are worse: they have lower survival times, and the error bounds decrease as you increase the diffusivity.

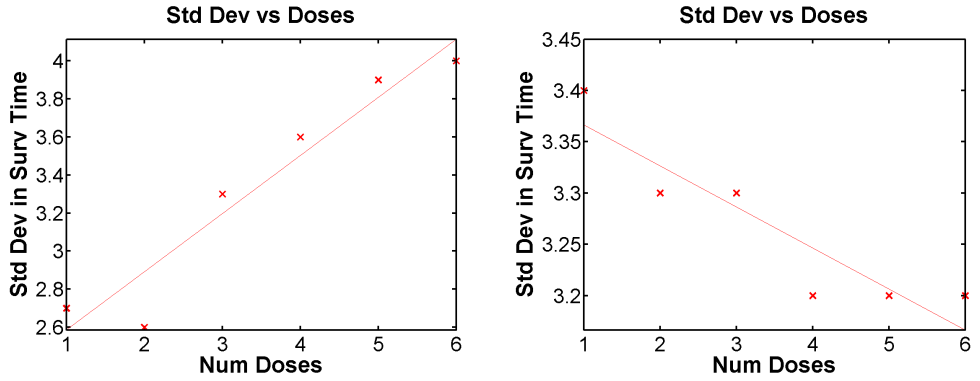

Figure 3.11: Plots of standard deviation versus number of doses of chemotherapy, external noise is on the left, internal is on the right. In this case although both kinds of noise predict that more doses leads to longer survival, external noise predicts larger error bounds for more doses, whereas internal noise predicts nearly identical error bounds regardless of the dose. In either case the error bound is roughly 3-4 days for any number of doses, and the slight change isn't significant.

Chapter 4

Noise in a Mitosis Model

Chang and Ferrel's model for mitotic trigger waves of the Xenopus cell cycle[31] consists of two PDEs that describe the concentration of B1-Cdk1 complexes in their active and inactive phosphorylation states (we will call them A and I respectively in the subsequent equations). It is a fairly straightforward activator-inhibitor type excitable model with both positive and negative feedback loops[30][32] (figure (4.1)), and as we have seen with the Vilar model, can generate a traveling waves under certain conditions (figure (4.2)). This traveling wave is called a "trigger wave" because it represents a signal traveling rapidly through the cell telling it to switch from a normal state to a mitotic state.

We will show in this chapter how just the right amount of noise can induce a traveling wave instability in an otherwise deterministically stable system, known as stochastic coherence or stochastic resonance[27][28]. Such a result would broaden the conditions under which the trigger wave can occur and imply that mitosis is more likely to occur than expected under the deterministic setting. As mentioned previously, it has been speculated that some biological systems (such as neural signalling in human brains) have evolved to make use of such phenomena[29], and it would stand to reason that noisy and chaotic growth of cancer cells would take full advantage of such situations as well.

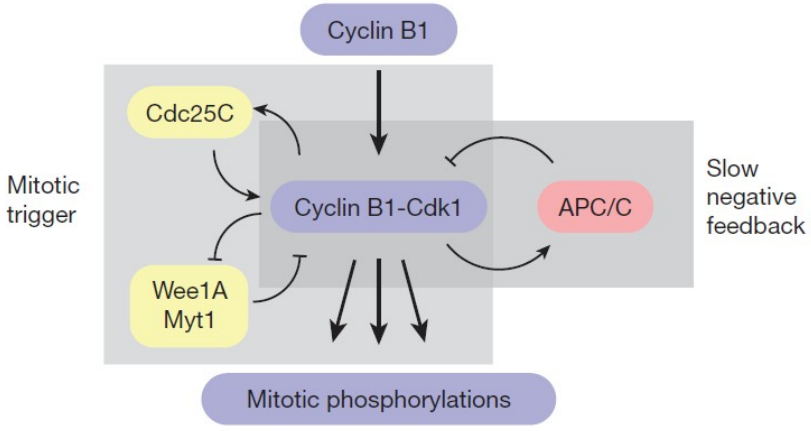

Figure 4.1: A schematic of system described by the mitotic trigger wave model. The three feedback loops correspond to the three hill functions in equations (4.1) and (4.2). Figure from Chang and Ferrel[31].

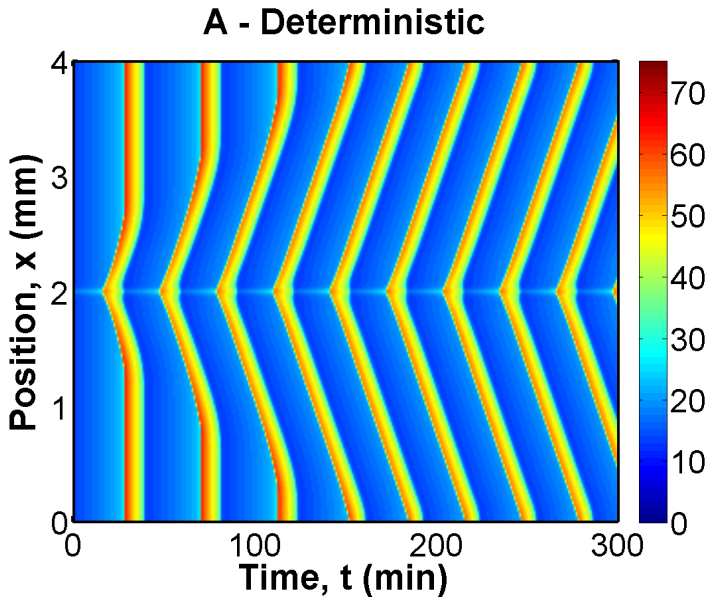

Figure 4.2: Traveling wave generated by Chang and Ferrel's model in 1 dimension. Y axis represents the cell stretched out in a straight line and the x axis represents time. Physically, the wave represents the signal to begin mitosis propagating from the middle out to the edges.

4.0.1 Possible future reinterpretation for Metastasis

There is a growing sense that metastasis - particularly the way cancer cells suddenly switch from non-metastatic to metastatic - can be modeled as an excitable system. Metastasis is described as a sequence of very distinct steps by Weinberg[14] (sometimes known as the Metastasis Cascade) and the very first step in the sequence is the switch from a normal to a metastatic tumour cell. Michor et al[16] have also considered this first step in metastasis, and they use a stochastic model based on Moran processes that examine random mutations in a group of tumour cells. However, in Michor's model, spatial aspects are essentially ignored, it does not consider how neighbouring tumour cells might affect each other, whereas we saw in both Fisher's equation and the Vilar model that excitable systems transmit signals in the form of a traveling wave. We know for example that a cell undergoing mitosis does so in a very specific spatially orientated way (which have been modeled in the past as Turing instabilites[6]) and it stands to reason that a normal tumour undergoing the change to a metastatic one would do so in a spatially correlated manner as well.

Very current and ongoing research suggests that there may be a link between excitable systems and metastasis. Of direct relevance is the paper by Iglesias and Devreotes (Curr Opin Cell Biol. 2012)[36] that discusses the importance of how random fluctuations in excitable systems can be used to explain the "spontaneous migration of cells", a key first step in metastasis. Djamgoz (2014)[37] and Brackenbury (2012)[38] discuss the role of ion channels (particularly sodium) as an excitable system that could possibly lead to metastasis. On the other hand, Prevarskaya et al (2011)[39] describe a non-excitable mechanism for metastasis based on calcium channels.

Chang and Ferrel's model is a very good starting point for a model of metastasis because the situation it models has obvious parallels with a cancer cell undergoing a switch from a normal state to a metastatic state. A reinterpretation of this model to metastasis would require finding an analogous set of signalling molecules to the B1-Cdk1 complexes in mitosis for metastasis. Once

those molecules are found, the trigger wave would then represent the mitosis signal spreading through the tumour. In an overview of current research of Brain metastases Eichler et al[15] say that the "propensity of cancer cells to spread to specific sites [is] dependent upon two factors: the cancer cell (the seed) and the receiving organ environment (the soil)." Internal and external noise would certainly be one way to model such aspects of the tumour microenvironment.

Other aspects of the Metastasis Cascade would have to be considered separately, and have been modeled by other researchers. For example, Anderson et al[17] have modified a model of angiogenesis (which itself is a modification of the tumour model in chapters 2 and 3) to describe how tumour cells that are already metastatic leave the primary tumour site and invade into a different part of the body.

4.1 Mathematical Details

The deterministic equations for the mitotic trigger wave model are as follows:

$$\begin{aligned}\frac{dA}{dt} &= D\nabla^2 A + k_{synth} + \left(a_1 + b_1\frac{A^{n_1}}{E_1^{n_1}+A^{n_1}}\right) I - \left(a_2 + b_2\frac{E_2^{n_2}}{E_2^{n_2}+A^{n_2}}\right) A \\ &\quad - \left(a_3 + b_3\frac{A^{n_3}}{E_3^{n_3}+A^{n_3}}\right) A, \qquad (4.1)\\ \frac{dI}{dt} &= D\nabla^2 I - \left(a_1 + b_1\frac{A^{n_1}}{E_1^{n_1}+A^{n_1}}\right) I + \left(a_2 + b_2\frac{E_2^{n_2}}{E_2^{n_2}+A^{n_2}}\right) A \\ &\quad - \left(a_3 + b_3\frac{A^{n_3}}{E_3^{n_3}+A^{n_3}}\right) I. \qquad (4.2)\end{aligned}$$

with Neumann boundary conditions at the ends of the domain. Here we have intentionally replaced the descriptive subscripts in the parameters with numbers to simplify the notation. Since it is made up of a series of Hill Functions, there are standard ways of estimating the various parameters and Hill coefficients. Moreover, it is a model that can actually be verified experimentally in a lab under controlled conditions[31]. Exact details on the what the parameters mean and their values can be found in Appendix C.

Two important features of the model to note is that 1) both species diffuse at the same rate D (so there are no spatial (Turing) instabilities), and 2) all the parameters and initial conditions are spatially homogeneous (i.e not a function of position), except for the parameters a_1 and b_1 which have a higher concentration in a narrow region around the middle of the domain. This higher concentration of a_1 and b_1 is what makes the wave start initially in the middle and then spread outwards. Assuming k_{synth}, which measures the production of A, is variable (while all other parameters are constant), one can show using standard linear stability analysis[57] that this system is unstable (i.e. produces traveling waves) for $k_{synth} > 0.76$ nM/min.

A useful next step is to non-dimensionalize the equations to identify any characteristic length or time scales, and any non-dimensional parameters of interest. Since A and I have units of $1/V$, an appropriate choice for non-dimensionalization would be $\hat{A} = A/E_2$ and $\hat{I} = I/E_2$. Similarly, all the a_i's and b_i's have dimension $1/T$, with a range of 0.01 min^{-1} to 4 min^{-1} so an appropriate non-dimensional time would be $\hat{t} = a_2 t$ (since a_2 measures the degradation of A).

Ignoring the diffusion term for the moment, the non-dimensionalized equations are then given by

$$\frac{d\hat{A}}{d\hat{t}} = \hat{k} + \left(\alpha_1 + \beta_1 \frac{\hat{A}^{n_1}}{\epsilon_1^{n_1} + \hat{A}^{n_1}}\right)\hat{I} - \left(1 + \beta_2 \frac{1}{1 + \hat{A}^{n_2}}\right)\hat{A} - \left(\alpha_3 + \beta_3 \frac{\hat{A}^{n_3}}{\epsilon_3^{n_3} + \hat{A}^{n_3}}\right)\hat{A}, \quad (4.3)$$

$$\frac{d\hat{I}}{d\hat{t}} = -\left(\alpha_1 + \beta_1 \frac{\hat{A}^{n_1}}{\epsilon_1^{n_1} + \hat{A}^{n_1}}\right)\hat{I} + \left(1 + \beta_2 \frac{1}{1 + \hat{A}^{n_2}}\right)\hat{A} - \left(\alpha_3 + \beta_3 \frac{\hat{A}^{n_3}}{\epsilon_3^{n_3} + \hat{A}^{n_3}}\right)\hat{I}, \quad (4.4)$$

where $\alpha_i = a_i/a_2$, $\beta_i = b_i/a_2$, and $\epsilon_i = E_i/E_2$. The non-dimensional parameter that governs whether oscillations occur is now given by $\hat{k} = \frac{k_{synth}}{a_2 E_2}$. Thus, in the deterministic case, non-dimensionalization simply re-scales the variables and in particular tells us that the characteristic concentration is E_2.

4.1.1 Stochastic Parameter for Intrinsic Noise

Using the non-dimensionalized deterministic equations above, we can add intrinsic noise to the model by writing it out as a system of chemical reactions. The stoichiometry and propensity are as follows:

$$\mathbf{S} = \begin{bmatrix} 1 & 1 & -1 & -1 & 0 \\ 0 & -1 & 1 & 0 & -1 \end{bmatrix}, \tag{4.5}$$

$$\boldsymbol{\nu} = \begin{bmatrix} \hat{k} \\ \left(a1 + \frac{b1\, A^{n1}}{E1^{n1} + A^{n1}}\right) I \\ \left(1 + \frac{b2}{1+A^{n2}}\right) A \\ \left(a3 + \frac{b3\, A^{n3}}{E3^{n3} + A^{n3}}\right) A \\ \left(a3 + \frac{b3\, A^{n3}}{E3^{n3} + A^{n3}}\right) I \end{bmatrix}. \tag{4.6}$$

From equation 1.51 of chapter 1, one can see that the size of the fluctuations (the second moment) are determined by the external forcing term given by the diffusion matrix $\mathbf{D} = \mathbf{S} \cdot \text{diag}[\boldsymbol{\nu}] \cdot \mathbf{S}^T$. Plugging in the expressions above we get

$$\mathbf{D} = \begin{bmatrix} \hat{k} + \left(\alpha_1 + \frac{\beta_1 A^{n_1}}{\epsilon_1{}^{n_1} + A^{n_1}}\right) I + \left(1 + \frac{\beta_2}{1+A^{n_2}}\right) A + \left(\alpha_3 + \frac{\beta_3 A^{n_3}}{\epsilon_3{}^{n_3} + A^{n_3}}\right) A & -\left(\alpha_1 + \frac{\beta_1 A^{n_1}}{\epsilon_1{}^{n_1} + A^{n_1}}\right) I - \left(1 + \frac{\beta_2}{1+A^{n_2}}\right) A \\ -\left(\alpha_1 + \frac{\beta_1 A^{n_1}}{\epsilon_1{}^{n_1} + A^{n_1}}\right) I - \left(1 + \frac{\beta_2}{1+A^{n_2}}\right) A & \left(a1 + \frac{\beta_1 A^{n_1}}{\epsilon_1{}^{n_1} + A^{n_1}}\right) I + \left(1 + \frac{\beta_2}{1+A^{n_2}}\right) A + \left(\alpha_3 + \frac{\beta_3 A^{n_3}}{\epsilon_3{}^{n_3} + A^{n_3}}\right) I \end{bmatrix} \tag{4.7}$$

If we rewrite the deterministic equations as

$$\begin{aligned} \frac{d\hat{A}}{d\hat{t}} &= \hat{k} + f_1(\hat{A})\hat{I} - f_2(\hat{A})\hat{A} - f_3(\hat{A})\hat{A}, \\ \frac{d\hat{I}}{d\hat{t}} &= -f_1(\hat{A})\hat{I} + f_2(\hat{A})\hat{A} - f_3(\hat{A})\hat{I}, \end{aligned}$$

and drop the hats to simplify the notation, we get

$$\mathbf{D} = \begin{bmatrix} k + f_1 I + f_2 A + f_3 A & -f_1 I - f_2 A \\ -f_1 I - f_2 A & f_1 I + f_2 A + f_3 I \end{bmatrix} \tag{4.8}$$

and at steady state

$$I^* = \frac{f_2}{f_1 + f_3} A^*, \quad \text{and,} \quad \hat{k} = -f_1 I^* + f_2 A^* + f_3 A^*. \tag{4.9}$$

so one possible way to rewrite $\mathbf{D}$ in steady state is

$$\mathbf{D}^* = \begin{bmatrix} 2(f_2 + f_3) A^* & -f_2 \left(\frac{1}{f_1 + f_3} + 1 \right) A^* \\ -f_2 \left(\frac{1}{f_1 + f_3} + 1 \right) A^* & 2 f_2 A^* \end{bmatrix}. \tag{4.10}$$

Notice that the diagonal terms now only depend on A^*. Following Scott et al[11], we compare the diagonal terms (ignoring the factor of 2 and all deterministic parameters) to the characteristic number of reactants $E_2\Omega$ (characteristic concentration E_2 multiplied by system size Ω). This means the non-dimensional size or volume parameter of interest is $\Delta = 1/E_2\Omega$, which represents the average change in the system with a birth or death ((1+1)/2) divided by the characteristic local density of A.

With these two non-dimensionalizations, one can then use a combination of linear stability analysis and a modification of the Linear Noise Approximation as described by Scott et al[12] (see Appendix D.) to produce a stability diagram that depends on Δ and k_{synth} (see figure (4.3)). This phase diagram tells us under which conditions temporal instabilities (and hence traveling waves) occur. Again, there are no spatial (Turing) instabilities, unlike the Vilar model mentioned in the background material, because both species diffuse at the same rate.

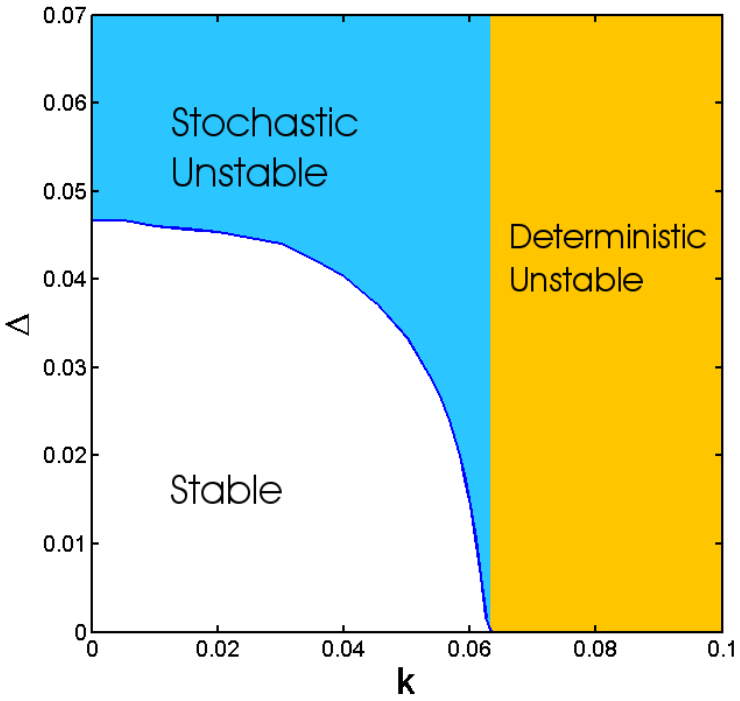

Figure 4.3: A schematic diagram of the (temporal) stability of the mitotic trigger wave model when internal noise is added. The x axis corresponds to the fully deterministic case ($\Omega \to \infty$).

4.2 Analysis of the system without spatial effects

It is useful to verify the results of our linear stability analysis without considering spatial effects first. It also gives us a sense of what to expect when we add space back into the system. Only intrinsic noise will be considered for the spatially homogeneous model.

Using the phase diagram we just computed in figure (4.3), figures (4.4) to (4.7) show plots from different regions of stability. In particular, figure (4.4) shows the difference between the stable and unstable modes of the purely deterministic system, figures (4.5) and (4.6) show the effects of noise induced oscillations when the deterministic system is stable, and figure (4.7) shows how noise affects an already unstable system. The key conclusion to draw from these graphs is that noise can cause the system to enter into an excited state even when the deterministic system is stable, but it cannot knock the system out of the oscillatory state if the system is already unstable.

One might then try to estimate the variance of the system with internal noise using Van Kampen's Linear Noise Approximation as we did with the tumour model. However figure (4.8) shows graphically how the Linear Noise Approximation does not work in either the stable or unstable modes of the trigger wave model. This means that we cannot develop an analytic expression for the second moment using the methods explained in this thesis.

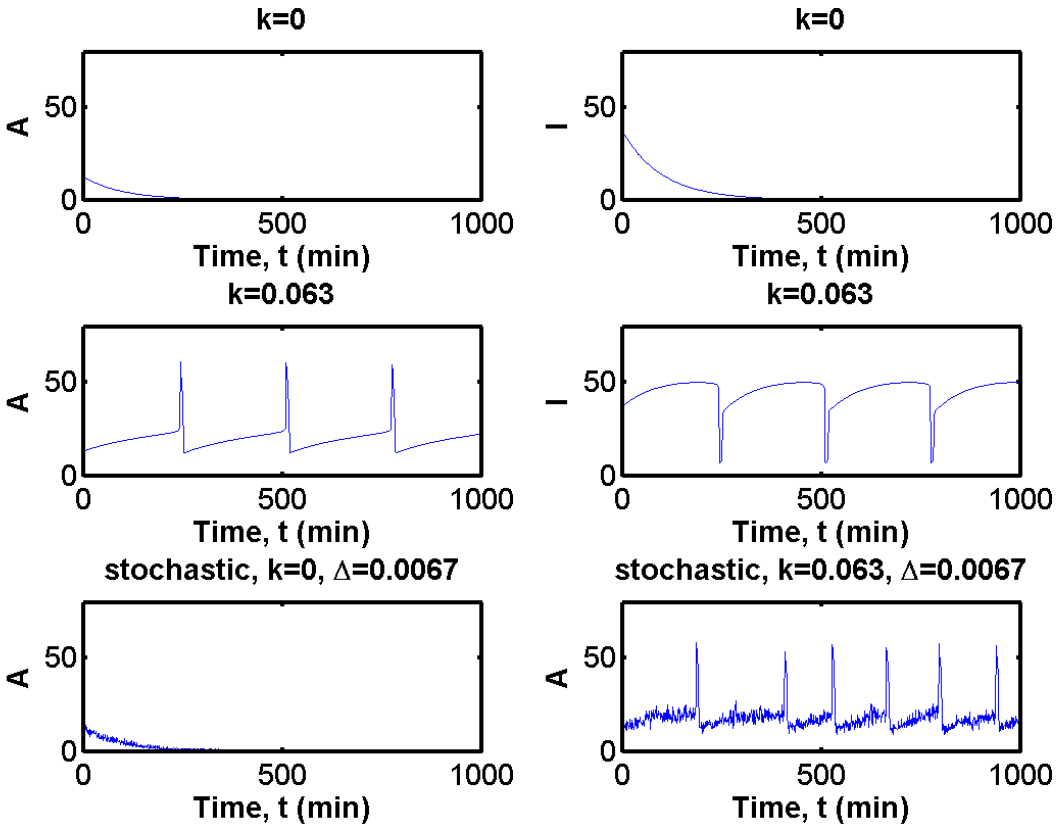

Figure 4.4: First two rows show the difference between the stable and unstable modes of the system without noise, with the left column as plots for A and right column as corresponding plots of I. The last row demonstrates how the stable and unstable modes retain their overall behaviour in the presence of low amounts of noise.

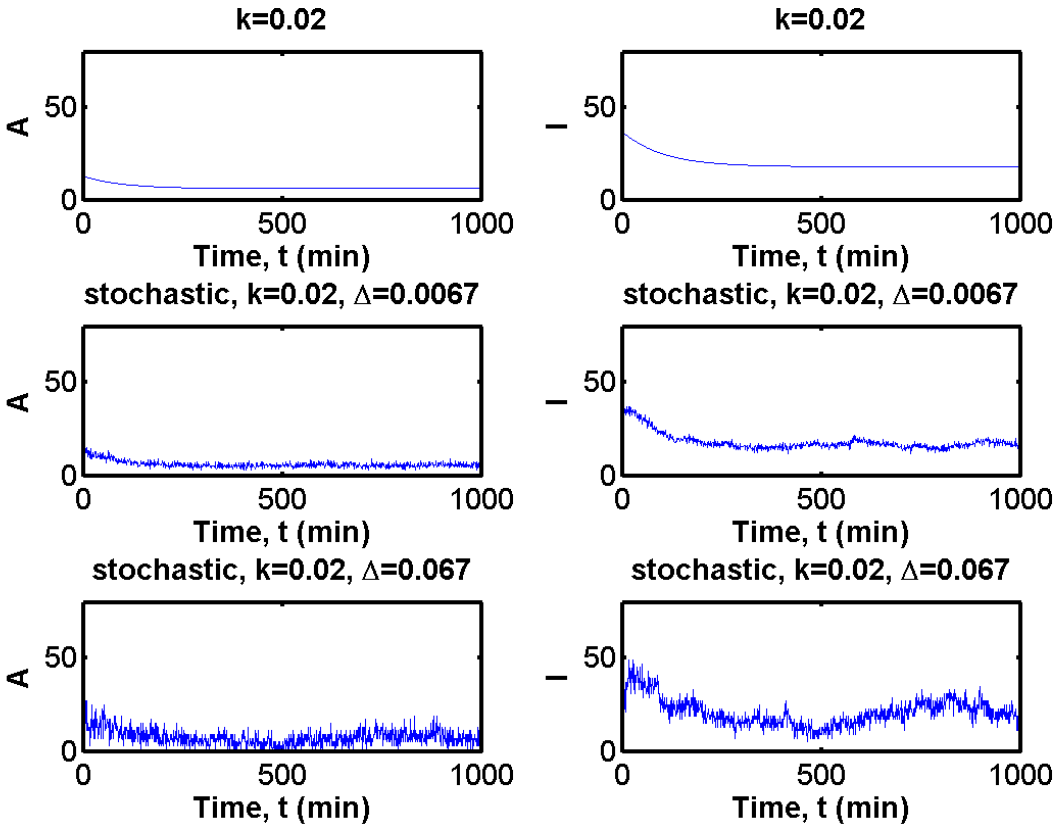

Figure 4.5: These plots show the system with a small value of k_{synth} so that it is far away from the temporal instability. The second and third rows show how adding more noise makes the system begin to oscillate.

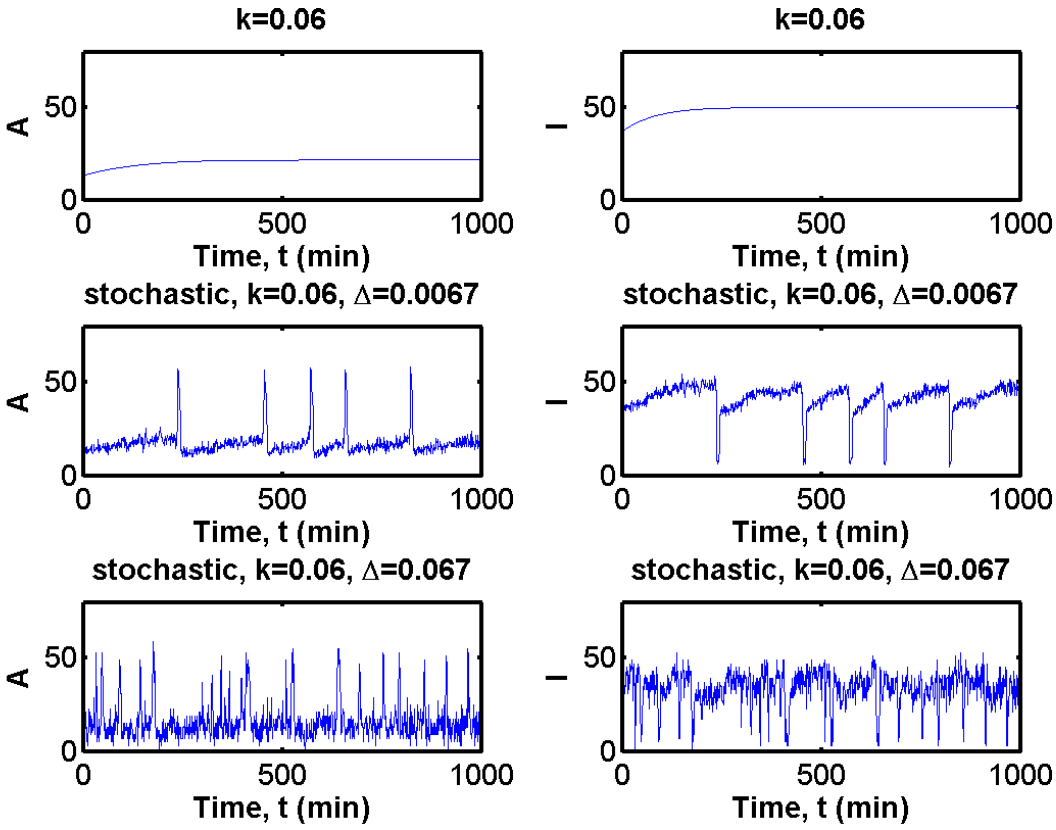

Figure 4.6: These plots show the system with k_{synth} close to the critical value for instability. Noise is now able to induce oscillations with a clear peak and period, causing the system to enter the excited state. When more noise is added we see the period of the osculations start to decrease in the third row.

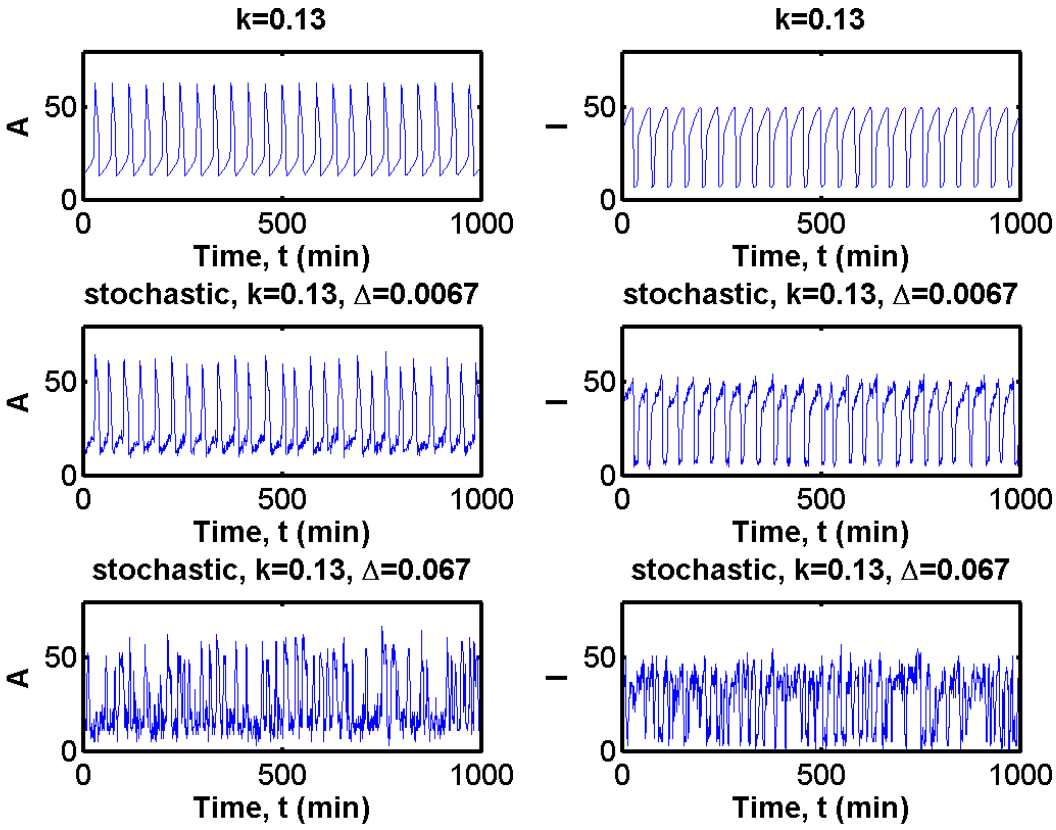

Figure 4.7: In these plots the system is already in its unstable mode. We can see here that the oscillations are qualitatively fairly robust to noise, as the period and value of the peaks don't seem to change much even when the noise parameter is increased by 10 times between the second and third rows.

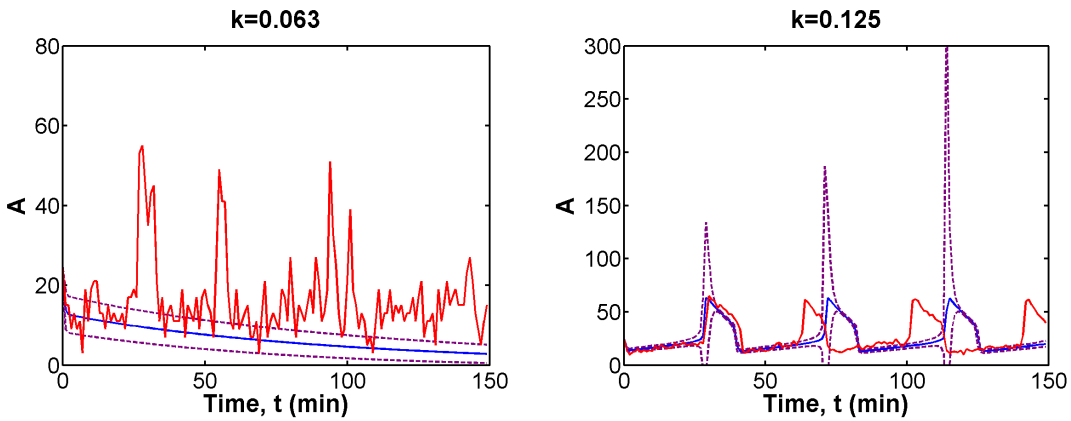

Figure 4.8: On the left is the system in its stable mode, and on the right is the system in its unstable mode. The linear noise approximation fails differently in each case. In the stable mode we can see that the variance envelope does not correctly capture the height of the noise induced oscillations. For the unstable mode, the variance envelope does not capture the oscillations happening at a different location to the deterministic model, and grows rapidly to infinity at the deterministic peaks. It's clear that this growth to infinity is not a numerical instability since the variance envelope reduces back to a reasonable width after each peak.

4.3 Analysis of the system in 1 dimension

We now add diffusion to the previous model and allow the reactants to move in one dimension. As with the tumour model, we will first consider external noise, then internal noise. It is more difficult to interpret what exactly the variance means in the case of the traveling wave (and the Linear Noise Approximation doesn't apply for internal noise) so only a mostly qualitative assessment of the results will follow.

4.3.1 External Noise

For external noise we once again consider a Langevin forcing term

$$\frac{dA}{dt} = D\nabla^2 A + k_{synth} + \left(a_1 + b_1 \frac{A^{n_1}}{E_1^{n_1} + A^{n_1}}\right) I - \left(a_2 + b_2 \frac{E_2^{n_2}}{E_2^{n_2} + A^{n_2}}\right) A - \left(a_3 + b_3 \frac{A^{n_3}}{E_3^{n_3} + A^{n_3}}\right) A + \sigma_A(x,t)\eta(x,t), \tag{4.11}$$

$$\frac{dI}{dt} = D\nabla^2 I - \left(a_1 + b_1 \frac{A^{n_1}}{E_1^{n_1} + A^{n_1}}\right) I + \left(a_2 + b_2 \frac{E_2^{n_2}}{E_2^{n_2} + A^{n_2}}\right) A - \left(a_3 + b_3 \frac{A^{n_3}}{E_3^{n_3} + A^{n_3}}\right) I + \sigma_I(x,t)\eta(x,t). \tag{4.12}$$

where $\eta(x,t)$ is space-time gaussian white noise, and for simplicity we once again set $\sigma_A(x,t) = \sigma_I(x,t) = \sigma$, a constant.

Figures (4.9) to (4.14) show various plots of the system when external noise is added, both in situations where we would and wouldn't expect oscillations in the deterministic model. In all the plots, the original deterministic model is shown for comparison, and 50 simulations of each parameter set were run to compute the average and standard deviation of the stochastic simulations.

Figures (4.9) and (4.11) show what happens when a low amount of noise is added to the unstable and stable systems respectively. Both systems demonstrate only a little deviation from the deterministic model. As we increase the noise, figures (4.10) and (4.12) are perhaps the most interesting as they show new behaviour not present in the deterministic model. Figure (4.10) shows how noise has changed the 'V' shape of the wave into a bump, making the entire system jump at the same time instead of a gradual signal propagation, and figure (4.12) shows how noise can cause certain parts of the otherwise stable system to jump into the excited state (the red dots) which may then propagate for a while and then dissipate. Figures (4.13) and (4.14) show the system can still undergo intermittent noise induced oscillations even for values of k_{synth} far away from the critical value.

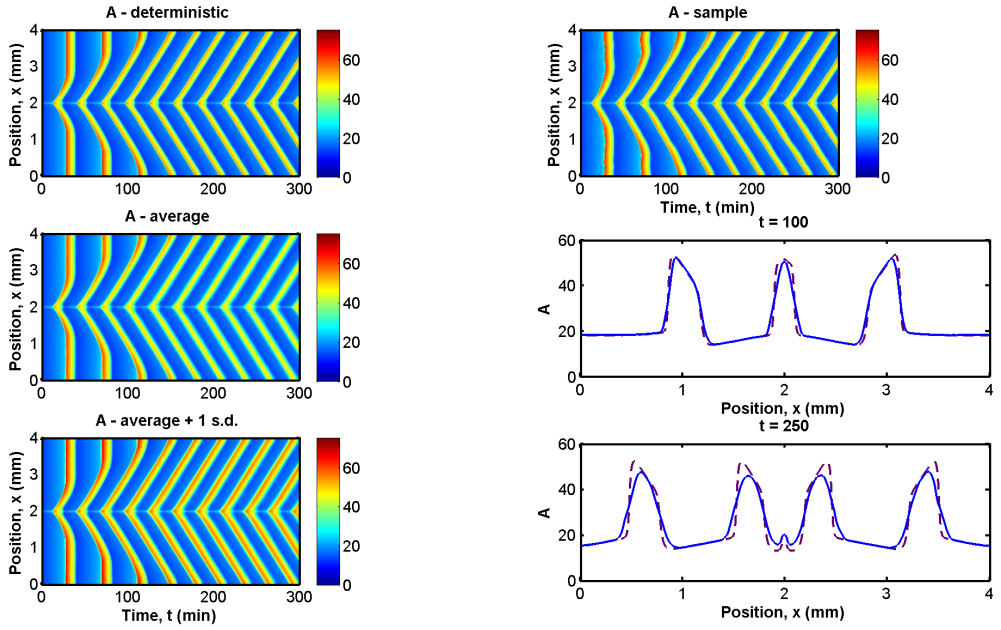

Figure 4.9: Plots for $k_{synth} = 1.5$ and $\sigma = 5$ in the original (unscaled) variables. 50 simulations of the system we run and the average and standard deviation were computed. Plots on the left column show the deterministic system, the average over 50 simulations, and the average plus one standard deviation. Plots on the right show one sample simulation. For the bottom two plots on the right, the solid blue line is the sample simulation and the dotted purple line is the corresponding deterministic system at the same point in time. The plots here show how the system is fairly robust to low levels of noise, retaining the 'V' shape of the wave, and not showing much variance between simulations.

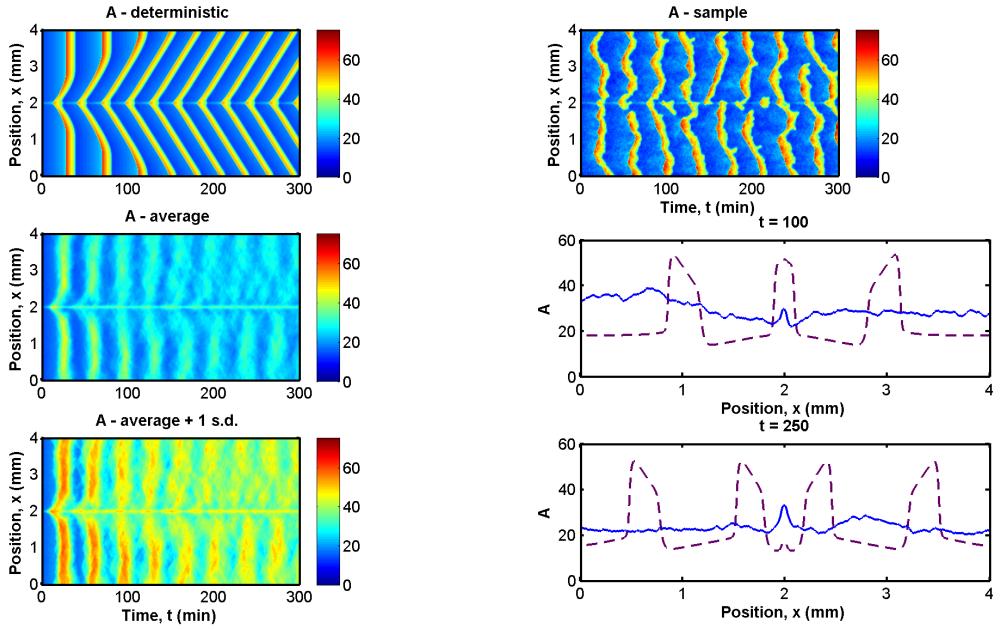

Figure 4.10: Plots for $k_{synth} = 1.5$ and $\sigma = 50$ in the original (unscaled) variables. In this case, the noise is 10 times stronger than before, and we see that 'V' shape is gone, but there is still clearly a traveling wave. On average, large parts of the system seems to jump all at once into its excited state, analogous to the spatially homogenous temporal instability in the Vilar model. Looking at the bottom left corner plot with shows the average + 1 standard deviation, we can also see that there is a probability that the system will enter its excited state earlier (i.e. lower refractory time).

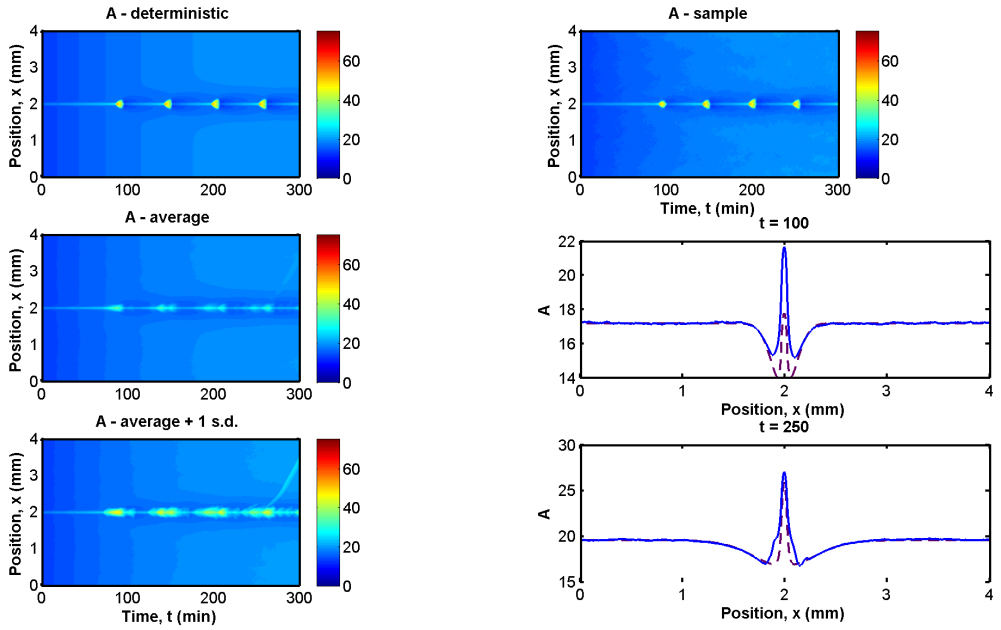

Figure 4.11: Plots for $k_{synth} = 0.7$ and $\sigma = 5$ in the original (unscaled) variables. In the stable state of the system, low levels of noise does not have much of an effect.

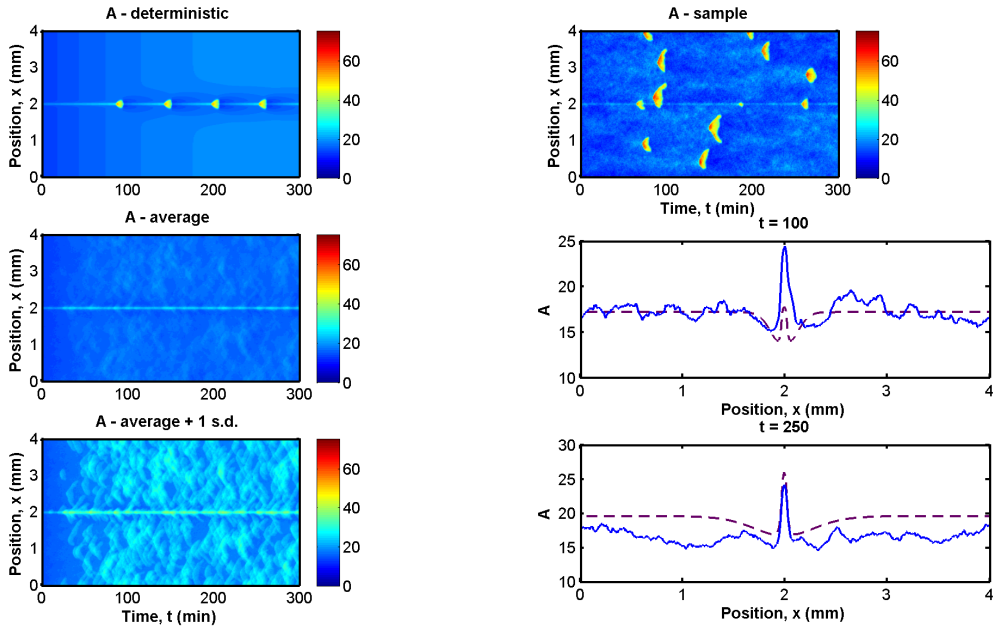

Figure 4.12: Plots for $k_{synth} = 0.7$ and $\sigma = 50$ in the original (unscaled) variables. When there is sufficient noise then we see that parts of the system can suddenly jump into the excited state and the signal can propagate outwards a little before settling back into the stable steady state.

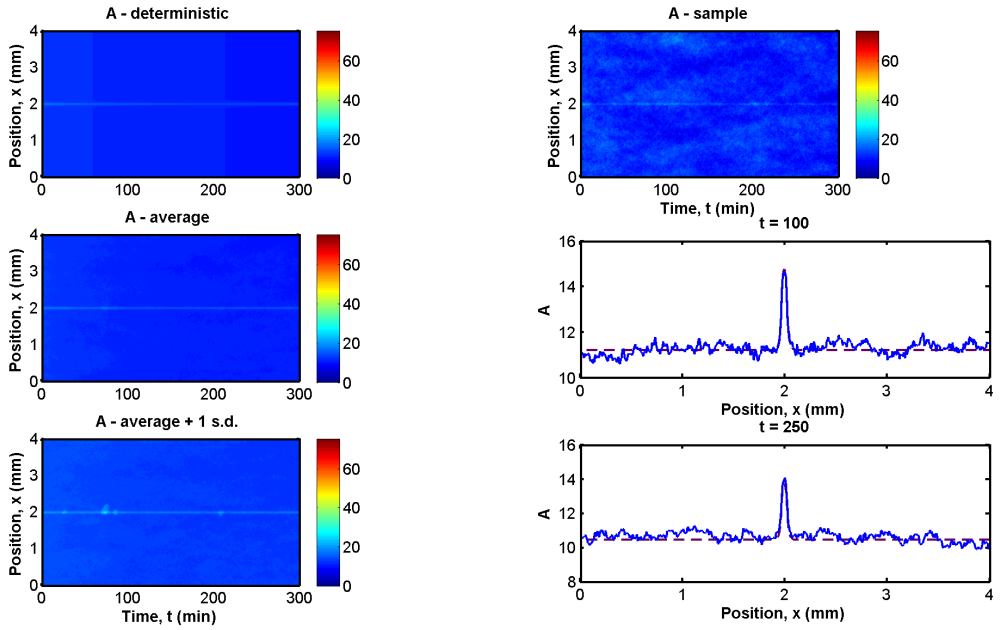

Figure 4.13: Plots for $k_{synth} = 0.4$ and $\sigma = 50$ in the original (unscaled) variables. Here the system is further away from the critical value of $k_{synth} = 0.76$ and the same level of noise that caused the previous plot to enter into the excited state is not enough this time.

4.3.2 Internal Noise

For internal noise, we will look at some Gillespie simulations of the system in different parts of the phase space based on the stability diagram we derived before in figure (4.3) and look at how adding a spatial dimension produces different results from the spatially homogenous model we studied earlier. As mentioned previously, the Linear Noise Approximation fails for this system, so we are unable to generate an analytic expression for the variance. Figure (4.15) demonstrates graphically how the variance envelope predicted by the Linear Noise Approximation increases rapidly to infinity after one oscillation.

Figures (4.16) and 4.17) show how intrinsic noise affects the system in its unstable state. The first set of plots shows results analogous to the situation with external noise where the noise disrupts the 'V' shape of the wave but there are still clearly temporal oscillations. Notice also that the wave starts in the stochastic simulation at an earlier time than the deterministic model.

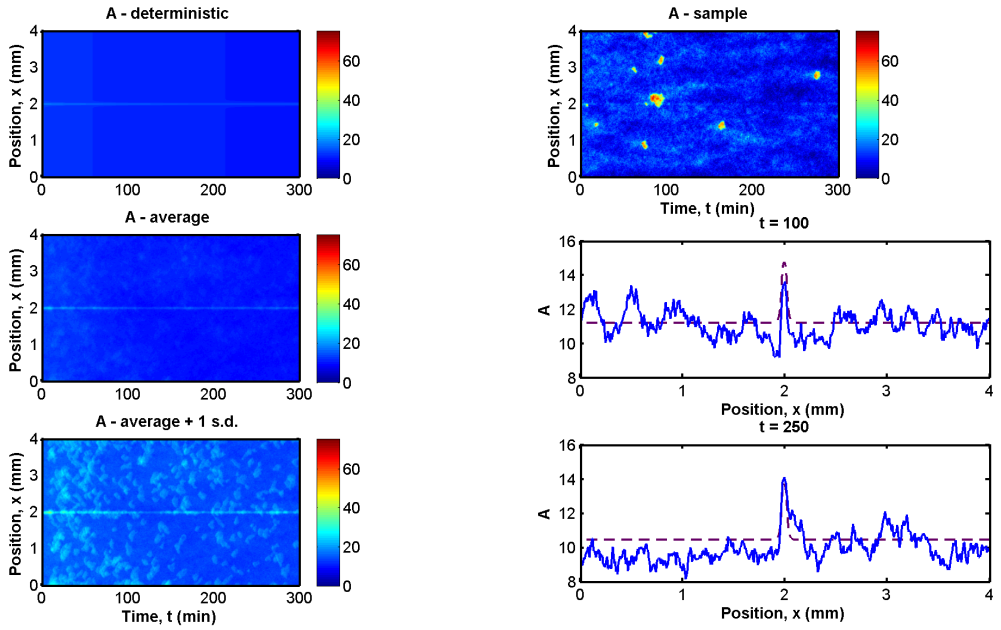

Figure 4.14: Plots for $k_{synth} = 0.4$ and $\sigma = 100$ in the original (unscaled) variables. Increasing the value of noise even more, we see that it is now possible for the system to enter into its excited state.

The second set of plots show how lowering the particle number to very low levels completely causes the wave to disappear. Although the system still oscillates, there does not seem to be any kind of spatially coordinated behaviour.

Figures (4.18) and (4.19) show how intrinsic noise affects the system in its stable state. Noise induced oscillations appear as expected (the two time slices on the right of the figures clearly show part of the system in it's excited state) but perhaps more interestingly figure (4.19) shows how we are able to form a nice traveling wave when there is a medium amount of noise, which is a case of stochastic resonance where medium amounts of noise produce the most regular results.

Finally, figure (4.20) is by far the most important result of this chapter. For this figure we have removed the higher concentrations of a_1 and b_1 in the middle of the domain so that there is nothing to spark the traveling wave to initiate from the middle. In the stable regime, the entire system simply converges to its spatially homogeneous stable steady state, but in the presence of

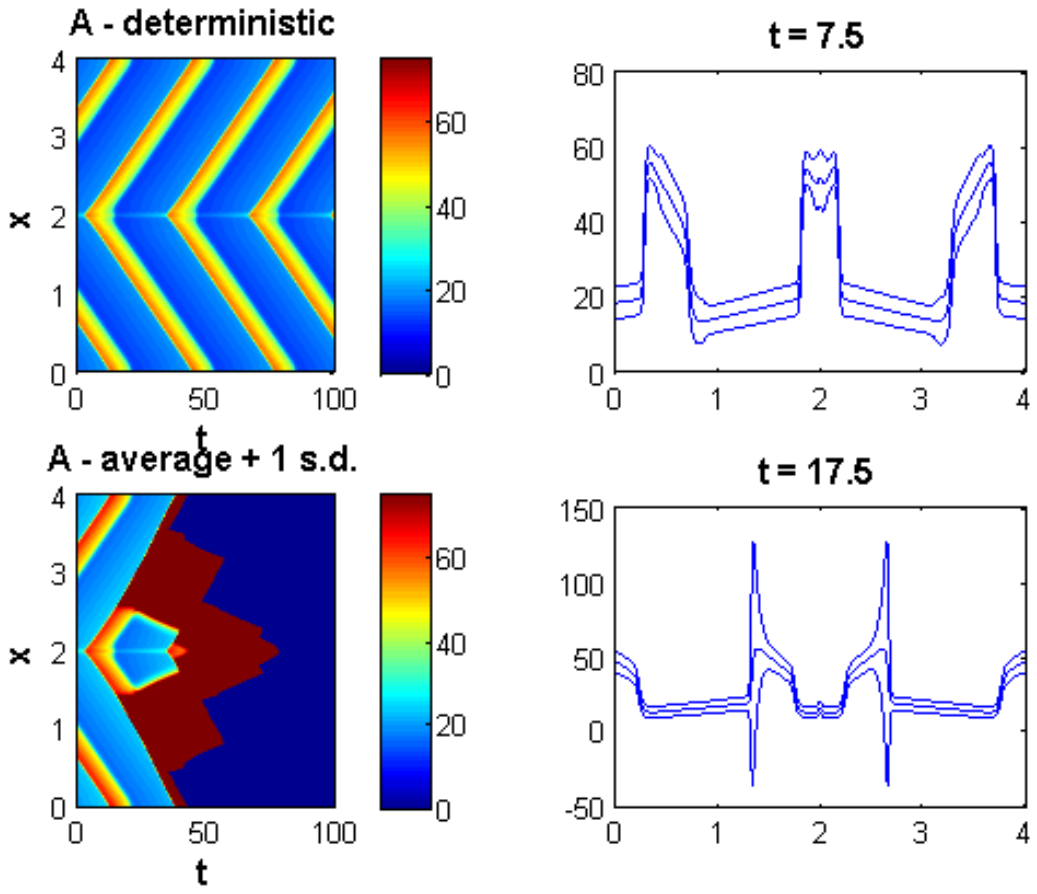

Figure 4.15: These are plots for $k_{synth} = 1.5$ and $\Omega = 1$ in the original (unscaled) variables with the variance envelope calculated using the extended version of the Linear Noise Approximation. As before, we see that the predicted variance at the peaks of the oscillations grow rapidly to infinity and the approximation fails.

noise, we see that oscillations occur in spatially heterogeneous manner. Again, only when the strength of the noise is just right is there a nice coherent traveling wave, when the noise is too strong we only get occasional isolated oscillations.

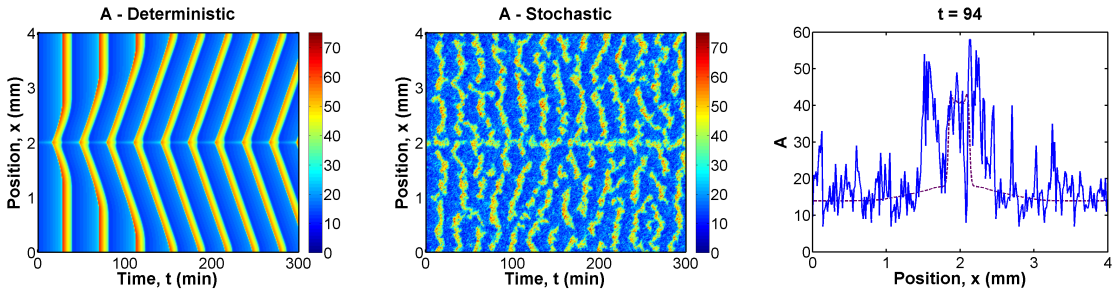

Figure 4.16: Sample internal noise simulation using the modified Gillespie algorithm as explained in Appendix B with $k_{synth} = 1.4$ and $\Omega = 5$ in original variables. Left most plot is the deterministic system. Middle plot shows a sample realization, and the right most plot shows a cross-section of this realization at fixed time point. For the right most plot the solid blue line represents the stochastic simulation, and the dotted purple line represents the deterministic system at the same time point.

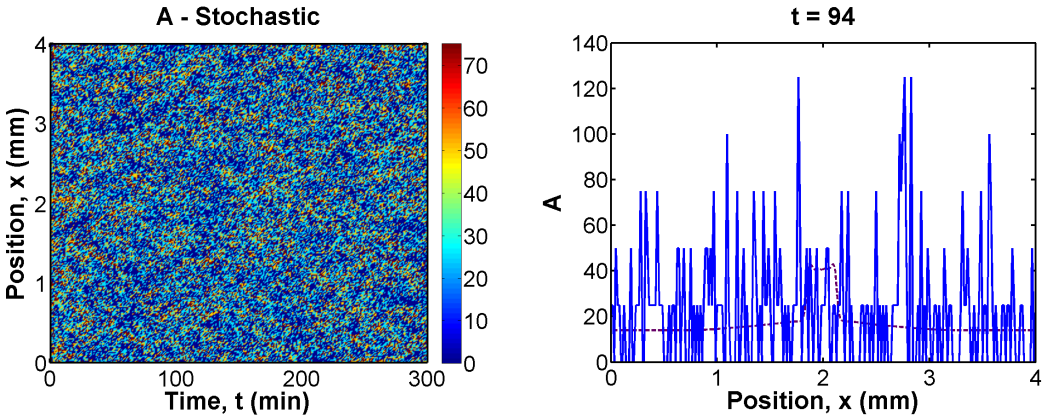

Figure 4.17: Sample internal noise simulation using the modified Gillespie algorithm as explained in Appendix B with $k_{synth} = 1.4$ and $\Omega = 1$ in original variables. Here we see how the traveling wave seems to have disappeared when the number of molecules is very small (and hence noise is very large).

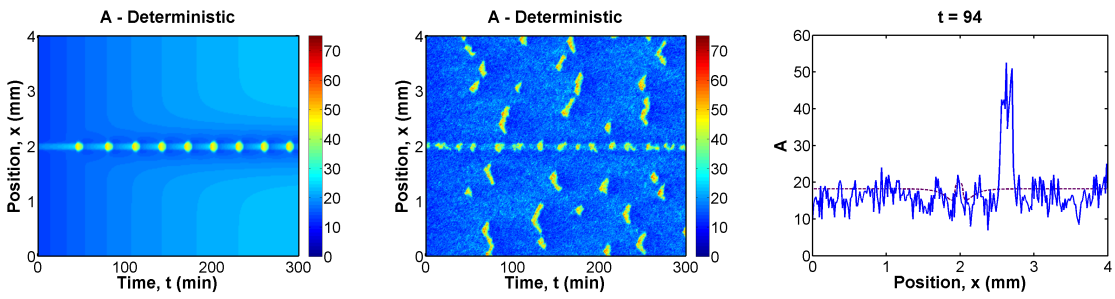

Figure 4.18: Sample internal noise simulation using the modified Gillespie algorithm as explained in Appendix B with $k_{synth} = 0.74$ and $\Omega = 2$ in original variables. Based on our earlier analysis of the spatially homogeneous model we expected there to be noise induced oscillations but not necessarily traveling waves. We see here that for this choice of k_{synth} and Ω there are some small localized traveling waves but they dissipate quickly.

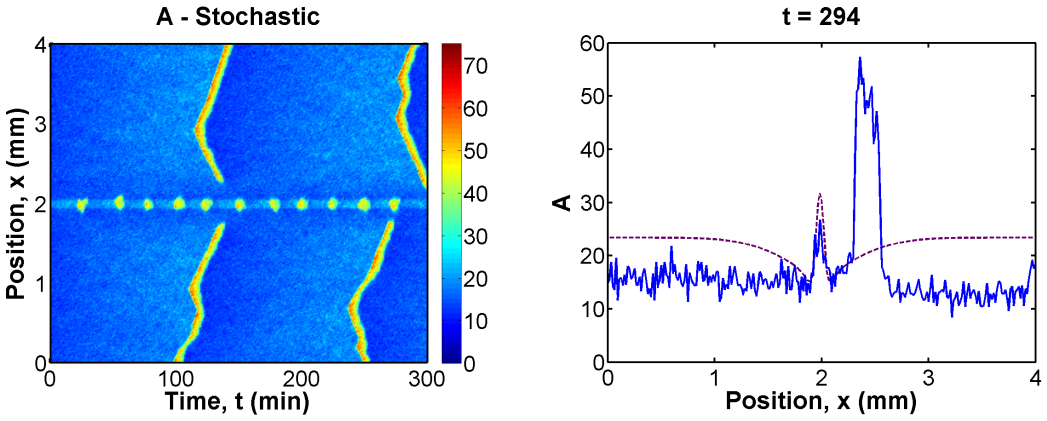

Figure 4.19: Sample internal noise simulation using the modified Gillespie algorithm as explained in Appendix B with $k_{synth} = 0.75$ and $\Omega = 5$ in original variables. If we increase Ω, we increase the number of molecules and this reduces the amount of noise. However, in this case it is possible to generate a nice looking traveling wave in the deterministically stable system. This could be a case of stochastic resonance as mentioned briefly in our earlier analysis of the Vilar model where medium amounts of noise produce well behaved results.

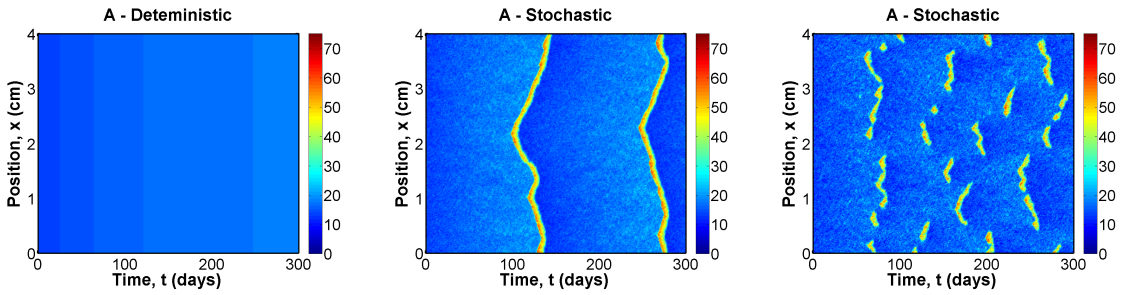

Figure 4.20: The plots show the system with the higher concentrations of a_1 and b_1 in the middle removed. Using the same $k_{synth} = 0.75$ as in figure (4.19) but with, from left to right, $\Omega = \infty$ (deterministic limit), $\Omega = 5$, and $\Omega = 2$. These plots show how definitively how the deterministically stable system can be induced into its excited state in the presence of noise. Moreover, it demonstrates the effects of stochastic coherence as the middle plot with a medium amount of noise produces a nice clear traveling wave signal, where as the right plot with more noise can only generate occasional and brief blips.

4.4 Analysis and Conclusion

For both extrinsic and intrinsic noise we saw how noise disrupts the 'V' shape of the traveling wave in the unstable mode of the system, and can generate noise induced traveling waves in the stable mode of the system. Just on a purely qualitative level, figure (4.21) demonstrates graphically how these noisy systems more closely match the experimental results. Figure (4.22) shows an alternate way of analyzing the traveling wave by looking at the Fourier spectra of the system. It doesn't offer any particular new insight but does demonstrate mathematically that there are spatio-temporal correlations in the noise induced system.

For the system in its unstable mode, we saw for both kinds of noise that noise can reduce the refractory time of the system and cause large parts of the system to oscillate at the same time, instead of sequentially like in the deterministic system. Physically, this means that noise can cause the system to enter into its excited state earlier and that signal propagation is faster in some regions than in others. Internal noise also allows for the wave to be completely disrupted under extreme conditions, which represents no signal propagation within the system.

In the stable mode, both kinds of noise were able to produce (intermittent) noise induced

oscillations, which means that the system is able to enter its excited state and propagate that excited state even in situations when the deterministic system is unable to do so. Moreover, the internal noise simulations produced a coherent looking traveling wave only when there was a medium amount of noise present which means that systems that are too small or too large would not be able to produce traveling waves.

In terms of interpreting these results as applicable to metastasis, this model only represents the first step in which a normal tumour cell becomes a metastatic tumour cell. The normal state is represented by the lower stable steady state of the system, and the metastatic state is represented when the system enters into the high state temporarily when it under goes oscillations. The refractory time of the excitable system can be used to explain why tumours normally do not become metastatic immediately, and noise induced oscillations broaden the possible situations under which the tumour can make such a change. External noise can be used to explain why tumours in different parts of the body have different rates of metastasis, by modeling environmental factors as extrinsic noise parameters. Internal noise could explain why only tumours of a certain size can undergo metastasis as we saw that too much noise (i.e. very small tumours) can disrupt the signalling process and only a moderate amount of noise (i.e. a moderately sized tumour) can produce noise induced oscillations.

Future work would need to identify analogous activator-inhibitor pairs appropriate to the type of metastasis being studied to apply the model. For external influences on the system, one would need to fit the system to some data to determine the noise amplitude σ and possibly consider a more complicated σ that may depend on space and time. For internal noise one would need to consider the typical size of the tumour to see what value of Ω would be appropriate.

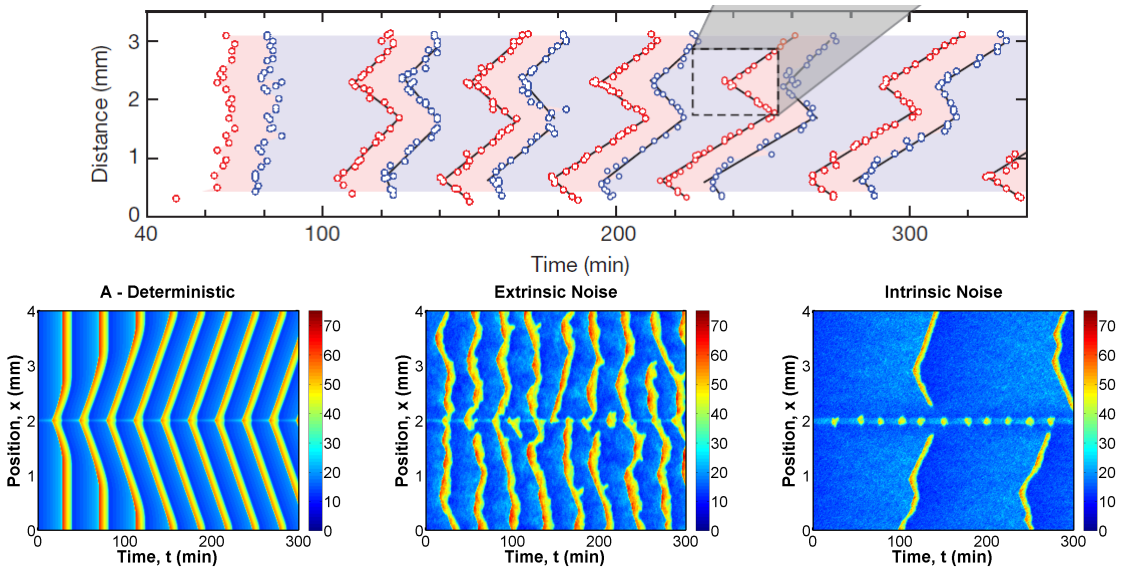

Figure 4.21: The top plot is from Chang and Ferrel[31] and shows some experimental results of the Xenopus egg in a lab. The red dots in the top plots indicate places where mitosis occurred and the blue dots indicate where the cell reformed into a normal rest state. These two states are represented mathematically by the peaks and troughs of the oscillations in the model. The bottom plots are sample numerical simulation results from this section. Just qualitatively, one can see that the two plots with noise more closely match those of the experiment and represents the random nature of actual cell signalling more accurately. Both plots with noise also recreate the phenomena of the top half of the system moving at a different speed from the bottom half. However, the sharpening of the 'V' shape in the deterministic model is lost in the stochastic models and that possibly needs to be represented somehow.

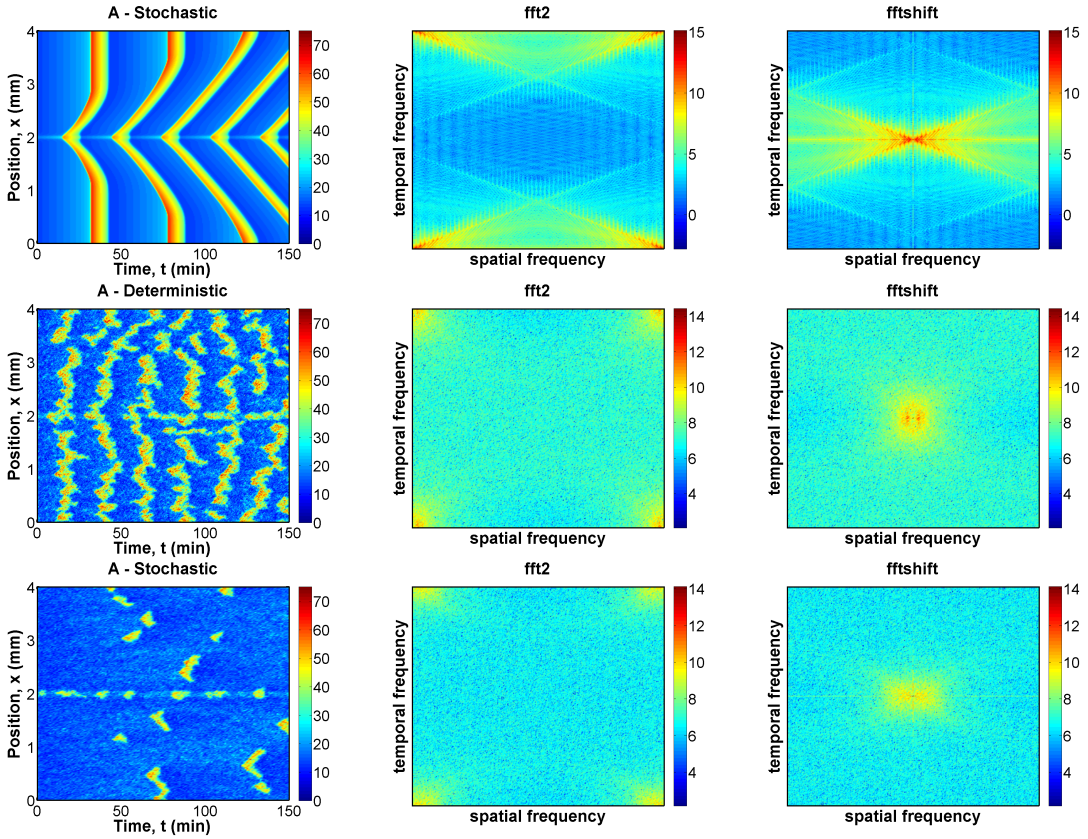

Figure 4.22: A more quantitative way of identifying traveling waves is to look at the fourier spectra and identify space-time correlations (i.e. peaks in the spectra away from the zero). Left most column are plots in normal space-time. Middle column is the (log-scaled) fourier spectra of the data, and the right most column uses the fftshift command in matlab which re-orientates the plot so that the low frequencies are in the middle, giving us a more intuitive representation of the fourier spectra. The top row is the deterministic case, the middle row is noise in the unstable mode, and the bottom row is noise in the stable mode. The diagonal lines in the top right plot tells us that spatio-temporal oscillations at certain space and time frequencies in the deterministic model (which is exactly what we would expect) and as we move down we see that there is definitely a peak away from the origin for the unstable mode with noise, and possibly even in the case for noise induced osculations in the stable mode even though the plot doesn't quite look like a traveling wave.

Chapter 5

Summary, Conclusion, and Future Direction

In this thesis we examined the effects of both extrinsic and intrinsic noise on a model for tumour growth and a model for mitosis. We saw that the difference between the two kinds of noise was in its mathematical treatment: extrinsic noise required solving a stochastic PDE, while intrinsic noise required solving a master equation. External noise is simple to implement and understand but the noise amplitude parameter σ is ill defined physically as it could represent any number (or any combination) of external influences. Internal noise is more difficult to understand but it represents the inherent randomness of a real physical system. The Linear Noise Approximation allows us to approximate internal noise as external, but we saw how it failed for noise induced oscillations and limit cycle behaviour.

For the reaction-diffusion tumour growth model, we found that both kinds of noise produced fairly intuitive results that agreed with each other. We saw in the case of extrinsic noise that increasing the strength of the noise increased the variance in visible tumour diameter and survival time in an almost linear fashion. Both kinds of noise agreed that increasing diffusivity led to a quicker and surer (smaller variance) survival time, and both also agreed that, when chemotherapy

is added to the model, the variance is roughly 3-4 days regardless of the number of doses. Although the uncertainty in this model is relatively small, we nonetheless have provided a method for calculating the error-bar for tumour diameter and survival time, which could eventually lead to more meaningful results with an improved model.

For the mitotic trigger wave model we used an excitable system that produced a traveling wave under certain conditions. This traveling wave represents a signal propagating from the centre of the embryo out towards the edges that tells the cells to undergo mitosis. Although the Linear Noise Approximation fails to predict the variance envelope in this case for intrinsic noise, we were still able to use it to determine the threshold for noise induced oscillations. Numerical simulations of both kinds of noise then allowed us to verify these noise induced oscillations and demonstrated possible stochastic coherence effects with a medium amount of noise. These noise induced oscillations in what would normally be a stable deterministic system demonstrates that travelling waves can occur under a broader range of conditions, and means that mitosis might occur more readily than one might expect. In terms of a possible interpretation for a metastasis model, noise induced oscillations might represent the ability for a tumour to suddenly become metastatic due to inherent random fluctuations or external influences.

5.1 Future Direction

The analytical methods developed in chapters 2 and 3 are general methods that are applicable to any reaction-diffusion type model. However, the numerical simulations for the tumour growth model were performed on a simple square 2D grid, so the most natural extension would be to extend the simulations to 3D and to incorporate a more accurate domain with a distribution of white and grey matter and properly shaped boundaries. This domain need not be specific to any one patient as we can tune the strength of the noise to account for the uncertainty in the domain (and possibly make the diffusion coefficient a random function as well). We can also examine different therapeutic strategies easily using the same general principles described in these two

chapters.

For the mitotic trigger wave model we were able to show how a specific level of noise was able to induce a sustained traveling wave within the embryo. Noise induced oscillations might possibly be used to explain how embryos survive in non-ideal situations for example (such as some kind of disease or malnutrition etc). Future work for a possible interpretation as a metastasis model would need to identify the activator-inhibitor pair appropriate for the particular tumour of interest. Once they have been identified we can then determine whether Chang and Ferrel's model is appropriate or whether a different excitable model needs to be used. The qualitative results pertaining to noise induced oscillations and traveling waves would still stand, but the details would differ. In particular, the fact that traveling waves do not occur when there is too much noise (i.e. when the population number is low, such as in the initial stages of tumour formation) could be a possible explanation for why metastasis only occurs after a tumour has reached a certain size.

APPENDICES

Appendix A

Finite Difference Scheme for Numerical Simulation of the Stochastic Heat Equation

Here are some details on how the stochastic partial differential equation was simulated numerically. The Euler method in this section applies directly to the mitotic trigger wave model in 1 dimension for chapter 4 and the tumour model in 2 dimensions for chapter 2. The deterministic counterparts were simulated by simply removing the random forcing in the preceding numerical schemes (i.e. setting the noise amplitude to zero) which makes it a standard Euler scheme[56]. A fast fourier transform based spectral scheme[56] modified to 4 dimensions was used to numerically integrate the equation for the cumulant in chapter 3.

A.1 One Dimension

We will consider the stochastic heat equation first in one dimension. The most general form is given by

$$\frac{\partial u}{\partial t} = D\nabla^2 u + f(x,t,u) + \sigma(x,t,u)\dot{W}(x,t), \tag{A.1}$$

- $u(x,t)$ is some quantity if interest at position x and time t.
- D is the diffusion coefficient (not random),
- $f(x,t,u)$ is the external forcing term (deterministic),
- $\sigma(x,t,u)$ is the amplitude function for the noise (deterministic),
- $\dot{W}(x,t)$ is space-time white noise (defined below),

with appropriate boundary and initial conditions.

We will define the space-time white noise function $\dot{W}(x,t)$ by specifying its first two moments

$$\langle \dot{W}(x,t) \rangle = 0, \tag{A.2}$$

$$\langle \dot{W}(x,t)\dot{W}(x',t') \rangle = \delta(x-x')\delta(t-t'). \tag{A.3}$$

The simplest numerical discretization of this equation would be the forward Euler scheme[35][58]

$$u_i^{m+1} = u_i^m + \Delta t \left[D\frac{u_{i+1}^m - 2u_i^m + u_{i-1}^m}{(\Delta x)^2} + f_i^m + \sigma_i^m \frac{W_i^m}{\Delta x \Delta t} \right], \tag{A.4}$$

where

- $u_i^m = u(i\Delta x, m\Delta t)$,
- $f_i^m = f(i\Delta x, m\Delta t, u_i^m)$,
- $\sigma_i^m = \sigma(i\Delta x, m\Delta t, u_i^m)$,
- and W_i^m are i.i.d. $N(0, \Delta x \Delta t)$ random variables evaluated at each grid point $i\Delta x$ and each time index $m\Delta t$.

According to Davie and Gaines[35], if the initial condition $u_0(x)$ is Holder continuous with exponent $1/2$ (i.e. $|u_0(x) - u_0(y)| \leq C|x-y|^{1/2}$ for some $C > 0$), then the above numerical scheme converges for $\Delta t/(\Delta x)^2 < 1/2$ (see theorem 1.1 on page 122 of their paper). Higher order methods, such as those analogous to implicit and Crank-Nicholson schemes for PDEs, exist for stochastic PDEs, but both Davie and Gaines[35], and Chong and Walsh[58] demonstrate that this simple Euler scheme is in a sense already one of the most accurate. Alternate methods for numerically integrating stochastic PDEs, that are not akin to the deterministic counterparts exist, for example, as described by Brissaud and Frisch[59] and van Kampen[22] where they give methods for approximating the first and second moments of the underlying stochastic process.

A.2 Two Dimensions

For the two dimensional tumour model in chapter 2 we were considering the specific equation

$$\frac{\partial n}{\partial t} = D\nabla^2 n + \rho\left[1 + A(\mathbf{x}, t)\right] n, \tag{A.5}$$

where

- $n(\mathbf{x}, t)$ is the number density of cells at position $\mathbf{x}$ and time t.
- D is the diffusion coefficient (not random),
- ρ is the growth rate,
- $A(\mathbf{x}, t)$ is a random function of time and space,

with no flux boundary conditions, and a gaussian or delta initial condition in the middle of the domain.

We also set $A(\mathbf{x},t)$ = $A\eta(\mathbf{x},t)$, where A is a constant, and $\eta(\mathbf{x},t)$ is once again given by

$$\langle \eta(\mathbf{x},t) \rangle = 0, \tag{A.6}$$

$$\langle \eta(\mathbf{x},t)\eta(\mathbf{x}',t') \rangle = \delta(\mathbf{x}-\mathbf{x}')\delta(t-t'). \tag{A.7}$$

A straight forward extension of the 1 dimensional numerical scheme to 2 dimensions, applied to the specific problem above gives

$$u_{i,j}^{m+1} = u_{i,j}^{m} + \Delta t \left[D\frac{u_{i+1,j}^{m} - 2u_{i,j}^{m} + u_{i-1,j}^{m}}{(\Delta x)^2} + D\frac{u_{i,j+1}^{m} - 2u_{i,j}^{m} + u_{i,j-1}^{m}}{(\Delta y)^2} + \rho\left(1 + A\cdot\frac{W_{i,j}^{m}}{\Delta x \Delta y \Delta t}\right) u_{i,j}^{m} \right] \tag{A.8}$$

where

- $u_{i,j}^{m} = u(i\Delta x, j\Delta y, m\Delta t)$,
- and $W_{i,j}^{m}$ are i.i.d. $N(0, \Delta x \Delta y \Delta t)$ random variables evaluated at each grid point (i,j) and each time index m.

Appendix B

Gillespie's Algorithm

This section of the Appendix explains how Gillespie's Algorithm works for simulating trajectories of a stochastic process, and describes how diffusion can be added to the algorithm.

B.1 Basic Algorithm

Following Gillespie's paper from 1977[40], this section is a short explanation of the exact simulation algorithm for stochastic processes governed by a master equation named after him. For a system of chemical reactions, in order to simulate trajectories of the master equation, we need to know two things:

- the time for the completion of the next reaction τ
- and the reaction that occurred, index these μ

Estimate

$$P(\mathbf{n} + \Delta\mathbf{n}, t + \tau | \mathbf{n}, t) d\tau, \tag{B.1}$$

the probability that, given the system is in the state $\mathbf{n}$ at time t, the next jump occurs between $t + \tau$ and $t + \tau + d\tau$, carrying the state from $\mathbf{n}$ to $\mathbf{n} + \Delta\mathbf{n}$ (caused by reaction of type μ). Since

the stoichiometry encodes how the state will change with each reaction, just knowing the type of reaction is enough.

- The stochastic process of interest is Markov.
- Non-reactive (elastic) collisions occur much more frequently than reactive (inelastic) collisions. This ensures ***spatial homogeneity*** by "randomizing and uniformizing the position of the particles" (Gillespie, 1976), which is another way of saying that the system returns quickly to thermal equilibrium (constant temperature) between each reactive collision.
- Only one reaction occurs in the time interval $d\tau$.

Let $q(\mathbf{n}, t; \tau)$ be the probability that ***any*** reaction will occur in the interval t to $t + \tau$. Then, over an infinitesimal interval dt we have that

$$q(\mathbf{n}, t; dt) = \nu_1(\mathbf{n})dt + \nu_2(\mathbf{n})dt + ... = \left[\sum_{j=1}^{N} \nu_j(\mathbf{n})\right] dt \equiv a(\mathbf{n})dt. \tag{B.2}$$

One can then show that, for a non-infinitesimal interval, we have

$$q(\mathbf{n}, t; \tau) = 1 - e^{-a(\mathbf{n})\tau} \tag{B.3}$$

this means that the probability of ***no*** reaction occurring in the time interval τ is

$$1 - q(\mathbf{n}, t; \tau) = e^{-a(\mathbf{n})\tau}. \tag{B.4}$$

Thus,

$$P(\mathbf{n}+\Delta\mathbf{n}, t+\tau|\mathbf{n}, t)d\tau \tag{B.5}$$

$$= \text{Probability that no reaction occurs in the interval } [t, t+\tau] \tag{B.6}$$

$$\times \text{ Probability that any reaction occurs in the interval } [t+\tau, t+\tau+d\tau] \tag{B.7}$$

$$\times \text{ Probability that it was reaction } \mu \text{ that occurred,} \tag{B.8}$$

$$= e^{-a(\mathbf{n})\tau} \times a(\mathbf{n})d\tau \times a_\mu(\mathbf{n}). \tag{B.9}$$

Note that

$$a_\mu(\mathbf{n}) = \frac{\nu_\mu(\mathbf{n})}{a(\mathbf{n})}, \tag{B.10}$$

which, upon substitution (and a bit of change in notation) into the preceding equation gives us Gillespie's original result

$$P(\tau, \mu) = \nu_\mu e^{-a\tau}. \tag{B.11}$$

This first form of the equation is more useful since

$$P(\mathbf{n}+\Delta\mathbf{n}, t+\tau|\mathbf{n}, t) = \underbrace{a(\mathbf{n})e^{-a(\mathbf{n})\tau}}_{\text{Exponential distribution}} \times \left[\frac{\nu_\mu(\mathbf{n})}{a(\mathbf{n})}\right] \tag{B.12}$$

This allows us to pick τ and μ using a random number generator, which we can then use to update the time and state of the system before the next reaction occurs. A schematic diagram of how this works is shown in figure (B.1), which is from Gillespie's paper[40].

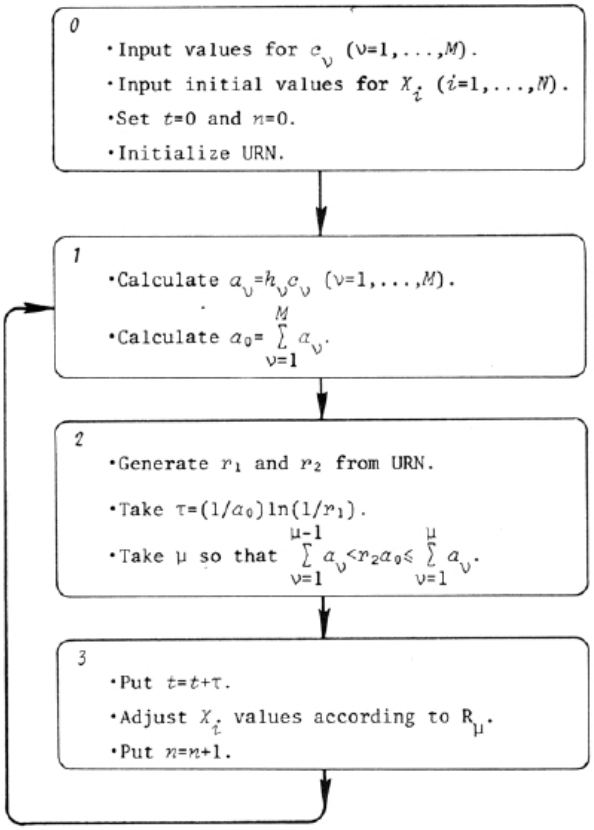

Figure 2. Schematic of the stochastic simulation algorithm.

Figure B.1: Figure from Gillespie's 1977 paper showing the main loop of the algorithm.[40].

B.2 Algorithm for Spatially Extended Processes

The strategy here is to treat diffusion as just another kind of chemical reaction. In order to turn diffusion into a reaction we will adapt Smoluchowski's analysis of Brownian motion (as explained by Kac[47], since Smoluchowski's original 1906 paper is in German[48]) to develop a relationship between the diffusion constant and transition rate. A consequence of treating diffusion as a reaction is that it will greatly increase the size of the stoichiometry matrix and propensity vector, and hence increase the computing time of the numerical simulation, especially if the spatial domain is discretized over a fine grid.

Let us consider the simplest case where there is only one reactant species and one dimension (say a straight line with reflecting boundary conditions at the two ends). The trick is now to discretize the space into separate bins, and to consider the reactants in each bin to be *different* species of reactants, that means the state of the system is now expressed as a vector $\mathbf{N} = (N_1, N_2, ...)$, where N_i is the number of reactants in bin i. We then consider movement between bins to be a reaction that decreases the number of reactants in the original bin, and increases the number of reactants in the destination bin. Again for simplicity, in one dimension we will only allow one reactant to move at each time, and only into an adjacent bin (either left or right, with reaction rates D_L and D_R), illustrated in figure (B.2).

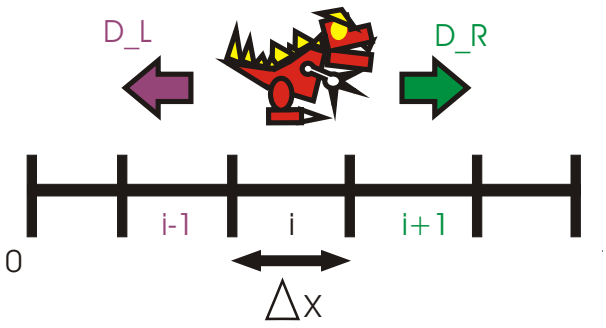

Figure B.2: In one dimension the reactant can either move to the left (with transition rate D_L) or to the right (with transition rate D_R) .

As a reaction scheme, we can write diffusion in the following way

$$N_i \xrightarrow{D_L} N_{i-1}, \tag{B.13}$$

$$N_i \xrightarrow{D_R} N_{i+1}. \tag{B.14}$$

This formulation of diffusion is analogous to a random walk for each reactant species. For simplicity, we will assume that diffusion is equal in all directions so that $D_L = D_R$. Then the situation is that of an unbiased random walk, and the master equation is

$$P(x, t + \Delta t) = \frac{1}{2}P(x - \Delta x, t) + \frac{1}{2}P(x + \Delta x, t), \tag{B.15}$$

where Δt is the time step, and Δx is the bin size. This is exactly Smoluchowski's formulation of Brownian motion. To find a relationship between the diffusion constant D and the transition rates D_L and D_R, we subtract $P(x, t)$ from both sides and divide by Δt to get

$$\frac{P(x, t + \Delta t) - P(x, t)}{\Delta t} = \left(\frac{\Delta x^2}{2\Delta t}\right) \frac{P(x - \Delta x, t) - 2P(x, t) + \frac{1}{2}P(x + \Delta x, t)}{\Delta x^2}, \tag{B.16}$$

which we recognize as the discrete version of the diffusion equation. Thus we must equate

$$D = \frac{\Delta x^2}{2\Delta t}, \tag{B.17}$$

and hence the discrete diffusion rate is $\frac{2D}{\Delta x^2}$ (since it needs to have dimensions of 1/time). This quantity is the total diffusion rate, it is the sum of both the left and right rates $D_L + D_R$; since we assumed that they are equal, we have that

$$D_L = D_R = \frac{D}{\Delta x^2}. \tag{B.18}$$

With these transition rates, it is then straightforward to modify the Gillespie algorithm by extending the propensity vector in a similar manner to the state vector (see figure (B.3)), and by

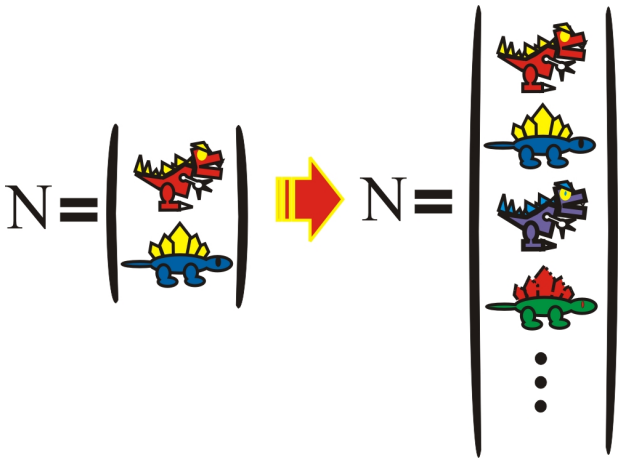

Figure B.3: Illustration of how the state vector changes. This illustration depicts two species of reactants in each bin (a red and blue dinosaur) and our extended algorithm then considers the species in each bin to be different species (different coloured dinosaurs).

extending the transition matrix as illustrated in figure (B.4).

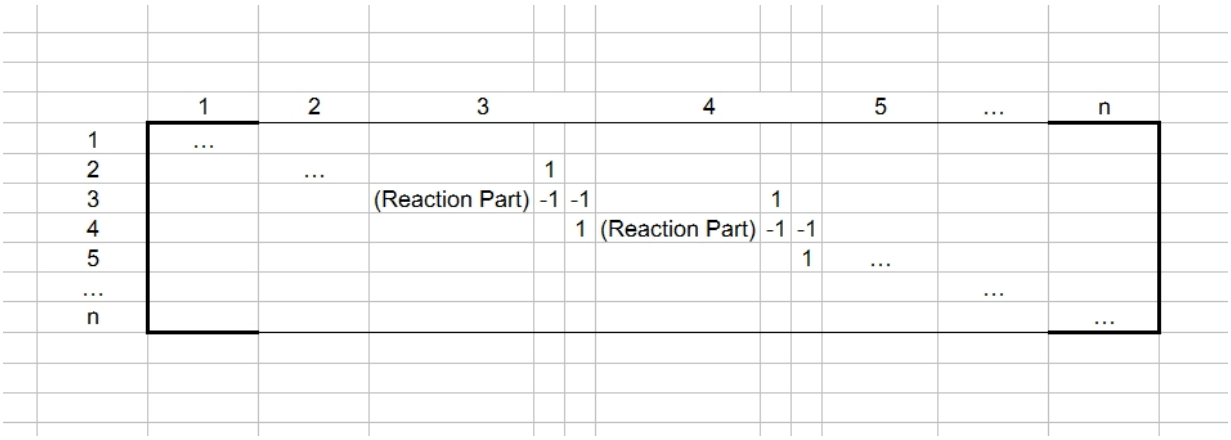

Figure B.4: Schematic diagram of the transition matrix in 1D. A generic middle section is shown where we encode the reaction part as in the original Gillespie algorithm, but then we also append two new reactions (movement left and right) which reduces the number of reacts in the original bin by 1 and increases the number of reacts in the adjacent bin by 1.

Appendix C

More Details On Numerical Simulations

This part of the Appendix provides more details on the grid size and time steps of the numerical simulations, and also lists the values of the parameters for the mitotic trigger wave model in chapter 4.

C.1 Tumour Model

Recall for the tumour model in chapter 2 we have

$$\frac{\partial n}{\partial t} = D\nabla^2 n + \rho\left[1 + \sigma(\mathbf{x}, t)\right] n, \tag{C.1}$$

where D and σ were varied. The numerical simulations were performed using the method in Appendix A on a 10cm by 10cm sized domain, with Neumann boundary conditions on all sides. Figure (C.1) demonstrates how a grid size of $2^5 \times 2^5$ gave virtually the same results as a grid size of $2^8 \times 2^8$ for the total number of cells and visible tumour diameter. The lower grid size was then chosen for the simulations to save time and computational cost as we needed to run a large ensemble of simulations.

For the time step, Δt, was chosen to be 1 day and the total simulation time was chosen so

that the tumour had ample time to reach a visible diameter of 6cm (approximately 400 days without chemotherapy and 900 days with chemothrapy). This Δt was chosen after some testing that showed a Δt of 1 day gave stable simulations and produced similar results to a Δt of 0.1 days. As explained by Chong and Walsh[58], large time steps are not recommended as they may smooth over the effects of the stochastic process, however, since we are only interested in the mean and variance over a large ensemble of simulations, some smoothing is not a big concern.

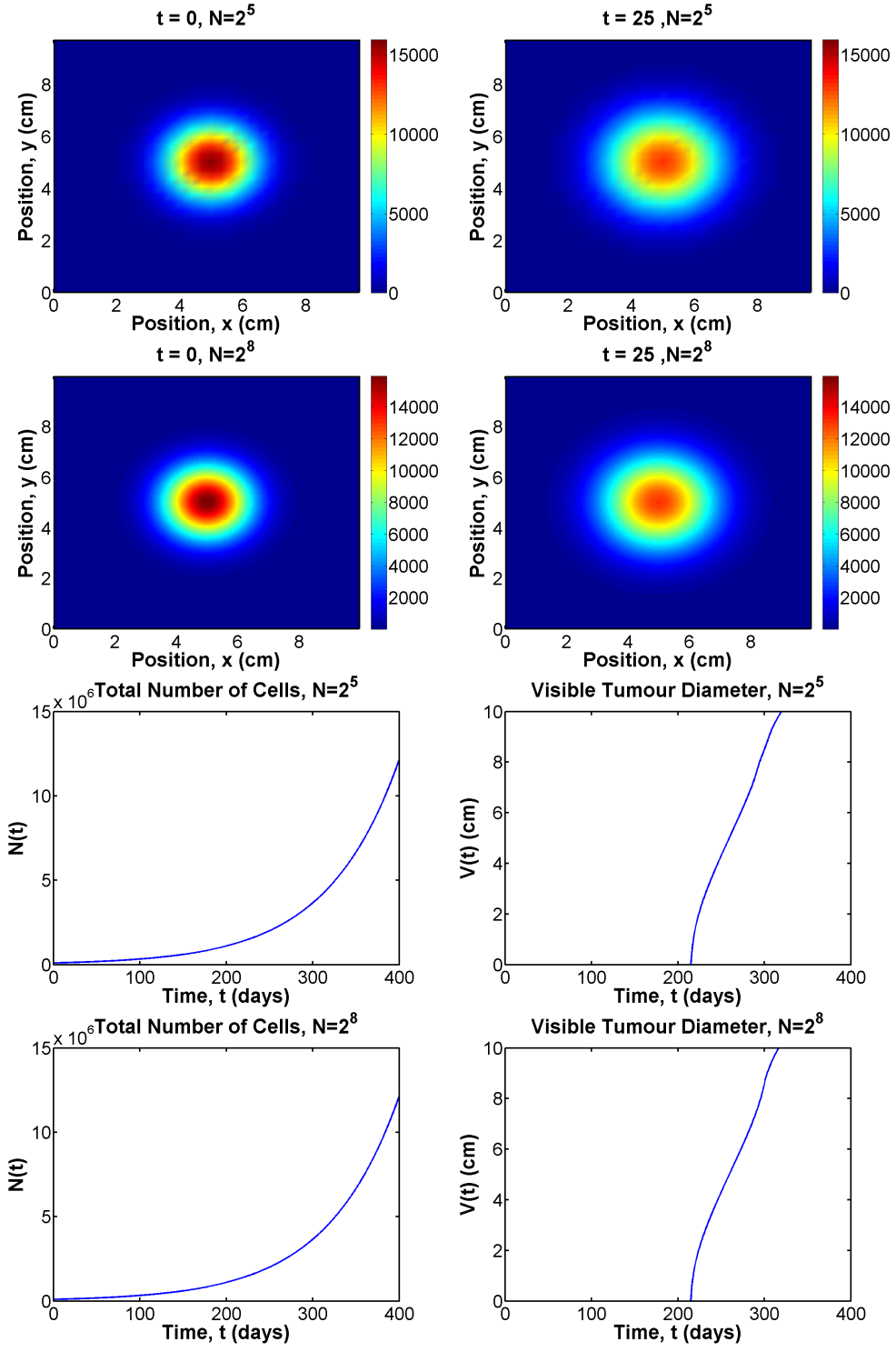

Figure C.1: Here are plots that compare the results from a grid size of $2^5 \times 2^5$ (first row) to $2^8 \times 2^8$ (second row). From the third and fourth rows, we can see that both grid sizes gave nearly identical results for the total number of cells and visible tumour diameter

C.2 Mitotic Trigger Wave Model

From Chang and Ferrel[31] the equations for the mitotic trigger wave model describe the synthesis and degradation of cyclin B1-Cdk1 complexes and a switch between its active and inactive phosphorylation states. In particular it is regulated by the proteins Cdc25, Wee1, and APC/C (denoted as deg in the preceding equations as it governs the degradation). A schematic of how each protein affects B1-Cdk1 is shown in figure (C.2).

As written in chapter 4, the deterministic equations for the mitotic trigger wave model are as follows:

$$\begin{aligned}\frac{dA}{dt} &= D\nabla^2 A + k_{synth} + \left(a_1 + b_1\frac{A^{n_1}}{E_1^{n_1} + A^{n_1}}\right) I - \left(a_2 + b_2\frac{E_2^{n_2}}{E_2^{n_2} + A^{n_2}}\right) A \\ &\quad - \left(a_3 + b_3\frac{A^{n_3}}{E_3^{n_3} + A^{n_3}}\right) A, \qquad \text{(C.2)} \\ \frac{dI}{dt} &= D\nabla^2 I - \left(a_1 + b_1\frac{A^{n_1}}{E_1^{n_1} + A^{n_1}}\right) I + \left(a_2 + b_2\frac{E_2^{n_2}}{E_2^{n_2} + A^{n_2}}\right) A \\ &\quad - \left(a_3 + b_3\frac{A^{n_3}}{E_3^{n_3} + A^{n_3}}\right) I. \qquad \text{(C.3)}\end{aligned}$$

where

- A = Cdk1$_{act}$, the active phosphorylation state of B1-Cdk1,
- I = Cdk1$_{inact}$, the inactive phosphorylation state of B1-Cdk1,
- D = 600 μm^2/min,
- k_{synth} = 1.5nM/min (this parameter was varied in chapter 4),
- $a_1 = a_{cdc25}$ = 0.8min^{-1},
- $b_1 = b_{cdc25}$ =4min^{-1},
- $n_1 = n_{cdc25}$ = 11,

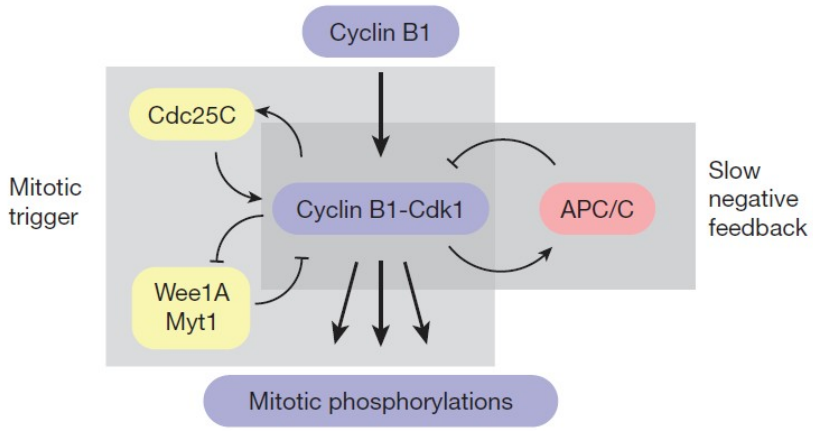

Figure C.2: A schematic of system described by the mitotic trigger wave model. Figure from Chang and Ferrel[31].

- $E_1 = EC50_{cdc25}$ =35nM,
- $a_2 = a_{wee1}$ = 0.4min^{-1},
- $b_2 = b_{wee1}$ =2min^{-1},
- $n_2 = n_{wee1}$ = 3.5,
- $E_2 = EC50_{wee1}$ =30nM,
- $a_3 = a_{deg}$ = 0.01min^{-1},
- $b_3 = b_{deg}$ =0.06min^{-1},
- $n_3 = n_{deg}$ = 17,
- $E_3 = EC50_{deg}$ =32nM,

and $EC50_a$ is the "half maximal effective concentration" of the protein a, which is the concentration that produces a response halfway between the baseline and maximum. Also, a_1 and b_1 had concentrations that were 50% higher in the middle of the domain.

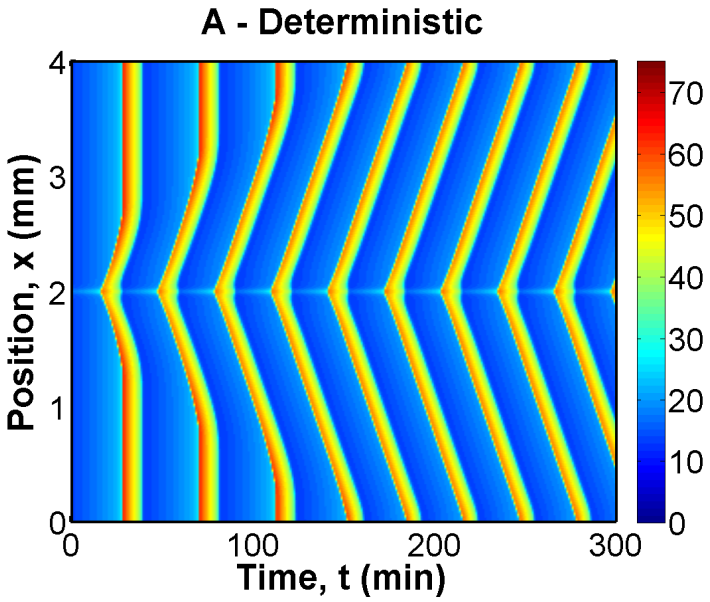

Figure C.3: Traveling wave generated by Chang and Ferrel's model in 1 dimension. Y axis represents the cell stretched out in a straight line and the x axis represents time.

As illustrated in figure (C.3), the numerical simulations were performed over a 1 dimensional domain that was 4mm long over a time of 300 minutes. Some testing showed that a minimum grid resolution of 2^8 was needed to resolve the traveling wave, and a time step of $\Delta t = 0.01$ minutes was used for all the simulations.

Appendix D

Effective Stability Analysis

This section provides some details on how to analyze the stability of a stochastic system in the presence of intrinsic noise, as explained by Scott et al[12].

D.1 Effective Eigenvalues

Suppose we have a deterministic system

$$\frac{d\mathbf{x}}{dt} = \mathbf{f}(\mathbf{x}), \tag{D.1}$$

and let $\{\lambda_i\}$ be the eigenvalues of the linearized system about its fixed points (obtained using standard linear stability analysis[57]). If $\mathbf{x_s}$ is a *stable* fixed point, then its corresponding eigenvalue λ_i has negative real part. For a small perturbation about the stable fixed point, $\mathbf{x} = \mathbf{x_s} + \mathbf{x_p}$, the linearized system is given by

$$\frac{d}{dt}\mathbf{x_p} = \left.\frac{\partial \mathbf{f}}{\partial \mathbf{x}}\right|_{\mathbf{x}=\mathbf{x_s}} \cdot x_p = \mathbf{J^{(0)}} \cdot \mathbf{x_p}. \tag{D.2}$$

Now in the presence of intrinsic noise, following the discussion in chapter 1 about the linear

noise approximation, we will let

$$\mathbf{x} = \mathbf{x_s} + \mathbf{x_p} + \omega\boldsymbol{\alpha}(t) \tag{D.3}$$

where $\omega = \sqrt{\Omega}$ and, denote the new eigenvalues by

$$\lambda_i' = \lambda_i + \lambda_{correct}, \tag{D.4}$$

where $\lambda_{correct}$ is the correction due to noise. If the real part of λ_i' is positive (when the real part of λ_i is negative) then we have found a noise induced instability.

The new Jacobian is given by

$$\mathbf{J} \equiv \left.\frac{\partial \mathbf{f}}{\partial \mathbf{x}}\right|_{\mathbf{x}=\mathbf{x_s}+\omega\boldsymbol{\alpha}(t)}. \tag{D.5}$$

As before, we take a system size expansion in the limit $\omega \to 0$:

$$\mathbf{J} \approx \mathbf{J}|_{\omega\to 0} + \left.\frac{\partial \mathbf{f}}{\partial \omega}\right|_{\omega\to 0} \equiv \mathbf{J^{(0)}} + \omega\mathbf{J^{(1)}}(t), \tag{D.6}$$

so the linearized system is now

$$\frac{d}{dt}\mathbf{x_p} = \left[\mathbf{J^{(0)}} + \omega\mathbf{J^{(1)}}(t)\right] \cdot x_p. \tag{D.7}$$

The equation above implicitly contains $\boldsymbol{\alpha}(t)$ so it is a stochastic differential equation. Since $\boldsymbol{\alpha}(t)$ has non-zero correlation time, $\mathbf{J^{(1)}}(t)$ also has non-zero correlation time, so the derivative of $\mathbf{x_p}$ exists in the ordinary sense as discussed in chapter 1). The mean stability of the system is hence governed by

$$\frac{d}{dt}\langle \mathbf{x_p} \rangle = \mathbf{J^{(0)}} \cdot \langle \mathbf{x_p} \rangle + \omega \left\langle \mathbf{J^{(1)}}(t) x_p \right\rangle. \tag{D.8}$$

One way to solve this equation is to use Bourret's integral formulation (Bourret's original paper

can be found in [60] and is explained by Brissaud and Frisch[59] and van Kampen[22]). If $\mathbf{J^{(0)}} \gg \omega \mathbf{J^{(1)}}(t)$, one can show that

$$\frac{d}{dt}\langle \mathbf{x_p} \rangle = \mathbf{J^{(0)}} \cdot \langle \mathbf{x_p} \rangle + \omega^2 \int_0^t \mathbf{J_c}(t-\tau)\langle \mathbf{x_p}(\tau) \rangle d\tau \tag{D.9}$$

where $\mathbf{J_c}(t-\tau) = \left\langle \mathbf{J^{(1)}}(t) e^{\mathbf{J^{(0)}}(t-\tau)} \mathbf{J^{(1)}}(\tau) \right\rangle$ is the time autocorrelation of the fluctuations (and $e^{\mathbf{J^{(0)}}(t-\tau)}$ is the matrix exponential of $\mathbf{J^{(0)}}$).

Using Laplace transforms, the solution is given by

$$\langle \hat{\mathbf{x}_p}(s) = \left[s\mathbf{I} - \mathbf{J^{(0)}} - \omega^2 \hat{\mathbf{J}}_\mathbf{c}(s) \right]^{-1} \langle \mathbf{x_p}(0) \rangle, \tag{D.10}$$

So the new eigenvalues can be found by solving

$$det \left[\lambda' \mathbf{I} - \mathbf{J_0} - \omega^2 \hat{\mathbf{J}}_\mathbf{c}(\lambda') \right] = 0. \tag{D.11}$$

Equation (D.11) is what was used to calculate the phase plot (figure (4.3)) in chapter 4. The original equations were input into a symbolic manipulation language such as maple, and the $\mathbf{J}$ matrices were then derived symbolically. Once we have the $\mathbf{J}$ matrices, maple can produce the appropriate laplace transforms, and different values of ω^2 were substituted into equation (D.11). The roots can then be found numerically until at least one of the λ' have positive real part (indicating a noise induced temporal instability).

Appendix E

Law of Mass Action for Chemical Reactions

The general rule that we employ to turn reaction coefficients in the differential equation into reaction rates for the master equation is known as the Law of Mass Action, first proposed by Guldberg and Waage in 1864[74] (reference is a review of their work by Lund, published in 1965). In short, they postulated that the reaction rate of a chemical reaction was proportional to the masses of the reactants, and inversely proportional to the volume. This rule was theorized so that they could find a way of mathematically writing down how the forward and backward reactions would balance in equilibrium.

Consider a chemical reaction $A + B \rightarrow A' + B'$, and denote P and Q as the number of molecules of A and B respectively, and let V be the volume of the system. Then the reaction rate of the forward reaction would be given by

$$\nu = \frac{kPQ}{V}, \tag{E.1}$$

where k is some unknown reaction constant that needs to be determined experimentally. In more modern notation, we might write the rate instead as $\nu = k[A][B]$ where the square brackets

denotes the concentration of the reactants (while remembering that this hides an extra factor of V in the denominator). This rule then allowed chemists to write ODEs to describe the change in mass of the system.

For our purposes, we wish to do the reverse: we will start with an ODE and extract the reaction rate from the equation to use as the transition probability in the master equation. For example, if we had exponential growth, where n is the concentration of the species

$$\frac{dn}{dt} = rn, \tag{E.2}$$

then the reaction rate ν would be rN/Ω where recall Ω is the volume parameter in the system size expansion of the master equation (and N is the number of reactants). On the other hand, if we had say a quadratic term,

$$\frac{dn}{dt} = rn^2, \tag{E.3}$$

then the reaction rate would be given by

$$\nu = r\left(\frac{N}{\Omega}\right) \cdot \left(\frac{N-1}{\Omega}\right) \tag{E.4}$$

where the $N-1$ in the second term arises from the fact that the reactant is colliding with another member of the same species so there is one less possibility for it to collide with.

References

[1] Robert A. Weinberg, *The Biology of Cancer.* Garland Science, New York 2007. 1

[2] Douglas Hanahan, Robert A. Weinberg, *The Hallmarks of Cancer.* Cell, 100(1):57-70, Jan 7 2000. 1, 41

[3] Douglas Hanahan, Robert A. Weinberg, *The Hallmarks of Cancer: The Next Generation.* Cell, 144(5):646-74, March 5 2011. 1, 41

[4] P. Tracqui, G.C. Cruywagen, D.E. Woodward, et al., *A mathematicl model of glioma growth: the effect pf chemotherapy on spatio-temporal growth.* Cell Prolif., 28, 17-31, 1995. 40, 52

[5] KR Swanson, EC Alvord Jr and JD Murray, *Virtual brain tumours (gliomas) enhance the reality of medical imaging and highlight inadequacies of current therapy.* British Journal of Cancer, 86:14-8, 2002. 3, 40, 42, 43, 48

[6] J. D. Murray, *Mathematical biology, 3rd Ed.* Springer, 2007. 3, 32, 40, 69

[7] J. M. Greenberg and S. P. Hastings, *Spatial Patterns For Discrete Models Of Diffusion In Excitable Media.* SIAM Journal on Applied Mathematics, Vol. 34, No. 3, 515-523, May 1978. 30, 33

[8] A. L. Hodgkin and A. F. Huxley, *A Quantitative Description Of Membrane Current And Its Application To Conduction And Excitation In Nerve.* J. Physiol. 117, 500-544, 1952. 30

[9] R. FitzHugh, *Impulses and physiological states in theoretical models of nerve membrane.* Biophysical J. 1:445-466, 1961. 30

[10] J. Nagumo, S. Arimoto, and S. Yoshizawa, *An active pulse transmission line simulating nerve axon.* Proc IRE. 50:20612070, 1962. 30

[11] Matthew Scott, Francis J. Poulin, and Herbert Tang, *Approximating intrinsic noise in continuous multispecies models*. Proceedings of the Royal Society of London - Series A. 467: 718-737, 2011. 57, 73

[12] Matthew Scott, Terence Hwa, and Brian Ingals, *Deterministic characterization of stochastic genetic circuits.* PNAS, May 1 2007, vol. 104, no. 18, 7402-7. 35, 36, 73, 116

[13] José M.G. Vilar, Hao Yuan Kueh, et al, *Mechanisms of noise-resistance in genetic oscillators*. PNAS, April 30, 2002, vol. 99, no. 9., 5988-92. 30, 36

[14] R. A. Weinberg, *Mechanisms of malignant progression*. Carcinogenesis, vol. 29, no. 6, 1092-5, 2008. 1, 2, 69

[15] April F. Eichler, Euiheon Chung, David P. Kodack, Jay S. Loeffler, Dai Fukumura and Rakesh K. Jain, *The biology of brain metastases - translation to new therapies.* Nature Reviews Clinical Oncology, advance online publication, Published online 12 April 2011. 70

[16] Franziska Michor, Martin A. Nowak, Yoh Iwasa, *Stochastic dynamics of metastasis formation.* Journal of Theoretical Biology 240, 521-30, 2006. 69

[17] A. R. A. Anderson, M. A. J. Chaplain, E. L. New Man, R. J. C. Steele And A. M. Thompson, *Mathematical Modelling of Tumour Invasion and Metastasis.* Journal of Theoretical Medicine. Vol 2, 129-151, 1999. 70

[18] N. G. van Kampen, *Stochastic Processes in Physics and Chemistry.* Elsevier Science & Technology Books, April 2007. 3, 5, 6, 13, 14, 25, 27

[19] N. G. van Kampen, *The expansion of the Master equation.* Adv. Chem. Phys. 34, 245-308, 1976. 14, 19

[20] N. G. van Kampen, *Fluctuations in continuous systems*. In Topics in statistical mechanics and biophysics: a memorial to Julius L. Jackson (ed. R. A. Piccirelli), 153-186. New York, NY: American Institute of Physics, 1976. 28, 58

[21] N. G. van Kampen, *Fluctuations in Nonlinear Systems*. Fluctuation Phenomena in Solids. Edited by R. E. Burgess. Academic Press, 1965, 139-177.

[22] N. G. van Kampen, *Stochastic Differential Equations.* Physics Reports, Volume 24, Issue 3, Pages 171-228, (March 1976). 6, 10, 100, 118

[23] Gibin Powathil, *Modeling of Brain Tumors: Effects of Microenvironment and Associated Therapeutic Strategies.* Ph.D Thesis, Waterloo, 2009. 32, 33, 40, 42, 52

[24] Hans Clevers, *The cancer stem cell: premises, promises and challenges.* Nature Medicine Volume 17, Number 3, March 2011, 313-9. 41

[25] Colin Turner, *Mathematical Modelling of Cancer Stem Cells.* Masters' Thesis, Waterloo, 2009. 41

[26] R. A. Fisher, *The wave of advance of advantageous genes.* Ann. Eugenics 7:353369, 1937. 30, 32, 41

[27] Robert C. Hilborn, Jessie D. Erwin, *Stochastic coherence in an oscillatory gene circuit model.* Journal of Theoretical Biology 253, 349 354, 2008. 37, 67

[28] Ralf Steuer, Changson Zhou, Jürgen Kurths, *Constructive effects of fluctuations in genetic and biochemical regulatory systems.* BioSystems 72, 241-251, 2003. 37, 67

[29] Mark D. McDonnell, Derek Abbot, *What is Stochastic Resonance? Definitions, Misconceptions, Debates, and Its Relevance to Biology.* PLoS Computational Biology, Volume 5, Issue 5, May 2009. 3, 37, 67

[30] Tsai TY, Choi YS, Ma W, Pomerening JR, Tang C, Ferrell JE Jr., *Robust, tunable biological oscillations from interlinked positive and negative feedback loops.* Science, Jul 4;321(5885):126-9., 2008. 30, 33, 67

[31] Jeremy B. Chang and James E. Ferrell Jr., *Mitotic trigger waves and the spatial coordination of the Xenopus cell cycle.* Nature 500, 603-7, August 2013. 3, 67, 68, 70, 92, 113, 114

[32] James E. Ferrell Jr., *Feedback loops and reciprocal regulation: recurring motifs in the systems biology of the cell cycle.* Current Opinion in Cell Biology, 25:676-86, 2013. 33, 67

[33] Pau Rué, Jordi Garcia-Ojalvo, *Gene circuit designs for noisy excitable dynamics*. Preprint submitted to Elsevier, February 22, 2011. 35

[34] Johan Elf, and Måns Ehrenberg, *Fast Evaluation of Fluctuations in Biochemical Networks With the Linear Noise Approximation.* Genome Res., 13: 2475-84, 2003. 20

[35] A. M. Davie and J. G. Gaines, *Convergence Of Numerical Schemes For The Solution Of Parabolic Stochastic Partial Differential Equations.* Mathematics Of Computation, 70(233):121-34, 2000. 13, 99, 100

[36] Pablo A. Iglesias and Peter N. Devreotes, *Biased excitable networks: How cells direct motion in response to gradients.* Curr Opin Cell Biol. 2012 April ; 24(2): 245253. 69

[37] Mustafa B A Djamgoz, *Biophysics of Cancer: Cellular Excitability (CELEX) Hypothesis of Metastasis.* J Clin Exp Oncol 2014, S1. 69

[38] William J. Brackenbury, *Voltage-gated sodium channels and metastatic disease.* Landes Bioscience; Channels 6:5, 352-361; September/October 2012. 69

[39] Natalia Prevarskaya, Roman Skryma and Yaroslav Shuba, *Calcium in tumour metastasis: new roles for known actors.* Nature Reviews Cancer, Volume 11, August 2011, 609-18. 69

[40] Daniel T. Gillespie, *Exact Stochastic Simulation of Coupled Chemical Reactions.* The Journal of Physical Chemistry, Vol. 81, No. 25, 1977. 3, 14, 102, 104, 105

[41] Daniel T. Gillespie, *Markov Processess - An Introduction for Physical Scientists.* Acadeemic Press, San Diego, 1992. 6

[42] Ronald A. Fisher, *Statistical Methods For Research Workers.* Oliver and Boyd, Edinburgh, 1925. 44, 48

[43] Ronald A. Fisher, *On the "Probable Error" of a Coefficient of Correlation Deduced from a Small Sample.* Metron, 1: 3-32, 1921. 44

[44] D. S. Sivia, *Data Analysis - A Bayesian Tutorial 2nd Ed.*. Oxford University Press, New York, 2006. 48

[45] Paul Langevin, *On the theory of Brownian motion.* CR Acad. Sci. Paris, 146:530, 1908. 10

[46] J. L. Doob, *The Brownian Movement and Stochastic Equations.* The Annals of Mathematics, Second Series, Vol. 43, No. 2, 351-69, Apr., 1942. 11

[47] Mark Kac, *Random Walk And The Theory of Brownian Motion.* The American Mathematical Monthly, Vol. 54, 369-91, 1947. 26, 106

[48] Marian Smoluchowski, *Zur kinetischen Theorie der Brownschen Molekularbewegung und der Suspensionen.* Annalen der Physik 326 (14): 756780, 1906. 26, 106

[49] Kiyosi Itô, *Stochastic integral.* Proceedings of the Imperial Academy 20 (8): 51924, 1944. 12

[50] Kiyosi Itô, *On a stochastic integral equation.* Proceedings of the Japan Academy 22 (2): 325, 1946. 12

[51] R. L . Stratonovich, *A New Representation for Stochastic Integrals and Equations.* SIAM Journal on Control, 4(2), 36271, 1966. 12, 13

[52] N. G. van Kampen, *Itô Versus Stratonovich.* Journal of Statistical Physics, Vol. 24, No. 1, 175-87, 1981. 12, 13

[53] N.G. van Kampen, *Diffusion Approximation For Markov Processes.* Thermodynamics & Kinetics Of Biological Processes, Edited by I. Lamprecht and A. I. Zotin. Walter de Gruyter & Co., New York, 181-95, 1982. 15

[54] Crispin Gardiner, *Stochastic Methods - A Handbook for thr natural and Social Sciences. Fourth Edition.* Springer-Verlag, Berlin, 2009. 6, 11, 13

[55] D. S. Lemons, *An Introduction to Stochastic Processes in Physics.* The Johhn Hopkins University Press, Baltimore and London, 2002. 6

[56] Arieh Isreles, *A First Course in the Numerical Analysis of Differential Equations.* Cambridge University Press, Cambridge, 2004. 98

[57] P. Glendinning, *Stability, instability and chaos: an introduction to the theory of nonlinear differential equations.* Cambridge university press, Cambridge, 1994. 71, 116

[58] Yuxiang Chong, John B. Walsh, *The Roughness and Smoothness of Numerical Solutions to the Stochastic Heat Equation.* Potential Analysis, Volume 37, Issue 4, 303-32, November 2012. 13, 99, 100, 111

[59] A. Brissaud, U. Frisch, *Solving Linear Stochastic Differential Equations.* J. Math. Phys., Vol. 15, No. 5, 524-34, May 1974. 100, 118

[60] R. C. Bourret, *Ficton Theory Of Dynamical Systems With Noisy Parameters.* Canadian Journal of Physics, 43(4): 619-39, 1965. 118

[61] P. Thomas, R. Grima R, *Approximate probability distributions of the master equation.* Physical Review E 92, 012120, 2015. 23

[62] McQuarrie, Donald A. *Stochastic Approach to Chemical Kinetics.* Journal of applied probability 4.3, 413-78, 1967. 19

[63] Kristin R. Swanson, Carly Bridge, J.D. Murray, Ellsworth C. Alvord Jr., *Virtual and real brain tumors: using mathematical modeling to quantify glioma growth and invasion.* Journal of the Neurological Sciences, 216, 1-10, 2003. 3, 40

[64] K. R. Swanson, E. C. Alvord Jr., and J. D. Murray, *Virtual Resection of Gliomas: Effect of Extent of Resection on Recurrence.* Mathematical and Computer Modelling, 37, 1177-90, 2003. 3, 40

[65] K. R. Swanson, R. C. Rostomily, and E. C. Alvord Jr., *A mathematical modelling tool for predicting survival of individual patients following resection of glioblastoma: a proof of principle.* British Journl of Cancer, Vol. 98, 113-9, 2008. 3, 40

[66] R Rockne, J K Rockhill, M Mrugala, A M Spence, I Kalet, K Hendrickson, A Lai, T Cloughesy, E C Alvord Jr and K R Swanson, *Predicting the efficacy of radiotherapy in individual glioblastoma patients in vivo: a mathematical modeling approach.* Phys Med Biol., 55(12): 327185, Jun 2010. 42

[67] Neal ML, Trister AD, Cloke T, Sodt R, Ahn S, Baldock AL, et al., *Discriminating Survival Outcomes in Patients with Glioblastoma Using a Simulation-Based, Patient-Specific Response Metric.* PLoS ONE 8(1): e51951, 2013. 42

[68] G. Powathil, M. Kohandel, S. Sivaloganathan, A. Oza, and M. Milosevic, *Mathematical modeling of brain tumors: effects of radiotherapy and chemotherapy.* Phys. Med. Biol., Vol. 52, 3291-306, 2007. 40, 42

[69] M. Kohandel, M. kardar, M. Milosevic, and S. Sivaloganathan, *Dynamics of tumor growth and commbination of anti-angiogenic and cytotoxic therapies.* Phys. Med. Biol., Vol. 52, 3665-77, 2007. 40, 42

[70] Anna Kane Laird, *Dynamics of Tumor Growth*. British Journal of Cancer, 18(3):490-502, 1964. iii, 42

[71] A. R. A. Anderson and M. A. J. Chaplain, *Continuous and Discrete Mathematical Models of Tumor-induced Angiogenesis.* Bulletin of Mathematical Biology, 60, 857900, 1998. 42

[72] E.S. Norris, J.R. King, H.M. Byrne, *Modelling the response of spatially structured tumours to chemotherapy: Drug kinetics.* Mathematical and Computer Modelling, 43, 820837, 2006. 42

[73] A. M. Yaglom, *An Introduction To The Theory of Stationary Random Functions.* Martino Publishing, Mansfield Centre, CT, 2014. 6, 8, 9

[74] E. W. Lund, *Guldberg and Waage and the Law of Mass Action.* J. Chem. Educ., 42 (10), 548-50, 1965, 57, 119

[75] Edited by: Rene A. Carmona, and Boris Rozovskii, *Stochastic partial differential equations : six perspectives*. American Mathematical Society, Providence, RI, 1999 13

[76] Martin Hairer, *An Introduction to Stochastic PDEs.* Lecture notes from the University of Warwick, July 24 2009. http://www.hairer.org/notes/SPDEs.pdf 13

[77] E. Pardoux, *Stochastic Partial Differential Equations* Lectures given in Fudan University, Shanghai, April 2007. https://www.i2m.univ-amu.fr/ pardoux/spde-fudan.pdf 13